LBL-6046

MICROSTRUCTURE AND MECHANICAL PROPERTIES OF AISI 4340 STEEL MODIFIED WITH ALUMINUM AND SILICON

Manjeshwar Shanthidas Bhat
(Ph. D. thesis)

February 1977

Prepared for the U. S. Energy Research and Development Administration under Contract W-7405-ENG-48

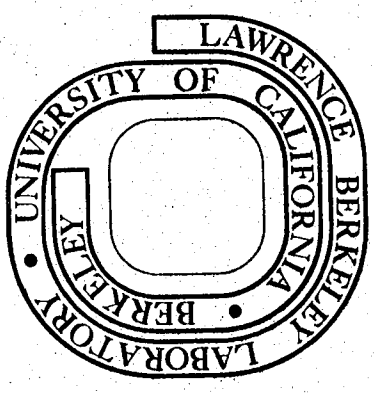

LBL-6046

Table of Contents

MICROSTRUCTURE AND MECHANICAL PROPERTIES OF AISI 4340 STEEL MODIFIED WITH ALUMINUM AND SILICON

Manjeshwar Shanthidas Bhat

Materials and Molecular Research Division, Lawrence Berkeley Laboratory and Department of Materials Science and Engineering, College of Engineering; University of California, Berkeley, California 94720

ABSTRACT

The influence of additions of aluminum and combinations of aluminum and silicon to AISI 4340 steels was investigated. The mechanical properties such as strength, fracture toughness (K_{Ic}), and impact toughness (C_v) were obtained for the modified steels in the quenched and tempered condition. The microstructure was characterized using optical and transmission electron microscopy. The fracture surfaces and inclusions were characterized using scanning electron microscopy and an energy dispersive analysis of x-rays unit.

It was observed that the softening which normally occurs on tempering AISI 4340 steel was retarded by additions of either aluminum or combinations of aluminum and silicon. The effect of aluminum on the tempering reactions in steel appeared to be similar to that of silicon. The tempered martensite embrittlement phenomenon in AISI 4340 steel occurred at higher tempering temperatures in the presence of silicon and/or aluminum. Significant improvements in the strength and toughness of quenched and tempered 4340 steel were obtained through silicon and/or aluminum additions. An attempt was made to correlate microstructure with the observed mechanical properties. The fracture surface features associated with the initiation of fast fracture for

all the heat treated conditions investigated indicated that the operative fracture mode was complex.

I. INTRODUCTION

Recent research on low alloy ultrahigh strength steels (yield strength 200-300 ksi) has been focused on improving properties such as strength, fracture toughness, and stress corrosion resistance. The relationship between strength and toughness has been studied extensively and so has the relationship between microstructure and mechanical properties. This investigation was undertaken to understand better these relationships in a specific class of steels.

In the past, a number of different approaches have been taken to improve the fracture toughness. The most promising of these are:

1. Improving the cleanliness of existing steels
2. Modifying the heat treatment of currently used steels
3. Utilizing new alloy compositions, and
4. Modifying the composition of the commonly used grades.

Studies directed toward improving the cleanliness of steels have been aimed at reducing the size and content of nonmetallic inclusions and lowering impurity concentrations.[1,2] Substantial improvements in fracture toughness have been obtained through these reductions.

A further improvement in the mechanical properties can be achieved by the utilization of heat treatment modifications. Higher temperature austenitizing treatments have been used to obtain microstructural features which improved the plane strain fracture toughness.[3,4] However, this increase in the fracture toughness (K_{Ic}) can be accompanied by a loss in Charpy V-notch values.[3-7]

Some work has been done on arriving at new alloy compositions which could result in alloys having favorable combinations of strength and toughness.[8-10] The ideas in these investigations have been aimed at achieving microstructural features which are expected to be beneficial to the fracture toughness in new steels.

An increase in the fracture toughness at high levels of strength can also be achieved by modifying the composition of an existing steel. For example, modifications of AISI 4340, such as 300-M and HP310, have been developed.[11,12] The major compositional modification in these steels is the addition of Si and V. Silicon raises the embrittlement temperature range and allows tempering to be carried out at higher temperatures[13,14] which allows a greater reduction in internal stresses.[15,16] It also retards the softening of the steel which normally occurs on tempering.[17,18] Vanadium was added presumably to promote toughness by reducing the grain size.[19]

The approach used in this investigation, for improving the fracture toughness, was to utilize the effect of inexpensive alloying modifications in a commercial steel. One of the alloying additions examined was aluminum and the commercial steel chosen was an ultrahigh strength steel, AISI 4340, on which substantial data is already available in the literature.[19-24]

Previous studies of the effect of Al in steels have been mainly related to its influence on grain size.[25,26] Some work has been reported on the effect of aluminum on phase transformation characteristics such as isothermal transformation behavior[27,28] and martensitic

transformation.[29] A summary of the work done in connection with effects of Al in steel upto the year 1952 has been published in a book.[30] Some investigators have felt that Al additions beyond the amount necessary to provide grain refinement are detrimental to mechanical properties, especially impact toughness.[31] In addition problems were encountered in steel melting practice when substantial amounts of Al were added to steel.[32,33] However, aluminum additions to steel can have beneficial effects such as improvement in corrosion resistance,[31] oxidation resistance[31] and resistance to sulfidation.[34] It has been suggested in the literature that Al would retard tempering reactions in a manner similar to that of Si.[35] It was of interest to study the effect of Al additions on the microstructure and mechanical properties of low alloy heat treatable steels. Since Si is known to be a much more effective strengthener of iron than Al,[36] combinations of Al+Si were also made to AISI 4340 to study any possible synergistic effects.

The influence of Al and Al+Si additions (to AISI 4340 steel) on the tempering behavior was investigated. The tensile properties and the fracture toughness of the modified AISI 4340 steels in various heat treated conditions were measured. The microstructure of the modified steels was studied using optical and transmission electron microscopy, and the fracture characteristics were studied using scanning electron microscopy.

II. EXPERIMENTAL PROCEDURE

A. Alloy Preparation and Processing

The base steel used in this investigation was commercial aircraft quality, annealed AISI 4340, obtained as 2 $\frac{1}{2}$ in. diameter rounds which met AMS-2300 and MIL-S-8844C specifications. Alloy modifications were made by remelting the commercial steel in an argon atmosphere in a vacuum induction furnace and adding Al, Si and C. The C was added to compensate for loss during remelting. The alloys were cast as 22 lbs., 2 $\frac{1}{2}$ in. diameter round ingots.

The ingots were upset and cross-forged at 1150°C to bars 2.7 in. wide and 0.8 in. thick. The bars were homogenized in argon at 1200°C for 24 hours. The chemical compositions of the steels used in this investigation are listed in Table I.

Specimen blanks for mechanical testing were obtained from the homogenized bars. In Fig. 1 are shown the orientations of specimen blanks with respect to the long direction of the bar. The dimensions of the blanks allowed for appropriate tolerances for final machining.

B. Heat Treatment

The specimen blanks were austenitized for 1 hour in an argon atmosphere in a vertical tube furnace and quenched in agitated oil. Specimen blanks were tempered for 1 hour in neutral salt baths and air cooled.

C. Mechanical Testing

1. Hardness Tests

Rockwell C hardness was measured using a Wilson hardness tester. An average of at least 3 measurements was taken for each specimen. For the tempering study, the hardness readings were taken on heat-treated specimen blanks. Hardness measurements were also made of tensile specimens and compact tension specimens.

2. Tensile Testing

Two types of specimens were used for determining the room temperature longitudinal tensile properties. Sketches of the two types are shown in Figs. 2 and 3. For obtaining the flat tensile specimens, blanks of the same thickness as the compact tension specimens were first austenitized and quenched. This procedure was followed in order to ensure that the tensile and fracture toughness properties corresponded to comparable cooling rates. The blanks were then sliced into 0.07 in. thick sheets prior to tempering at different temperatures. Following tempering, the slices were machined to the dimensions shown in Fig. 2. The round tensile specimen blanks were austenitized, quenched, and tempered prior to final machining.

The flat tensile specimens were tested using a 11,000 lbs. capacity Instron machine. The strain rate was 0.02 per minute. The round tensile specimens were tested using a 300,000 lbs. capacity MTS Universal testing system. For both types of specimens, yield strength was determined by the 0.2 pct. offset method. The total elongations for the flat specimens were determined from the load vs. crosshead

displacement record. For the round specimens the plastic elongation to fracture was obtained by measuring the distances between fixed points, before and after testing, using a Vernier travelling microscope.

3. Fracture Toughness Testing

Room temperature fracture toughness tests were conducted using specimens of the compact tension type as shown in Fig. 4. Prior to heat treatment, compact tension specimen blanks were machined to their final size except for the thickness dimension. Following heat treatment the flat faces were wet ground to remove the decarburized layer (0.02 in. on each face) and a 0.008 in. wide slot of about 0.1 in. length was ground into the specimen. Grooves for holding the crack opening displacement (COD) gauge were also ground in at this stage.

The tests were performed in accordance with ASTM specifications E-399-72. Fatigue precracking was performed using either a 300,000 lb capacity MTS Universal testing system or a high cycle MTS fatigue machine. Following precracking, the specimens were tested using the 300,000 lbs. capacity MTS Universal testing machine at a ram speed of 0.005 in/sec (0.00125 cm/sec) and load - COD curves were recorded. The fracture toughness was calculated according to the standard ASTM procedure.

4. Charpy Impact Tests

The specimen used for the Charpy tests is sketched in Fig. 5. The impact tests were performed at room temperature using a 223 ft-lb capacity testing machine. The tests were performed according to ASTM E-23-72 specifications.

D. Phase Transformation Measurements

1. Dilatometry

A commercial dilatometer (Theta Dilatronic model) was used in this investigation. A sketch of the specimen used is shown in Fig. 6. The M_s and M_f temperatures were determined.

2. Magnetic Saturation

The transformation of austenite to martensite during a tensile test was detected by a magnetic saturation technique in which the proportion of martensite in a specimen was measured prior to, and during testing using a permeameter attached to an Instron testing machine. Figure 7 shows a sketch of the permeameter system. The technique is described in detail in Appendix I.

E. Microstructural Analysis

1. Optical Microscopy

Samples for optical metallography were prepared by mechanical grinding and polishing followed by chemical etching. The etchants used were standard Nital solutions or Picral. This technique was used to study the general microstructure of heat treated specimens and to detect the different phases present in the steel. For the prior austenite grain-size determinations, the as-quenched polished specimens were etched in picral. The etched surface was observed at a magnification of 100X and the grain diameters were compared to standard ASTM charts to determine the ASTM grain size number.

2. X-ray Metallography

Metallographically polished specimens were examined in a Norelco x-ray diffractometer using CuK_α radiation and a crystal monochromator (lithium fluoride) to reduce the fluorescent radiation. The amounts of retained austenite present in some of the heat treated specimens were determined using standard techniques.[37,38]

3. Transmission Electron Microscopy

Thin foils for transmission electron microscopy were prepared by the twin-jet electropolishing technique using a solution containing 75 gms of Cr_2O_3, 400 ml of CH_3COOH and 20 ml of H_2O. The samples for electro-polishing were obtained in the following way. Slices, 0.025 in. thick, were cut from fractured compact tension specimens taking care to introduce the minimum possible amount of deformation during slicing. These slices were chemically thinned to 0.002 in. in a solution of hydrogen peroxide containing a few drops of hydrofluoric acid. Round discs, 3 mm in diameter, were punched out of the thin sheets and were used for electropolishing.

A Hitachi HV-125 and a Phillips 301 electron microscope was used in this study. The operating voltage was 100 kV. Both microscopes were equipped with a goniometer stage. Dark field microscopy was performed by beam tilting.

F. Scanning Electron Microscopy

Fracture surfaces of broken compact tension specimens were examined in an AMR-1000 scanning electron microscope operated at 20 kV. An

Energy Dispersive Analysis of X-rays (EDAX) unit, attached to the microscope, permitted semi-quantitative chemical analysis of inclusions and of fracture surfaces.

III. RESULTS

A. Transformation Temperatures and Heat Treatment

The addition of Al and/or Si to AISI 4340 resulted in an increase in the temperatures required for solution treating in a single phase austenite region. The solution treatment temperatures were determined by using optical metallography. Each steel was heated to some temperature, and either quenched directly to room temperature or isothermally transformed at some temperature in the neighborhood of the M_s temperature in a dilatometer. The polished specimens were etched in nital to reveal the presence of ferrite.

In Fig. 8 are shown the results of such a study for the 4340+3Al steel. In Fig. 8a is shown the microstructure resulting from the specimen held at 900°C and quenched. The light etching phase is ferrite. Ferrite is still present in the specimen solution treated at 1000°C as seen in Fig. 8b. However following solution treating at 1075°C, no ferrite was observed, as shown in Fig. 8c. In all these microstructures the morphology of the ferrite precludes the possibility of it having formed during cooling from the austenitization temperature. In a steel containing 4 pct. Al it was found that solution treatment in a single phase austenite region was not possible at any temperature. The microstructures obtained by solution treating at different temperatures between 900° and 1300°C are shown in Fig. 9. Although at some intermediate temperature the amount of ferrite decreased, it was found

that at no temperature was there a total absence of ferrite in the microstructure. The austenitization temperature determined in this manner for each of the modified steels is listed in Table II.

The microstructures of the modified steels, especially the ones containing higher amounts of Al and Si, were found to be very sensitive to the carbon concentration. A drop in carbon level caused the appearance of ferrite in the microstructure. The steels containing 3.0 Al and 2.0Al+2.0Si required a minimum of about 0.38-0.4 pct. C to allow austenitization in a single phase region.

The M_s temperatures of all the steels used in this investigation were determined with the help of a dilatometer. The technique allowed fairly accurate determinations (±5°C) of the M_s temperature. However, it was found that the M_f temperatures could not be accurately determined. The M_s and M_f temperatures which were measured are listed in Table II.

The variation of M_s of AISI 4340 as a function of Al content is shown in Fig. 10. All the steels were austenitized at the same temperature to attain the same grain size. It was found that the addition of Al to AISI 4340 resulted in a slight increase in the M_s. The significance of being able to raise the M_s (or at least keep it the same) in AISI 4340 type steels will be discussed in a later section.

The information obtained was used to design the heat treatments in this investigation. The steels were austenitized at the temperatures shown in Table II and oil quenched. They were tempered at temperatures from 250° to 500°C.

B. Effect of Composition on Tempering

The effect of Al additions on the tempering response of AISI 4340, as indicated by hardness measurements, is shown in Fig. 11. Also plotted in the figure are similar data for AISI 4340. The hardness data for AISI 4340 was obtained from the literature.[14] A sharp drop in hardness was observed for the AISI 4340 steel following tempering at temperatures beyond about 200°C. This sharp drop in hardness was not observed in the modified steels at tempering temperatures lower than 225°C. With increasing amounts of Al in the steel, the hardness was maintained at increasingly higher levels especially following tempering at temperatures higher than 250°C. Following tempering at 600°C, the steel with the highest amount of Al had the highest hardness.

A similar behavior was observed for the steels modified with combinations of Al and Si. The results are shown in Fig. 12. However, higher hardness values were obtained for these steels than for steels containing only Al. Also, there appeared to be an indication of a mild secondary hardness peak at higher tempering temperatures. It was observed that the higher the combined additions of Al and Si to the steel, the higher was the hardness following tempering at high temperatures.

The variation in microstructure with tempering was also investigated using optical and electron microscopy. The results will be discussed in later sections.

C. Mechanical Behavior

1. Tensile Properties

The variation in the 0.2 pct offset yield and ultimate strength with tempering temperature for the 4340+Al steels is shown in Fig. 13. Following an initial drop in the ultimate strength, a plateau in strength appears which extends to higher tempering temperatures with higher Al contents. The precipitous drop in the ultimate strength of the AISI 4340 on tempering beyond 200°C is clearly not seen in the Al containing steels. The drop in ultimate strength of modified steels occurs at increasingly higher temperatures and is a reflection of the hardness drop discussed in the previous section.

The 0.2 pct offset yield strength increases with tempering temperature upto about 300-400°C, beyond which there is a sharp drop in strength. The peak in yield strength occurs at increasingly higher tempering temperatures with increasing amounts of Al in the steel.

The variation in yield and ultimate strengths of the steels modified with combinations of Al and Si was similar to that of steels containing only Al. The results are shown in Fig. 14. Higher strength levels were obtained in the Al+Si steels than in the plain Al steels.

As mentioned in the section on experimental procedure, two types of specimens were used to measure the tensile properties, viz., flat and round tensile specimens. In Fig. 15 are plotted the results of tests using the two types of specimens. There are data points on either side of the line representing similarity of strengths obtained by the two different types of specimen given similar heat treatments.

The total elongation values (1" guage length) obtained are shown in Tables III to VI in which the 0.2 pct offset yield and ultimate strengths are also shown.

2. Fracture Properties

The plane strain fracture toughness of the experimental steels were measured in the as-quenched and quenched and tempered conditions. With the limited amount of material available, not all the tempering temperatures could be characterized. In the cases where material was available, Charpy tests were also run, and the impact energy values at room temperature were measured. The results of the study are presented in Figs. 16 to 26. Also plotted in the figures are the 0.2 pct offset yield and ultimate strengths.

For the 4340+1Al and 2Al steels, a maximum in the K_{Ic} fracture toughness occurred around a tempering temperature of 250°C. For the 2Al steel the maximum in impact energy also occurred around 250°C. In the steel containing 3 pct Al there appears to be a maximum in both K_{Ic} and C_v at around 300-350°C. The series of steels containing combination of Al+Si behave in a similar manner and the variation in properties are shown in Fig. 19 to 23. There are two sets of data available for the steel to which 1.5Al+1.5Si was added. These were obtained for two different ingots using two different austenitization temperatures. In all the experimental steels except the one containing 1 and 2 pct Al, the peak in the fracture toughness curve occurred around a tempering temperature of 300°C. The steel containing additions of 1.5Al+1.5Si, austenitized at 1000°C and the one containing a 2Al+2Si addition, austenitized at 1100°C showed a sharp drop in

the K_{Ic} and C_v values following tempering beyond 350°C.

Fracture toughness data were also obtained from 4340+Si steels and are shown in Figs. 24 to 26. The 1 pct Si steel exhibited a peak in the toughness (both K_{Ic} and C_v) at a tempering temperature of 250°C following which the toughness dropped on tempering to temperatures upto 400°C. The 2 and 3 pct Si steels showed a maximum in both the K_{Ic} and C_v energy at about 300°C following which there was a sharp drop in the toughness.

The variation in fracture toughness in the as-quenched condition with different austenitization temperatures was measured for the 4340+1Al steel and the data is shown in Table VII. It was observed that K_{Ic} was the same for the 900°C and 1100°C austenitizing temperatures and there was a slight increase in K_{Ic} when the austenitizing temperature was raised to 1200°C. For the 4340+2Al+2Si steel K_{Ic} was measured for the 1100°C and 1200°C austenitizing temperatures in both the as-quenched, and quenched and tempered (300°C) condition. The results are shown in Table VII. The K_{Ic} values were essentially the same for the two different austenitizing temperatures.

D. Behavior of Retained Austenite

The amount of retained austenite present in the steels in the as-quenched, and quenched and tempered condition was obtained with the help of the magnetic saturation technique described in Appendix I. In some of the samples the amount of retained austenite was also measured with the x-ray technique.

The variation in the retained austenite content as a function of strain under tensile loading was also measured by the magnetic saturation technique and the results are plotted for the different steels in Figs. 27 to 33. The amount of retained austenite present in the tensile specimens at yield (0.2 pct plastic strain) and at 2 pct plastic strain are plotted along with the amount present before loading (0 pct strain). The following general observations were made. The amount of retained austenite present in the specimens decreased following tempering. In the steels containing lower amounts of Al ($< 2Al$) and Al+Si ($< .5Al+.5Si$), the amount of austenite present following tempering at 400°C was very low (around 1 pct) as compared to the steels containing higher amounts of Al and Al+Si. In all the steels the austenite present in the as-quenched condition was the most unstable with respect to stress and strain. This can be seen easily by comparing the difference in amounts of austenite present at 0 pct strain and at 0.2 pct or 2 pct strain. The stability of the austenite, with respect to stress or strain, appears to increase with tempering upto 250°C, beyond which the stability either remains the same or decreases depending on the composition of the steel.

E. Fracture Surface Morphology

The fracture surfaces of almost all the broken compact tension specimens were examined in a scanning electron microscope taking care to study the fracture area near the fatigue precrack/fast fracture interface. The fracture surfaces of some representative compositions are discussed.

In Fig. 34 are shown the fracture surfaces observed in the 4340+2Al steel. Figure 34(a) is for the as-quenched condition, and Figs. 34(b), (c) and (d) are for the quenched and tempered conditions for tempering temperatures of 250°, 325°, and 375°C, respectively. The as-quenched condition was characterized by mostly shallow dimples and quasi-cleavage, and some tearing. The fracture surface of the specimen tempered at 250°C showed evidence of mostly dimpled rupture (both shallow and deep dimples) and some quasi-cleavage. Higher magnification examination showed that many of the dimples appeared to be associated with particles. The specimens tempered at 325°C and 375°C exhibited fracture features similar to these in the specimen tempered at 250°C.

The fracture surfaces of the 4340+3Al steel are shown in Fig. 35. Figure 35(a) is from the as-quenched specimen and Figs. 35(b), (c), and (d) correspond to fracture surfaces obtained in specimens tempered at 300°C, 400°C, and 450°C respectively. The fracture features observed in the 3.0 pct Al steel were in general larger than those observed in the 4340+2Al steel. Fracture in the 4340+3Al steel was in general characterized by failure near prior austenite grain boundaries, and consisted of both shallow and deep dimples, tearing and quasi-cleavage. Shallow dimples appeared to be associated with failure regions in the immediate proximity of the grain boundaries and the deeper dimples with regions at greater distances from the boundaries. There were only small differences in the relative amounts of dimpled areas, quasi-cleavage and tearing between the as-quenched, and quenched and tempered specimens, although the dimples observed in the as-quenched specimens were mostly shallow.

Figure 36(a), (b), (c), (d) are fracture surfaces observed in the 4340+.5Al+.5Si steel in the as-quenched, quenched and tempered at 250°, 300°, and 400°C conditions. The as-quenched and 250°C temper specimens showed mainly shallow dimples associated with quasi-cleavage. However, for the 300°C temper, the fracture was mostly dimpled rupture. The specimen tempered at 400°C showed areas of dimpled rupture, quasi-cleavage and grain-boundary tearing.

The series of fractographs shown in Fig. 37(a), (b), (c) and (d) were observed in broken specimens of 4340+1.5Al+1.5Si steel austenitized at 950°C. The shallow dimples and quasi-cleavage areas characteristic of as-quenched specimens of the other steels were also observed for the as-quenched 4340+1.5Al+1.5Si steel. At a tempering temperature of 300°C the fracture becomes mostly dimpled rupture associated with some quasi-cleavage. The amount of dimpled rupture was lower for higher tempering temperatures; most of the dimples were shallow and the areas of quasi-cleavage increased as shown in Figs. 37(c) and (d). For the 4340+1.5Al+1.5Si steel austenitized at 1000°C, the fracture surfaces shown in Figs. 38(a), (b), (c), and (d) were observed. The fracture surface of the as-quenched specimen was characterized by unusually flat features, most of which were very shallow dimples and some quasi-cleavage facets. The 300°C tempered specimen showed mostly dimpled rupture with some large dimples. Tempering at 350°C increased the areas of quasi-cleavage and in a specimen given a 450°C temper, large areas of quasi-cleavage and evidence of intergranular fracture were observed as seen in Fig. 38(d).

The 4340+2Al+2Si steel exhibited fracture features shown in Fig. 39(a), (b), (c), and (d). The as-quenched specimen showed features similar to those observed in the as-quenched 4340+1.5Al+1.5Si steel austenitized at 1000°C, shown in Fig. 39(a). In addition, several deep troughs were in evidence. On tempering at 300 and 350°C, the fracture surface changed to dimpled rupture with mostly shallow dimples of various sizes, and some areas of quasi-cleavage. Following tempering at 450°C large areas of quasi-cleavage and troughs similar to those in the as-quenched specimen were observed as shown in Fig. 39(d).

The fracture surface features observed for the 4340+3Si steel, Fig. 40, were very similar to those observed in the 4340+1.5Al+1.5Si steel austenitized at 1000°C (Fig. 39). The 300°C tempered specimen exhibited mostly dimpled rupture and the 450°C tempered specimen showed mostly intergranular failure and quasi-cleavage facets.

Figure 41(a) and (b) show the fracture features observed in the 4340+2Al+2Si steel, austenitized at 1200°C, in the as-quenched, and quenched and tempered at 300°C condition respectively. The features in Fig. 41 appear to be similar to those observed in the as-quenched and 300°C tempered specimens of the same steel austenitized at 1100°C (Figs. 40(a) and (b)). However there is evidence of a greater amount of grain boundary tearing and dimple formation in the 1100°C austenitized specimens than in the 1200°C austenitized specimens, both for the as-quenched and the 300°C tempered conditions.

The fractographs obtained from as-quenched specimens of 4340+1Al steel austenitized at 900°, 1100° and 1200°C are shown in Fig. 42(a), (b), and (c) respectively. The general morphology of the fracture surfaces was similar and consisted of dimpled rupture and quasi-cleavage. In addition, several deep troughs were observed in the specimens austenitized at 1100°C and 1200°C.

F. Inclusion Characterization

The inclusions observed in some of the 4340+Al and 4340+Al+Si series of steels were characterized in terms of shape, size and chemistry with the help of the scanning electron microscope and an attached Energy Dispersive Analysis of X-rays (EDAX) unit. The chemical analysis of the inclusions was qualitative. Figures 43 through 47 illustrate the various types of inclusions observed along with the x-ray energy spectrums obtained from the inclusions. The inclusions shown in Figs. 43 through 45 are rich in aluminum. The inclusions shown in Fig. 46 give rise to x-ray peaks of Al, S, Mn and Fe and the inclusion shown in Fig. 47 shows x-ray peaks of the elements Fe, Mn, S, Al and Mg.

The inclusions vary from almost spherical, as observed in Figs. 46 and 47, to angular as in Fig. 43, and plate-like as observed in Fig. 45. The sizes of the inclusions were measured and were found to range from 0.5 μm to 6.8 μm. Almost all of the Mn containing inclusions were much smaller than the inclusions rich in Al and not containing Mn. All the inclusions that were observed on fracture surfaces were associated with large dimples.

It is apparent from the above observations that the addition of Al to the 4340 steel resulted in an increase in the inclusion content. Although most of the larger inclusions were found to have a high Al content, they could not be definitely identified as oxides or nitrides. The fairly large size and shape of the inclusions suggested that they could be oxides. Since all the inclusions observed, irrespective of their size and morphology, had large dimples associated with them, it is obvious that a part of the fracture in these steels is associated with initiation of failure at inclusion-matrix interfaces. In spite of this fact, the values of fracture toughness obtained at high levels of strength were superior to those found in the base 4340 steel. This indicates that the beneficial effect of Al in solution in the ferrite is greater than the detriment caused by the formation of oxide inclusions in the presence of Al in the melt.

G. Microstructural Characterization

1. Optical Metallography

The prior austenite grain-size and general microstructure of the experimental alloys were observed by optical metallography. The observed ASTM grain size numbers are shown in Table VIII for the steels used in this investigation. The microstructures observed in some representative steels are shown in Figs. 48 to 54. Some of the general features observed are discussed below.

Figure 48(a), (b), (c), and (d) are micrographs obtained from the 4340+2Al steel in the as-quenched and quenched and tempered at 250°,

350° and 375°C conditions respectively. The microstructure was mostly martensitic in the as-quenched condition with some ferrite retained from the austenitizing treatment. Ferrite was not observed in the dialtometer specimens which were previously used to determine the austenitizing temperatures. Carbide precipitation appeared to have occurred on tempering. The light etching ferrite can be been clearly in Figs. 48(b) and (d). The morphology and distribution of carbides are not clearly resolved in these micrographs.

Micrographs were obtained from the 4340+3Al steel for the as-quenched, and quenched and tempered at 300°, 400° and 450°C conditions and are shown in Fig. 49(a), (b), (c), and (d), respectively. The only difference between the optical micrographs observed for the 4340+2Al steel and the 4340+3Al steel is that, in the latter steels, larger features were present. There also appeared to be some plate martensite present in as-quenched 3Al steel as observed in Fig. 53(a).

The micrographs obtained from the 4340+1Al+1Si steel are shown in Figs. 50(a), (b), (c), and (d) for the as-quenched, and the quenched and tempered at 300°, 350°, and 400°C conditions respectively. Only martensitic structures were observed in this steel. The microstructures appear to be similar to the ones observed in the 4340+2Al steel.

Figures 51(a), (b), (c), and (d) are microstructures observed in 4340+1.5Al+1.5Si steel in the as-quenched, and quenched and tempered at 300°, 350° and 400°C conditions, respectively. Again, the general microstructure observed in this steel is similar to those observed in the 4340+2Al steel and were mostly martensitic. Some plate martensite is present in these structures.

Micrographs obtained from the 4340+2Al+2Si steel is shown in Figs. 52(a), (b), (c), and (d) which are for the steel in the as-quenched, and for the quenched and 350°, 400° and 450°C tempered conditions respectively. The microstructures consisted mostly of martensite, with very large plates of martensite being present. The large plates of martensite showed midribs. This was the only steel studied in which large amounts of martensite plates were observed. Figure 53(a) and (b) are microstructures observed in the same steel austenitized at a higher temperature (1200°C). Figure 57(a) is from the as-quenched specimen and 57(b) is from the 300°C tempered specimen. Both microstructures were similar to those observed in the steel austenitized at the lower temperature (1100°C).

The set of optical micrographs shown in Figs. 54(a), (b), (c), and (d) were obtained from specimens of 4340+3Si steel in the as-quenched, and quenched and tempered at 250°, 300° and 400°C conditions respectively. Some martensite plates were observed with most of the structure being martensitic as in the case of the other steels. There appeared to be some carbide precipitation in the specimens tempered at 300° and 400°C.

2. Transmission Electron Microscopy

The microstructures of two of the experimental steels were characterized at the electron optical level using transmission electron microscopy. Each steel was investigated in three heat-treated conditions, viz. the as-quenched, and the quenched and tempered at 300°C and 400°C conditions. The steels studied were 4340+3Al and

4340+1.5Al+1.5Si. The tempering temperature of 300°C was chosen because the highest level of toughness was obtained at this temperature and the temperature of 400°C was chosen arbitrarily. The as-quenched condition was characterized for comparison purposes.

Microstructure of 4340+3Al Steel

The typical microstructures observed in the as-quenched steel are shown in Figs. 55 and 56. Figure 55 shows a pair of bright and dark field micrographs. The dark field picture was obtained using the austenite reflection $(002)_\gamma$ shown in the diffraction pattern. The presence of austenite in the as-quenched steel was established by magnetic saturation measurements. Transmission electron microscopy showed that the austenite was present in the form of interlath films of varying thickness (200-800 Å). The other features observed in the bright field micrograph are typical dislocated martensite with some laths showing precipitates. Microtwinning was not present to any substantial degree. A higher magnification micrograph of the steel is shown in Fig. 56. The microstructure in this figure is characterized by a high dislocation density (A), some microtwinning (B), and wavy precipitates (C).

Transmission electron micrographs obtained from the steel tempered at 300°C showed additional precipitation of carbides and the same general features as in the as-quenched steels. Some austenite transformation occurred on tempering at 300°C as was established by magnetic measurements. Transmission microscopy showed that the untransformed austenite was present as interlath films. Figure 57

shows a bright field micrograph of a martensite lath in which the carbides had precipitated in two definite directions during tempering at 300°C. The diffraction pattern was indexed as shown in the figure and the approximate traces of the three low index directions, namely, $[011]_M$, $[0\bar{1}1]_M$ and $[002]_M$ are shown on the picture. In addition, three other directions are shown on the micrograph which correspond to the streak directions observed in the diffraction pattern. The directions marked 1 and 2 are perpendicular to the two sets of precipitates and the one marked 3 is parallel to one of the set of precipitates that are perpendicular to direction 2.

The micrographs in Fig. 58 were also obtained from a foil given the same heat treatment as above. The diffraction pattern was indexed as shown and the three directions observed, namely $[\bar{1}10]$, [002] and $[11\bar{2}]$ are shown on the micrograph. The dark field picture was obtained using the diffraction spot marked D.F. on the figure and shows reversal of contrast for one set of carbides.

An attempt was made to determine the habit plane of the observed carbides by trace analysis of Figs. 57 and 58. As shown in Fig. 59 it appeared that a possible habit plane is $(12\bar{2})$. However, since only two orientations of the foil were available, the validity of this habit plane could not be confirmed. The interesting fact remains that the observed carbides did not lie parallel or perpendicular to the ⟨100⟩ or ⟨112⟩ directions observed in Figs. 57 and 58, and neither do they appear to be close to {110}. A higher magnification picture of the area in Fig. 58 was taken and is shown in Fig. 60. The carbides observed were of different sizes; the largest carbide was about 5000Å

long and 225Å wide and the smallest one was about 530Å long and 25Å wide.

Figure 61 shows a typical microstructure observed in foils obtained from specimens tempered at 400°C. The foil orientation was close to $(100)_M$ and the diffraction pattern was indexed as shown in the figure. The maximum precipitate size observed was about 7400Å long and 90Å wide and the smallest one was 425Å long and 20Å wide in the steel tempered at 400°C. In the diffraction pattern of Fig. 61 streaks were observed which were perpendicular to the two precipitate sets as indicated in the bright field picture. One general observation which was made in the specimens tempered both at 300°C and 400°C was that precipitation was observed only in some laths and not in all the laths.

Microstructure of 4340+1.5Al+1.5Si Steel

The microstructural features observed in the as-quenched 4340+3Al steel was also present in the as-quenched 4340+1.5Al+1.5Si steel. As in the case of the Al modified steel, not much twinning in the martensite was observed and the laths were mostly dislocated. Figure 62 shows the general microstructure observed in the as-quenched 4340+1.5Al+1.5Si steel. The dark-field picture was obtained by using the $(20\bar{2})_\gamma$ diffraction spot and shows the presence of interlath films of austenite. The austenite exhibited the Kurdjumov-Sachs orientation relationship[39] with the martensite. Evidence of autotempering in the as-quenched steel is shown in Fig. 63. The laths in which no precipitation was observed was characterized by a high dislocation density.

The microstructural features present in the steel tempered at 300°C were the same as those in the as-quenched steel except additional carbide precipitation and growth was observed. Some austenite transformation occurred during tempering as established by magnetic measurements, and the remaining austenite was observed to be present in the form of interlath films. Figure 63 shows a lath in which carbides were observed for this heat treated condition. The diffraction pattern was indexed as shown in the figure. It is seen that the carbides do not lie parallel or perpendicular to any of the three low index martensite directions, namely, [002], $[0\bar{1}1]$, and $[0\bar{1}\bar{1}]$. The maximum size of the carbides in the steel tempered at 300°C appeared to be about 3750Å long and 60Å wide and the minimum was around 900Å and about 60Å wide.

Following tempering at 400°C, it was found that retained austenite was still present in the microstructure as established by magnetic measurements. The general microstructure obtained by transmission electron microscopy was similar to those of the steel tempered at 300°C. The maximum observed dimensions of the carbides in the steel tempered at 400°C appear to be about 3750Å long and about 110Å wide.

In both the 4340+3Al and the 4340+1.5Al+1.5Si steel specimens, the carbides did not produce a sufficient number of diffraction spots for unambigous identification of their crystal structure. In addition the carbides were not found to be on known habit planes for ε-carbide. Trace analysis of the carbides which appear to lie in two principal directions indicate that the traces are not in {112} (as expected, since not much twinning was observed), and neither do they

appear to be in {110}. A more detailed crystallographic study using symmetric orientations of the foil are needed to determine the exact habit planes of the observed carbides.

DISCUSSION

A. Effect of Composition on Phase Transformation

The modification of the AISI 4340 steel by additions of Al and Si led to substantial changes in the phase transformation behavior. This discussion will concentrate on the effect of these alloying elements on the phase boundaries of the $\alpha \rightleftharpoons \gamma$ transformations and on the tempering reactions in the experimental steels.

From the iron-rich section of the Fe-Al and Fe-Si phase diagrams it is observed that both the elements Al and Si lead to the formation of γ loops.[41,42] Thus both Al and Si are ferrite stabilizers, although Al has an fcc crystal structure and Si has a diamond cubic structure. The tendency for the formation of a body centered cubic structure when Al or Si is alloyed with iron has been explained by using the Engel-Brewer theory.[40] The extent to which each of these elements are soluble in the austenite phase are different; Al is soluble in γ to a maximum of about 0.95 wt% and Si is soluble to the extent of about 2.00 wt% in austenite.[41] Hence Al has a much stronger ferrite stabilizing tendency as compared with Si in binary Fe-Al and Fe-Si systems respectively. That this is indeed true in the more complex alloy systems based on the 4340 steel was made very clear from the present study. The 4340 steel containing about 3 pct. Al could be completely austenitized only at a temperature of about 1075°C whereas the steel containing 3.0 pct Si required a lower temperature (950°C) for complete austenitization. Limited studies of 4340 containing

4.0 pct. of either Al or Si indicated that with 4.0 pct. Al, it was not possible to austenitize in a single phase γ region at any temperature, whereas with the same steel containing 4.0 pct. Si, the steel could be austenitized in a single phase γ region. The steel containing 2.0 pct. Al+2.0 pct. Si could be austenitized in a single phase γ region at 1100°C which again indicated that Si was less effective than Al as a ferrite stabilizer.

The effect of alloying elements on the M_s temperature has been the subject of several investigations[43,44] and many empirical formulae have been derived to estimate the M_s temperature as a function of composition.[45-59] It has been reported by some investigators that Si decreases the M_s temperature,[46] and by others that Si has no effect on the M_s.[50] Aluminum is among the very few alloying elements which is reported to raise the M_s temperature.[43,46] In the present investigation it was found that when these elements were added to a commercial 4340 steel, Si lowered the M_s temperature slightly whereas Al raised the M_s temperature slightly. The effect of alloying elements on the M_s temperature is important because, as pointed out by several investigators,[16,51,52] it is necessary to keep the M_s temperature as high as possible to promote toughness. The mechanisms by which the toughness is improved (by raising the M_s) has been attributed to a number of factors, viz., reduction in distortion and transformation stresses,[51] reduction in the amount of twinned martensite plates,[53] and increased autotempering of martensite on quenching from the austenitization temperature.[51] The slight increase in M_s by the

addition of Al to the 4340 steel could thus have a beneficial effect on the toughness of the as-quenched steel. Whether this was indeed the result will be discussed in a later section.

The difference between the M_s temperature and the measured apparent M_f is shown in Table II. An empirical formula has been derived to relate the volume fraction of austenite transformed to martensite at temperatures below the M_s.[53] The equation reported can be written as

$$f = 1 - \exp - \{0.011(M_s - M_f)\}$$

where f is the volume fraction of martensite formed at a temperature M_x and M_s is the martensite start temperature. Using this equation to estimate the percentages of martensite formed corresponding to the (M_s-'M_f') temperature differences measured, it was found that the temperature measured as M_f actually corresponded to temperatures of M_{61} to M_{80}. Thus it is clear that the dilatometer technique used in this investigation did not give the real values of M_f, and this observation is also supported by the fact that another investigator[47] has reported that the difference between M_s and M_f should be around 200°C.

B. Tempering Behavior

A number of investigations on the tempering behavior of plain carbon[54-56] and alloy steels[15,57-60] have been conducted and many papers have been written on the process of tempering.[59-62] The variation in physical and mechanical properties with tempering in a wide variety of steels has been reported as well as the types of microstructures

observed in these steels.[51,63-66] A recent review by Speich and Leslie[61] has summarized the knowledge gained on the subject and the following paragraphs use their paper as a base for discussion.

a. Tempering in plain carbon steels. When a plain carbon steel, whose M_s is above room temperature, is quenched from the austenitization temperature there is a segregation of the carbon atoms to low energy sites such as dislocations and cell walls. This process has been termed as auto-tempering. When the carbon content of the steel is below 0.2 pct, it has been shown that, during the quench, almost 90 pct of the carbon atoms segregate to lattice defects.[61] In steels where the carbon content is greater than 0.2 pct, the low energy sites are saturated and the remaining C atoms remain in the interstitial lattice positions. On heating to temperatures around 100°C, the carbon atoms cluster and grow and some investigators have reported clusters along {001} planes.[67] On tempering the steels containing more than 0.2 pct C between temperatures of 100°C to 200°C, ε-carbide is precipitated with the habit plane of the carbide being $\{100\}_M$.[65,68] On tempering at higher temperatures, cementite precipitates. The habit plane of the cementite is $\{112\}_M$ when the martensite is twinned and $\{110\}_M$ when it is dislocated.[64,69-71] The morphology of the cementite is initially needle-like and changes to spheroids on tempering at temperatures beyond 400°C. Other intermediate carbides, such as Hägg carbide, have been reported[72] but have not been positively identified. When retained austenite is present in the steel, it decomposes in the temperature range of 200 to 300°C with the decomposition product being reported

as bainite.[75] Based on the observations, the process of tempering in plain carbon steels is comprised of the following:

1. Autotempering
2. Preprecipitation clustering
3. Precipitation of ε-carbide
4. Decomposition of retained austenite
5. Precipitation of cementite

The first two processes are generally not classified as parts of the different stages of tempering. The precipitation and growth of ε-carbide in the temperature range of 100-200°C is generally called the first stage of tempering. The second stage of tempering is usually associated with the decomposition of retained austenite. The precipitation of and growth of cementite is classified as the third stage of tempering. A fourth stage of tempering appears in the presence of sufficient amounts of carbide forming alloying elements in the steel. This stage will not be discussed further in this thesis because, for the steels studied in this investigation, the fourth stage is absent.

b. Influence of silicon on tempering. The presence of alloying elements such as Mn, Si, Cr, Al etc. can affect the different stages of tempering. A discussion of the effect of alloying elements on tempering will be long and complicated. A number of papers are available in the literature on this subject.[15,57-60,74,75] Hence only the effect of Si on the tempering process will be first presented, and then the results of the effect of Al on the tempering behavior of 4340 steels will be discussed.

The effect of Si on the tempering behavior of steels containing a wide range of carbon contents has been studied extensively.[13,14,17,18,57,76,77] It has been reported that Si drastically affects the kinetics, carbide composition and size, and consequently the mechanical properties of steels. Whether there is any definite effect on the autotempering process is not clear although a few investigators[17] have reported that it is possible that Si inhibits autotempering during quenching. Also there are no reports in the literature on the effect of Si on precipitation clustering which occurs in steels on tempering at temperatures upto 100°C. However, in one investigation, where the formation of a new silicon carbide has been reported, the existence of a pre-precipitation stage of clusters/zones, which are silicon rich, in the tempering range of 150-250°C has been indicated.[78-80] These clusters/zones are reported to grow into a silicon rich phase which has been called a τ-carbide by the investigators. In plain carbon steels the clusters which form at temperature below 100°C, grow at temperatures of 100°C and higher to eventually form ε-carbide, which constitutes the first stage of tempering.[61] Silicon affects the temperature range over which the first stage of tempering occurs. It has been reported that silicon has no effect on the temperature of the beginning of Stage I, but the end temperature of this stage is raised.[57] Thus Si essentially extends the temperature range of the first stage of tempering and appears to expand the range of temperatures in which ε-carbide is stable. It has also been reported that Si increases the

activation energy of the first stage of tempering in a high carbon steel (1.0 wt pct C).[58]

The effect of Si on the second stage of tempering consists essentially of raising the temperature range over which the retained austenite decomposes to a mixture of ferrite and carbide.[76]

Silicon influences the third stage of tempering dramatically. The studies on the effect of Si on the third stage have been easier and a number of papers are available in the literature on the subject.[13,60,76] By virtue of the effect of Si on stabilizing ε-carbide to higher temperatures the third stage of tempering occurs at higher temperatures.[60,76] The nucleation and growth of cementite not only occurs at higher temperatures but also the kinetics of the whole stage are slowed down. The temperature at which the third stage commences depends on the amounts of Si present in the steel and the kinetics of the third stage are mainly controlled by the diffusion of Si and not that of carbon in solution.

c. Hardness variation with tempering. All the effects mentioned above influence the mechanical properties of steels. The changes in mechanical properties, for example, hardness, are mostly due to changes in the s-ate of the matrix solid solution and the precipitation and growth of carbide phases.[61,62] Consider the hardness vs tempering curve for a 4340 steel shown in Fig. 11. On tempering to a temperature of about 100°C there is a slight increase in hardness. This slight increase in hardness is usually attributed to increased carbon segregation to dislocations and in a low carbon steel when all the

carbon has already segregated to dislocations there would effectively be no change in the hardness.[61] Beyond 100°C and upto about 200°C the hardness is observed to drop gradually. In this temperature range, ε-carbide is being precipitated. The matrix is thus loosing carbon from solid solution and is softening. At the same time, at the lower temperature range of ε-carbide precipitation, the dispersion of the carbide is fine and coherent and can thus lead to precipitation hardening. There is thus a balance between the loss in hardness due to carbon loss from solution and increase in hardness due to ε-carbide precipitation. Towards the higher temperature range, of the first stage of tempering, the growth of ε-carbide results in a hardness decrease, which, in combination with the softening due to further loss of carbon from solution, causes an increasing rate of softening in the steel. On tempering the steel beyond 200°C there is a drastic reduction in hardness. This is the range in which the precipitation and rapid growth of cementite occurs, and accounts for the large drop in hardness due to the depletion of the matrix of most of the carbon and the presence of coarse particles of cementite.[61] At higher tempering temperatures, the spheroidization of the carbides, accompanied by recovery and recrystallization, cause further decreases in the hardness. The 4340 type steels contain about 3.0 pct of retained austenite in the as-quenched state and this austenite decomposes on tempering beyond 200°C.[81] Apparently the decomposition has no visible effect on the hardness curve. Based on the discussion above it is feasible to use a tempering temperature vs. hardness curve as an indicator of the

different tempering reations in a steel.

d. Modification of tempering of 4340 steel by Al and Al+Si addition. Very little information is available in the literature on the effect of Al on tempering of steel. In the discussion section of one paper it was reported that higher tempering temperatures are required to obtain the third stage of tempering in the presence of 1.2 wt pct Al in a 4140 type of steel.[35] One other reference available in the literature reported that in low carbon (0.05C) iron alloys the presence of 1.5 pct of Al led to an increase in activation energy for the conversion of ε-carbide to cementite.[82] No kinetic studies of the effect of Al and Si on the tempering of 4340 steel were made in this investigation. The tempering behavior was mainly followed by measuring the hardness as a function of tempering temperature and also by studying the microstructure of the tempered steels by transmission electron microscopy. The results are discussed below.

1. Autotempering and Preprecipitation Clustering

From the as-quenched structures obtained in the 4340+3Al steel (Fig. 55) and the 4340+1.5Al+1.5Si steel (Fig. 63) it was clear that autotempering had taken place. Thus although other investigators have reported that addition of Si might lead in a reduction in autotempering,[17] the present study indicated that the 4340 steels modified with additions of Al and Al+Si did autotemper. The autotempering could have seen assisted by the fact that the M_s temperature

of the steels of the present investigation were relatively high (around 300°C). The presence of autotempering indicated that Al and combinations of Al+Si did not inhibit the initial stage of tempering in these steels.

2. Stage I Tempering

Hardness data were not available for tempering temperatures below 250°C for the experimental steels. Hence, although a continuous decrease in hardness with tempering temperature to 250°C is shown in Figs. 11 and 12, it was quite possible that on tempering at lower temperatures, there was an increase in hardness as in the case of the 4340 steel.

Beyond a tempering temperature of 250°C, the retardation of the tempering processes was clearly observed, with the retardation being more effective at the highest Al and Al+Si levels. From the discussion on the behavior of the hardness versus tempering temperature curve presented before, it appeared that the first stage of tempering was extended to higher tempering temperatures in the presence of Al and Al+Si. From Figs. 57 and 58 it is observed that precipitation of a carbide occurred in some laths in the 4340+3Al steel tempered at 300°C. The presence of streaks in the diffraction pattern in Fig. 57 suggested the presence of thin sheets of precipitate.[83] The type of carbide and its habit plane could not be identified due to an insufficient number of carbide reflections in the diffraction patterns.

Also the carbides were found not to lie parallel to the $\langle 100 \rangle_M$ (Fig. 57) or the $\langle 112 \rangle_M$ directions (Fig. 58) which also precluded the identification of the carbide by known habit plane relationships. In a normal medium carbon steel it has been found that ε-carbide precipitates on $\{100\}_M$ planes[65,68] and cementite on $\{110\}_M$ planes in dislocated martensite and on {112} planes in twinned martensite.[57,64,69-71] Thus, had either the ε-carbide or cementite conformed to these habit planes, they would have appeared as sets of carbide perpendicular to one another when the foil orientation was $(100)_M$ or $(110)_M$. A similar behavior was observed for the 4340+1.5Al+1.5Si steel tempered at 300°C (Figs. 63).

An interesting observation made from the electron micrographs obtained from the 300°C tempered specimens was the range of sizes of the carbides observed. For the 4340+3Al steel the length of the maximum dimension of the largest carbide observed was 5000Å and that observed in the 4340+1.5Al+1.5Si steel was 3750Å. In the work of Keh and Leslie[84] it was shown that in an Fe-0.45Mn-0.017C alloy, the carbides (Fe_3C) grew to a maximum dimension of 14,500Å on tempering at 200°C and in an Fe-3.34Si-0.018C alloys, the carbide (not Fe_3C) grew to a maximum dimension of 3000Å at 200°C and 8000Å at 300°C. Based on these observations it was proposed that Si inhibits the growth of carbides. Making a similar comparison, the present investigation showed that Al and combinations of Al+Si are effective inhibitors of carbide growth in 4340 steels. The exact mechanism by which carbide growth is inhibited will be discussed in a separate section.

From the hardness curves it appeared that for the 3Al and 1.5Al+1.5Si steels, the first stage of tempering extended to 400°C. The problem of precipitate identification is still present for this tempering temperature. Extensive precipitation was not observed at 400°C in either steel and only some of the martensite laths showed evidence of precipitation. Streaking in the diffraction patterns was still present (e.g. Fig. 61) which showed that some of the carbides were in the form of thin sheets which were either coherent with the matrix or at least partially coherent.[83] The maximum dimensions of carbides observed for both steels (7400Å for the 3Al steel and 3750 for the 1.5Al+1.5Si steel) indicated that the amount of alloying elements present were still effective in inhibiting growth. A comparison of these dimensions suggested that a combiantion of Al and Si was more effective in retarding growth than just Al.

Stage II Tempering

The Stage II tempering behavior of the experimental steels can be analysed by using Figs. 27-33 where the percentage of austenite are plotted as a function of tempering temperature. It is clear by a comparison of Figs. 27-29 that Al extends the temperature of Stage II to higher temperatures. The higher the amount of Al the higher was the temperature to which Stage II was extended. From the magnetic saturation measurements it is obvious that retained austenite was still present in the 4340+3Al steel following tempering even at 400°C.

A similar behavior was observed for the Al+Si steels, with steels containing the highest combination of Al+Si having the Stage II temperature extended to the highest tempering temperature. The appearance of a mild hardening peak for the 4340+1.5Al+1.5Si and 4340+2Al+2Si could not be satisfactorily explained by the decomposition of retained austenite. There have been reports in the literature that a silicon rich carbide called τ carbide is formed in steels containing 2-3 pct of Si which leads to the appearance of a peak in the hardness curve.[78-80] However the peaks were reported to appear at 300°C, whereas the mild hardness peaks observed in the steel used in this investigation were located at a tempering temperature of 400°C. Since identification of the carbide was not possible with the data available no definite conclusions can be made as to the nature of the carbides present in the experimental steels used in the present investigation.

Stage III Tempering

Rapid softening of all the steels was observed beyond a tempering temperature of 400°C. Thus is appeared that the stage III tempering reaction in the Al and Al+Si steels occurred at a tempering temperature of greater than 400°C. Whether the rapid softening was due to the precipitation and growth of cementite could not be confirmed since the electron microscopy was not conducted of steels tempered at temperatures higher than 400°C.

e. ε-Carbide Stabilization and inhibition of carbide growth.

It is known that silicon inhibits the tempering of martensite by expanding the range of temperature in which ε-carbide is stable and by slowing down the growth of carbides.[60] A number of reasons have been given for the expansion of the range of temperatures over which the ε-carbide is stabilized. In a study of the influence of alloying elements on the kinetics of the first stage of tempering, it was found that elements such as Si and Ni, which promote graphitization in steel, increase the activation energy Q for the first stage process.[58] The activation energy Q is associated with the interstitial diffusion of carbon atoms, and is affected by the presence of alloying elements through an interaction of the elements with carbon. This effect can be interpreted in terms of how the thermodynamic activity coefficient of carbon in solution in ferrite/martensite is influenced by alloying elements. Elements such as Si and Ni increase in the activity of carbon in both austenite and ferrite and thus raise the activity coefficient, which, in turn, increases the activation energy to a value which is characteristic of a higher carbon content austenite or ferrite.[58] Thus the presence of Si in solid solution in martensite would slow down the kinetics of the first stage of tempering and possibly extend it to a higher temperature. Also it has been reported that large amounts of Si can stay in solution in ε-carbide and this may cause it to be

stabilized to higher temperatures.[18] The increase of carbon activity by the presence of Si also explains the inhibition of the growth of cementite. When cementite is first formed it contains some silicon in its structure. As it grows the silicon is rejected from the particles so that there is a build up of silicon atoms at the carbide/matrix interfaces resulting in a raising of the activity of carbon at these locations. The carbon activity gradient is thus reversed near the carbide particle and silicon has to diffuse away from the interface before the carbon from the matrix can diffuse to the carbide. Thus the growth of the carbide is controlled by the silicon diffusion away from it, and hence, is slowed down. The above explanation has been proposed as the reason for the inhibition of cementite growth.[60] Whether a similar explanation can be proposed for the growth of either ε-carbide or any other carbide that may form is not clear at present. However, it is interesting to note that carbides formed at 200°C in an Fe-3.3Si-0.018C alloy, which could not be identified as cementite, did grow at a much slower rate than the cementite formed at the same temperature in an Fe-0.45Mn-0.017C alloy.[61]

Although it was pointed out in the previous section that the first stage of tempering of the 4340+Al and 4340+Al+Si steels extended to higher temperatures, it was not possible to identify the carbides observed. However, a comparison of the carbide sizes with those observed by Keh and Leslie[61,84] showed that the growth of carbides formed in the experimental steels did slow down. Since Al is known to promote graphitization in steel it would not be surprising to find that Al would increase the activity coefficient of carbon in ferrite.

There is a reference in the literature[85] where studies of internal friction in a low carbon steel containing Al, have suggested that the interaction of carbon with aluminum atoms lowers the mean diffusivity of carbon and inhibits its precipitation as a carbide. Obviously a further detailed study of this problem is warranted.

C. Influence of Composition on Tensile Properties

The influence of composition on the yield and tensile strengths of the modified steels used in this investigation are shown in Figs. 13 and 14. The higher the amount of Al present, the higher was the strength of the steel (Fig. 13). This difference in strength can be due to a combination of factors such as solid solution strengthening, and due to the retardation of tempering. At tempering temperatures beyond 300°C and especially at 400°C the difference in strengths were strongly affected by the tempering processes taking place in the steels. The effect showed up very clearly in both the ultimate and yield strength curves. Thus the presence of higher amounts of Al are very effective in retarding the tempering reactions to higher temperature and thereby increasing strength. A similar behavior was observed for the steels modified with Al+Si (Fig. 14) and the explanations used above apply. However, it is seen clearly that combined additions of Al+Si were more effective in obtaining higher strength levels than just Al additions to steel. The reason for this is that Si is a much more effective strengthener of ferrite than Al.[36] That this is true is shown clearly in Fig. 65-67 where the yield and tensile strengths

are plotted as a function of the tempering temperature of steels containing equivalent amounts of Al, Si and Al+Si. Since the atomic weights of Al and Si are about the same such a comparison is feasible. However, a little caution is required in comparing the strength levels of the steels containing 3.0 pct of alloying elements (Fig. 67) since the austenitization temperatures used were different which resulted in different grain sizes.

There are many theories of solid solution hardening and they have been discussed in a recent paper by Leslie[36] for the case of solid solution strengthening of iron by alloying elements. It has been concluded that most elements appear to strengthen iron through the size misfit parameter when present in small amounts. Aluminum is one of the elements which appears to strengthen iron in this manner. However, it has been pointed out that elements which contract the lattice of α iron such as Si, P and Be, produce a disproportionate amount of strengthening from relatively small size misfits. The reasons for this behavior are presently not known. The results obtained in this study also agreed with the observations above since the size difference between Si and Fe atoms is smaller than that between Al and Fe and yet, the strength levels are enhanced more by Si additions to 4340 steel than by Al additions. The part of the strengthening due just to solid solution hardening could not be separated from that due to a difference in tempering responses for the different steels and hence no comments can be made as to the quantitative effects of Al and Si on the solid solution strengthening of 4340 steel.

D. Correlation of Microstructure with Mechanical Properties

The mechanical properties of steel such as strength, ductility, and toughness are drastically affected by microstructural features, impurity levels, temperature, environment, state of stress and strain rate.[86] When the last five parameters are kept constant, then, the mechanical properties are chiefly controlled by the microstructural constituents present in the steel. Thus it is essential to be able to correlate microstructure with mechanical properties. Before discussing the specific microstructures found in the experimental alloys used in this investigation it would be fruitful to discuss in general the reported effects of microstructure on mechanical properties.

The effective correlation of microstructure with mechanical properties has been the subject of many investigations and numerous papers are available in the literature which have attempted to identify different features of microstructure which control properties.[86-92] Through the increased use of research techniques such as transmission and scanning electron microscopy impressive advances have been made in interrelating microstructure, strength, fracture toughness and the micromechanisms of fracture.[89,92] Recent work has attempted to classify microstructural features which are either beneficial or detrimental to strength and fracture toughness. Inspite of all these advances there is yet a volume of work to be done in this area especially because there is some controversy over the relative effects of microstructural constituents on mechanical properties such as K_{Ic} and C_v.

This investigation is concerned mainly with the martensitic structures encountered in medium carbon, medium alloy content, ultra high strength steels. Although it has been pointed out that at high levels of carbon (> 0.4 pct C), bainitic structures have potential for combinations of strength and toughness superior to those found in martensitic structures,[52] it appears at the present time that for medium and low carbon steels (< 0.4 pct C) martensitic structures are preferred. In general tempered dislocated martensite gives the best combination of strength, toughness, and ductility.[51,88] However, it is essential that tempering be done in the proper temperature range.

The microstructural features present in tempered martensitic structures which appear to be beneficial to strength and toughness are

(a) High dislocation density, and

(b) Fine, coherent carbide dispersions within the laths of martensite.

The microstructural features present in the martensitic structure which could be detrimental to strength and toughness are

(a) Presence of large amounts of twinned martensite plates, and

(b) Coarse non-coherent plate-like carbides, especially at lath boundaries.

In addition to these intrinsic features of tempered martensite, there are other features which could affect strength and toughness. These are

(a) Retained austenite

(b) Decomposition products of retained austenite on tempering

(c) Decomposition products of retained austenite on applicaton of load.

(d) Non metallic inclusions

(e) Impurity element segregations

(f) Grain size

(g) Pro-eutectoid ferrite

The retained austenite in quenched and tempered steels can be either beneficial or detrimental to toughness depending on its morphology and the transformation products which might form as a result of tempering[8] or the application of stress/strain.[93,94] When the retained austenite is present in the form of interlath films in tempered or as-quenched steels which are stable to stress/strain it appears to be beneficial to toughness.[52,87] However, the presence of large amounts of austenite can lower strength.[95] In addition, if the retained austenite transformed to a high carbon martensite on the application of load, it could lead to a deterioration of toughness.[93] If the retained austenite decomposes during tempering to give continuous networks of carbides there could be a loss in toughness.[8,81] Thus the role of retained austenite in quenched and tempered steels is subtle and should be considered with care. Non-metallic inclusions in steels are considered to be detrimental to toughness and it has been shown that fracture initiates at inclusion-matrix interfaces.[1,96,97] The presence of substantial amounts of impurity elements such as Sn, Sb, S, P is considered to be very detrimental to toughness since these elements have the tendency to segregate to sites such as grain boundaries and cause a reduction in toughness.[2,98]

There is a definite influence of grain size on strength - a smaller grain size favors higher strength.[99-101] However, its influence on toughness appears to be controversial. This is so, essentially because grain size can affect toughness both directly and indirectly. For example a controversy exists over the role that grian size has on fracture toughness (K_{Ic}) and impact toughness (C_v). A smaller grain size favors impact toughness and ductility.[102] However it has been reported that steels heat treated to higher austenitizing temperatures can have high values of fracture toughness K_{Ic} and slightly lower impact energies C_v as compared to steels austenitized at lower temperatures.[3,4] One of the reasons suggested for the improvement in K_{Ic} was, that due to the larger grain size, the chances of obtaining proeutectoid ferrite and upper bainite were reduced as a result of increased hardenability.[4] However, it has been reported that the observed higher fracture toughness (K_{Ic}) can be explained in terms of the influence of notch root radius on toughness.[7] Although this may explain the behavior for a particular class of steels, it is not clear whether this explanation can be generalized because, in addition to the change in grain size, other microstructural features could be present, which can improve fracture toughness (K_{Ic}) and not improve impact energy (C_v). There is no apriori reason why microstructural features which improve K_{Ic} should also improve C_v. The fact remains that a large grain size is detrimental to impact energy and ductility, and this is not controversial. A smaller grain size is also preferred to allow a larger grain boundary area for impurity segregation so that the effect of impurities can be

minimized.[7,103]

Proeutectoid ferrite can be present in quenched and tempered steels as a result of two different reasons. The ferrite can form at prior austenite grain boundaries on quenching the steel from the austenitization temperature due to insufficient hardenability. The ferrite can also be present in the microstructure as islands, if the austenitization temperature is such that the steel is in a ferrite plus austenite region or a ferrite plus austenite plus carbide region at the solution treatment temperature. In either case its presence in the microstructure is considered undesirable because it is a soft phase and thus lowers strength and also at the same time lowers toughness because ferrite tears easily and leads to early fracture.[86]

The presence of other decomposition products of austenite, such as upper bainite or pearlite, due to lack of sufficient hardenability, is undesirable because they cause a reduction in strength and toughness.[53,86] Even lower bainite in the structure is not desired because it causes a reduction in strength and does not improve the toughness of tempered martensite.[104]

Based on the discussion presented above an attempt was made to evaluate the role of microstructure on the mechanical properties of the modified steels investigated. The following generalized discussion was based on the transmission electron microscopy conducted on two representative alloys, viz., the 4340+3Al and 4340+1.5Al+1.5Si steels.

As-Quenched Steels

The as-quenched structures of the experimental steels was characterized by the following microstructural features

(a) Mostly dislocated martensite

(b) Retained austenite films at lath boundaries

(c) Autotempered carbides in some laths.

(d) In some of the higher alloyed steels the presence of blocky ferrite (~2%) was observed even though the dilatometry specimens had failed to show ferrite in the microstructure following solution treating at the temperature used. An example is shown in Fig. 68 which is an optical micrograph of the 4340+1.5Al+1.5Si steel in the as-quenched condition following austenitization at 950°C.

The microstructure of the as-quenched 4340 austenitized at 870°C has been characterized[81] as being predominantly martensitic with very little retained austenite present. There were plates of internally twinned martensite present along with autotempered laths. Thus the difference in microstructure between the base 4340 steel and the modified alloys appeared to be the presence of twinned martensite plates and the absence of substantial amounts of retained austenite films in the 4340 steel. Whether this difference in microstructure can account for the observed difference in properties is not easy to assess. In general, the yield strength of almost all the modified alloys was about the same or slightly higher than that of the 4340 steel and yet the fracture toughness was either comparable or higher than that of 4340. However, the ultimate strength of the as-quenched

4340 steel is higher than or comparable to those of the modified steels. The higher ultimate strength of the 4340 could be due to slight changes in composition and less retained austenite in the microstructure.

The observed lower yield strengths obtained for the modified steels in the as-quenched condition can be rationalized if the behavior of the retained austenite under stress/strain is examined. From Figs. 27 to 33 it is seen that the retained austenite present in the as-quenched steels was unstable to stress and a substantial portion of the retained austenite transformed before yield. This factor, in addition to the fact that retained austenite was present, would account for the lower yield strengths of the as-quenched experimental steels.[105] Recently it was reported that high toughness with high strength is possible in an as-quenched steel because of the presence of retained austenite films and autotempering.[52]

Based on these observations it can tentatively be concluded that the better toughness of some of the modified steels as compared to the base 4340 steel could be due, in part, to the presence of retained austenite films, absence of extensive amounts of twinned martensite, and autotempering.

Steels Tempered at 300°C

The microstructure of the modified steels tempered at 300°C was characterized by

(a) Mostly dislocated martensite

(b) Retained austenite films at laths boundaries,

(c) Carbide precipitation in some laths, and

(d) Any ferrite present from the austenitization treatment in some steels.

As in the case of the as-quenched microstructures not much internal twinning was observed. The retained austenite films present at the lath boundaries in the quenched and tempered at 300°C steels behave in an entirely different manner than the austenite present in the as-quenched structure when subjected to stress/strain as shown in Figs. 27 to 33. It was seen that, following tempering at 300°C, the austenite was stabilized with respect to stress and strain. The carbides which were observed were comparatively fine as discussed in a previous section. The comparison of this microstructure with that found in a 4340 steel tempered at 300°C is interesting. It has been reported[81] that in a 4340 steel tempered at 280°C, cementite was the predominant carbide detected. The little retained austenite present decomposed completely on tempering at 280°C and cementite precipitation was observed both at lath boundaries and within the laths and plates of martensite. Discrete platelets of cementite were also observed at prior austenite boundaries but no continuous networks of carbide were observed at boundaries. The difference in mechanical properties, for example, between the 4340+3Al steel or the 4340+1.5Al+1.5Si steel and the 4340 following tempering at 300°C can be explained on the basis of the differing microstructure. Both the yield and ultimate strengths of the modified alloys were higher than those of the 4340 and yet the fracture toughness of the modified alloys was much higher than that of 4340. The loss in strength of the 4340 at 300°C is mainly due to the extensive precipitation of cementite and this feature has already been discussed in detail in the section on tempering. The modified

alloys retained their strength due to less carbide precipitation and a fine distribution of the precipitated carbide. Although there is no loss in K_{Ic} observed for the 4340 steel in this tempering temperature range, the value of K_{Ic} does not appear to change much. It has been pointed out that the embrittlement occurring in the 4340 steel in this tempering temperature region is clearly seen by studying the charpy impact toughness at temperatures below the room temperature.[106] In the experimental alloys it appeared that the highest value of yield strength was obtained in this temperature range along with a peak in the K_{Ic} and C_v energy values.

The appearance of embrittlement in 4340 can probably be attributed to the presence of carbide particles at lath boundaries. This type of precipitation was not observed in the modified Al or Al+Si alloy at 300°C and so embrittlement was not observed. In the place of interlath precipitation of carbides there was the presence of fairly stable austenite films in the modified alloy and this could be an additional factor for the higher toughness in these alloys.

Steels Tempered at 400°C

The Al and Al+Si steels tempered at 400°C showed basically the same microstructure as that observed at 300°C except for the following important differences

(a) Precipitation of carbides had occurred in more laths and the carbides were larger.

(b) There was not as much retained austenite observed.

The mechanical properties of the 4340+3Al and 4340+1.5Al+1.5Si

steels are discussed here. From Fig. 18 it is seen that for the 3Al steel, following tempering at 400°C, the yield strength, K_{Ic} and C_v notch impact energy values peak to a maximum. For the 1.5Al+1.5Si steel (Figs. 21 and 22) there were drops in ultimate strength and K_{Ic} but the yield strength remained high. From Fig. 29 it is observed that the retained austenite in the 3Al steel was stable with respect to stress and strain. For the 1.5Al+1.5Si steel, the retained austenite was less stable as compared to the 3Al steel. The embrittlement is much more severe in the case of the 1.5Al+1.5Si steel austenitized at 1000°C (Fig. 22) as compared to the same steel austenitized at 950°C. It appeared that the larger prior austenite size obtained following austenitization at 1000°C could be an additional factor responsible for the more severe embrittlement. Some investigators have reported that one of the factors responsible for tempered martensite embrittlement is the segregation of impurity elements to grain boundaries.[2,61] Since the prior austenite grain size was larger in the steel austenitized at 1000°C there was less grain boundary area available for the impurity elements to distribute themselves and hence this could also partly account for the observed severity in loss of toughness. At the same time it should be pointed that the 3Al steel was austenitized at 1100°C and had a much larger grain size than the 1.5Al+1.5Si steel austenitized at 1000°C and yet the Al steel does not appear to have suffered the embrittlement phenomenon at this tempering temperature. No microstructural data of the 4340 steel tempered at 400°C was available. However, the fracture toughness of the steel goes up and the strength goes down.

Although no transmission electron microstructural study was done of the modified alloys tempered at temperatures beyond 400°C, it is to be expected that the rapid drop in strength observed is due to precipitation and growth of cementite. No fracture-toughness data was available for the modified alloys tempered at temperatures higher than 450°C.

It thus appears that for the 4340 steels modified with Al and Al+Si the microstructural features which are required for optimum combination of strength and toughness in the quenched and tempered heat treated condition are:

(1) Fine dispersions of carbides in dislocated laths of martensite

(2) Retained austenite films of the right stability to stress and strain at lath boundaries.

(3) Smaller grain sizes.

The presence of features such as islands of ferrite, retained austenite which is not stable to stress and strain, and coarse lath boundary carbides are not desirable.

Fracture of Modified Steels

A study of the fracture surface of broken specimens provides a means for studying the different fracture modes encountered in steels. A comprehensive study of fracture surfaces encountered in ultra high strength 4340 and 300-M steels was reported by Bucher et al.[92] and the following discussion draws on this paper. Since all the fracture testing in the present investigation was conducted at room temperature,

the discussion with regards to the different modes of fracture observed is necessarily restricted to failure of the modified alloys at room temperature. In addition, the fracture surface appearance was characterized only near the fatigue and fast fracture interfaces and hence the fractographs are representative of the fracture modes associated with the initiation of unstable fracture in these steels.

Fracture mechanisms in quenched and tempered steels, can be characterized in general as below:

(a) Cleavage

(b) Quasi-Cleavage

(c) Microvoid coalescence resulting in dimples.

(d) Tearing

(e) Intergranular failure, and

(f) Mixture of above.

The terms used to describe the surface appearance resulting from mechanisms mentioned above have been defined elsewhere.[92,107] In the present investigation, fracture surface morphology was studied as a function of tempering temperature and composition, with the maximum tempering temperature being 450°C. Only the fracture surface of the broken compact tension specimens were studied and hence the conclusions are restricted to fracture under the low strain rates encountered in K_{Ic} tests. All the fracture surface appearances described by Bucher et al.[92] were observed on broken Charpy specimens. Hence a direct comparison of surfaces obtained in a K_{Ic} test, as obtained in the present investigation, with that obtained from surfaces obtained from

Charpy tests should be made with caution.

It was observed from the work of Bucher et al. that the fracture surface of as-quenched AISI 4340 steel was characterized mainly by "cleavage and some intergranular failure." From the work of Wood et al. it was observed that the fracture surface of broken as-quenched K_{Ic} specimens of AISI 4340 (austenitized at 870°C and oil quenched) was charcterized by "quasi-cleavage with pockets of ductile rupture." On tempering at about 200°C, Bucher et al. observed mainly "dimpled rupture and some cleavage". On tempering at temperatures between 230 and about 400°C, it was found that "intergranular fracture at prior austenite boundaries" was present and was attributed to the occurrence of tempered martensite embrittlement. On tempering beyond 400°C mostly dimpled rupture surfaces were observed. A similar behavior was observed for 300-M steel except for the fact that the tempered martensite embrittlement features were observed only on tempering in the temperature range of about 390°C to 600°C.

The fracture surface appearance observed in the experimental steels (as described in the section on results) indicated that for all the steels, whether they were in the as-quenched or quenched and tempered condition, the operative fracture mode was complex. Features such as dimples (shallow and deep), quasi-cleavage, and tearing were observed in almost all the as-quenched specimens and also some mode of intergranular failure was observed in some cases (4340+3Al steel). In most of the larger dimples inclusions were observed. On tempering to temperatures to 300°C, not much indication of prior austenite

boundary failure was observed and mostly dimpled rupture along with some quasi-cleavage was observed. In almost all the steels, the dimples observed following tempering at 300°C were deeper as compared to the ones observed at higher or lower tempering temperatures. Depending on the composition, tempering at temperatures between 300 and 400°C resulted in a change mainly in the relative amounts of dimpled and quasi-cleavage areas. In the steels containing higher amounts of Al and Si (especially for the steels austenitized at higher temperatures) tempering at temperatures greater than 400°C resulted in mainly intergranular and quasi-cleavage failure features.

It appeared that the failure mechanism in the modified steels was, in general, similar to that observed in the 4340 steel, except for the fact that the features characterizing tempered martensite embrittlement occurred at higher tempering temperatures, as was observed for 300-M steel. The appearance of brittle fracture features such as cleavage and intergranular failure was found to correlate with the fracture toughness trough observed in the modified steels. In the steels containing higher combinations of Al and Si for which the toughness trough observed at the higher tempering temperatures was severe, the main fracture features which appeared to characterize the embrittlement were intergranular failure and transgranular cleavage.

It has been reported that some of the factors responsible for the occurrence of tempered martensite embrittlement can be attributed to the precipitation of cementite films along martensite plates at austenite boundaries,[63] thin ferrite films along prior austenite boundaries[106,108] and the segregation of impurity elements to prior

austenite boundaries.[16] More recently it has been suggested that the embrittlement is associated with a critical carbide morphology present when Fe_3C first forms and may be caused by the precipitation of film-like carbides on grain boundaries and subboundaries.[61] The present investigation showed that the third stage of tempering is delayed by the addition of Al and Si to 4340 steel, and that tempered martensite embrittlement (as indicated by a decrease in K_{Ic} or C_v) occurred following tempering at higher temperatures in the modified 4340 steels. The evidence appeared to support the proposal that the embrittlement phenomenon was related to the precipitation of carbides in some way. Whether the phenomenon could be aggravated by the presence of impurity elements was not clear from this investigation.

Comparison of Mechanical Properties of 4340+1.5Al+1.5Si with Those of Commercial Steels

A comparison of the mechanical properties of the 4340+1.5Al+1.5Si, AISI 4340 and 300-M steels is shown in Figs. 69 and 70. From Fig. 69 it is observed that the modified steel, on tempering at 300°C, has a yield strength as high as the ultimate strength of 4340 and yet possessed a K_{Ic} which was higher than that of 4340 by about 33 pct. However, on tempering the modified steel beyond 350°C, the appearance of tempered martensite embrittlement resulted in it having K_{Ic} values lower than that of AISI 4340. The strength of the modified steel was still high at a tempering temperature of 400°C, compared to that of 4340 steel.

The comparison of the properties of 4340+1.5Al+1.5Si and 300-M (Fig. 70) showed that, following tempering at 300°C, the modified steel not only had yield and ultimate strengths comparable to those of 300-M, but also, it had a K_{Ic} value which was higher than that of 300-M by about 33 pct. It thus appeared that there was a beneficial effect of Al addition to 4340 steel.

The improvement in strength and toughness of the modified steel, following tempering at 300°C, over that of AISI 4340 can be explained in terms of the behavior of the microstructural features such as stability of retained austenite and size and coherency of carbides. This has already been discussed in detail in the section on correlation of microstructure with mechanical properties. However, the reason for improvement in toughness over that of the 300-M steel following tempering at 300°C needs more discussion. Figure 71 shows the behavior of retained austenite in quenched and tempered 300-M obtained from work done recently by Horn.[94] The retained austenite behaves in a manner similar to that found in the 4340+Al+Si steels. However, no microstructural data on the size of carbides in the 300-M was available and a comparison of coherency and growth rates of carbides could not be made. Hence, at the present time there is no conclusive evidence available to explain the improvement in toughness observed in the 4340+1.5Al+1.5Si steel over that of 300-M. It should be noted that although the yield strengths of the two steels were similar, the ultimate strength of the 300-M was slightly higher and could be a factor in explaining the difference in toughness.

In Fig. 72 K_{Ic} versus yield strength bands are shown for AISI 4340, 300-M, 18NiCoMo maraging alloys and the 4340+Al, 4340+Al+Si steels in the quenched and tempered condition. The steels containing higher amounts of Al and Si are located at the higher strength levels. The comparison in Fig. 72 indicates that although the modified steels used in this investigation possessed a better combination of yield strength and toughness than either 4340 of 300-M, they did not have properties as good as those of the maraging steels. However, if the fracture toughness of the same steels is plotted as a function of ultimate strength as shown in Fig. 73, the location of the band of the modified steels overlaps with that for the maraging steels at high strength levels. This is because the maraging steels have a low work hardening rate and hence have similar yield and ultimate strengths, whereas the modified 4340 steels have significantly higher ultimate strengths than their yield strengths.

Thus, this investigation has shown that it is possible to modify existing steels with inexpensive alloying modifications and obtain better mechanical properties.

SUMMARY AND CONCLUSIONS

The following conclusions were drawn from this investigation.

1. The addition of aluminum and combinations of aluminum and silicon to AISI 4340 steel resulted in an increase in the temperature needed for complete austenitization. Complete austenitization was not possible when the amount of aluminum added exceeded a critical amount which depended on the carbon content of the steel.

2. The M_s temperature of AISI 4340 steel was raised slightly by the addition of aluminum.

3. The addition of aluminum and combinations of aluminum and silicon to AISI 4340 affected the reactions which took place on tempering. These effects were

   (a) The first stage of tempering appeared to extend to higher tempering temperatures.

   (b) The temperature for the second stage of tempering was also raised.

   (c) The third stage of tempering appeared to occur in the modified 4340 steels (containing higher amounts of aluminum and silicon) at temperatures greater than about 400°C.

4. In addition to the above conclusions, the following observations were made based on the electron-microstructural study of the 4340+3Al and 4340+1.5Al+1.5Si steels.

   (a) Autotempering occurred in the as-quenched modified 4340 steels.

   (b) The carbides formed on tempering at 300°C and 400°C appeared to precipitate in two principal directions.

(c) Trace analysis indicated that the traces of the observed carbides do not lie in {100}, {112} and also did not appear to lie in {110} planes.

(d) The presence of streaking in the diffraction patterns obtained from steels tempered at temperatures as high as 400°C indicated that the carbides were in the form of thin sheets.

(e) Aluminum and combinations of aluminum and silicon appear to be effective inhibitors of carbide growth in 4340 steel, and the combined additions appear to be more effective in retarding growth of carbides than aluminum additions alone.

5. The effects of aluminum and aluminum plus silicon additions on the mechanical behavior of 4340 steel are summarized below.

(a) The alloying additions retarded the softening which normally occurs on tempering 4340 steel

(b) Tempering the modified steels at temperatures to 300-350°C appeared to stabilize the retained austenite to stress/strain.

(c) Combined additions of aluminum and silicon were more effective in obtaining higher strength levels than just aluminum additions in equivelent amounts.

(d) The addition of silicon alone to steel led to greater strengthening than the addition of equivalent amounts of either aluminum or combinations of aluminum plus silicon.

(e) The "500°F embrittlement" phenomenon (also known as tempered martensite embrittlement) occurs at higher tempering temperatures in the modified 4340 steels.

(f) It was possible to improve both the strength and toughness of 4340 steel by the addition of appropriate amounts of aluminum or aluminum plus silicon.

(g) Strength levels comparable to those of 300-M steel following tempering at 300°C were obtained in a modified 4340 steel containing combinations of aluminum and silicon in conjunction with a fracture toughness (K_{Ic}) which was significantly higher than that of 300-M.

6. The microstructural study of the modified steels led to the following conclusions

(a) The microstructural features which appeared to result in an optimum combination of strength and toughness in the modified 4340 steels were

(i) Fine dispersions of carbides in dislocated martensite

(ii) Retained austenite films at lath boundaries of the right stability to stress/strain.

(iii) Smaller piror austenite grain sizes.

(b) There appeared to be some evidence to support the proposal that the tempered martensite embrittlement phenomenon is related to the precipitation of carbides at lath boundaries.

7. A study of the fracture surfaces of the modified alloys indicated that

(a) The initiation of fast fracture in the modified 4340 steels was associated with complex fracture modes for all the heat treat conditions investigated.

(b) Brittle fracture features such as cleavage and intergranular failure correlated well with the fracture toughness troughs observed on tempering at high temperatures.

(c) The modified alloys contained inclusions which were rich in aluminum in addition to the normal sulfide inclusions found in this class of steels. The large dimples associated with these inclusions suggested that a part of the fracture initiation process was associated with the failure of matrix-inclusion interfaces.

ACKNOWLEDGEMENTS

The author would like to express his deep gratitude to Professors Victor F. Zackay and Earl R. Parker for their continued support and guidance throughout the course of this investigation. He would also like to extend his appreciation to Drs. Ron Horn, Dilip Bhandarkar, Gabriel Kohn, and Rob Ritchie not only for many valuable discussions, but also for their friendship over the past few years.

The author wishes to thank Professors Ian Finnie and G. Thomas for reviewing the manuscript.

Special thanks are extended to Yoshi Mishima, David Curtiss, Steve Bandel, and Eric Dittmar whose help during this study was very valuable. The invaluable technical assistance provided by the support staff of the Materials and Molecular Research Division is gratefully acknowledged; thanks are due in particular to Brian Pope (alloy preparation), John Holthius (alloy processing), Ed Edwards, Julian Patenaude and Duane Newhart (machining), Don Krieger (mechanical testing), Richard Lindberg (scanning electron microscopy), Lee Johnson (metallography), Jim Severns (electronics), Glenn Baum (vacuum systems), Carolyn Gosnell (electron microscopy), Sandy Stewart and Paul Stagnaro (purchasing), Gloria Pelatowski (preparation of line drawings), and Alice Ramirez (manuscript preparation).

This work was supported by the United States Energy Research and Development Administration through the Materials and Molecular Research Division of the Lawrence Berkeley Laboratory.

APPENDIX I

Determination of the Level of Retained Austenite in Thin Tensile Specimens Using a Magnetic Saturation Technique

The amount of retained austenite present in thin (0.05 in.) tensile specimens before applying load, and during tensile straining can be determined using a magnetic saturation technique used previously in another investigation.[110] A sketch of the system is shown in Fig. 7. The experimental set-up essentially consists of a permeameter containing two coils, placed between the poles of an electromagnet, to measure flux changes in a specimen. The whole device is attached to an Instron testing system. One of the coils encloses the specimen guage-length and is bucked against the other coil to eliminate the effect of the applied field and allow the measurement of the flux change in the specimen, which depends upon the amount of magnetic phase present. The field is applied by passing current through the large electromagnet making sure that the value of the field is enough to saturate the specimen. In this way, the voltage corresponding to the integrated signal from the coil containing the specimen is measured and is used for determining the amount of retained austenite.

In order to determine accurately small amounts of austenite it is essential to calibrate the measuring system. One of the steps in calibration involves the measurement of the magnetic saturation induction of a material whose reported value is known. In the present investigation a pure iron standard was used and the saturation induction was determined using the formula

$$B_s = \frac{1}{2NA} \times \Delta\phi_{SLFS} \times \frac{V}{V_o}$$

where

B_s = saturation induction

N = Number of turns of coil

A = Cross sectional area of specimen

$\Delta\phi_{SLFS}$ = Flux change due to square loop flux standard

V_o = Voltage corresponding to the square loop flux standard and

V = Voltage corresponding to the integrated signal from the coil containing the specimen.

The saturation induction values measured for pure iron was 21,300 gauss, which agreed well with the value reported in the literature.[111]

Since the saturation induction is a function of the composition, it is necessary to prepare standards made of the same composition as the steels in which the amount of austenite is to be determined. This was done by austenitizing specimens of each composition, quenching and tempering at a high enough temperature (650°C) to ensure that no austenite was present and using these specimens as standards. The amount of retained austenite could be determined using the formula

$$\text{Pct. Austenite} = \left(1 - \frac{V_{spec.}}{V_{std.}} \times \frac{A_{std.}}{A_{spec.}}\right) \times 100$$

where $V_{spec.}$ = voltage corresponding to specimen in coil

$V_{std.}$ = voltage corresponding to standard in coil

$A_{std.}$ = cross sectional area of standard

$A_{spec.}$ = cross sectional area of specimen.

The above formula allowed determination of retained austenite in specimens before loading. Following the application of load and plastic strain in the specimen, the amount of retained austenite was calculated using the formula

$$\text{Pct Austenite} = \left(1 - \frac{V_{spec.}}{V_{std.}} \times \frac{A_{std.}}{A_{spec.}} \times \frac{1}{\Delta \ell}\right) \times 100$$

where $\Delta \ell$ is the change in length of specimen at a particular plastic strain. It was possible to use this formula since it was assumed that (1) there was no change in volume on plastic deformation of the specimen, and (2) Elastic Strain, which are very small, can be ignored.

REFERENCES

1. T. B. Cox and J. R. Low, Jr., Met. Trans. 5, 1457 (1974).

2. J. M. Capus and G. Mayer, Metallurgia 62, 133 (1960).

3. W. E. Wood, E. R. Parker and V. F. Zackay, Lawrence Berkeley Laboratory Report, LBL-1474, 1973.

4. G. Y. Lai, W. E. Wood, R. A. Clark, V. F. Zackay and E. R. Parker, Met. Trans. 5, 1663 (1974).

5. D. Dulieu, Discussion to paper by V. F. Zackay, E. R. Parker and W. E. Wood, The Microstructure and Design of Alloys, Proc. Third Intl. Conf. on the strength of Metals and Alloys, Inst. of Metals, London 2, 383 (1973).

6. W. G. Ferguson, N. E. Clark and B. R. Watson, Metals Technology, p. 208, April 1976.

7. R. O. Ritchie, B. Francis and W. L. Server, Met. Trans. A 7A, 831 (1976).

8. J. M. McMahon and G. Thomas, Microstructure and Design of Alloys, Proc. Third Intl. Conf. on Strength of Metals and Alloys, Inst. of Metals, London 1, 180 (1973).

9. R. A. Clark and G. Thomas, Met. Trans. A 6A, 969 (1975).

10. E. A. Wylie, M. S. Thesis, LBL-4574, Lawrence Berkeley Laboratory, Berkeley, California.

11. J. W. Sands and O. O. Miller, Materials and Methods 43(3), 94 (1956).

12. R. T. Ault, G. M. Waid and R. B. Bertolo, Development of an Improved Ultra-High Strength Steel for Forged Aircraft Components, AFML-TR-71-27, Feb. 1971, Air Force Materials Laboratory, Wright-Patterson Air Force Base, Ohio.

13. A. G. Allten and P. Payson, Trans. ASM 45, 498 (1953).

14. C. H. Shih, B. L. Averbach and Morris Cohen, Trans. ASM 48, 86 (1956).

15. E. C. Bain and H. W. Paxton, Alloying Elements in Steel, American Society for Metals, Ohio, 1966, p. 182.

16. K. J. Irvine, JISI 200, 820 (1962).

17. C. J. Altstetter, Morris Cohen and B. L. Averbach, Trans. ASM 55, 287 (1962).

18. B. G. Reisdorf, Trans. Met. Soc. AIME 227, 1334 (1963).

19. A. M. Hall, "Introduction to Today's Ultrahigh-Strength Structural Steels," ASTM Spec. Tech. Publ. 498, American Society for Testing and Materials, Philadelphia.

20. A. M. Hall, Nickel in Iron and Steel, John Wiley and Sons, New York, 1954, p. 595.

21. E. A. Steigerwald, Eng. Frac. Mech. 1, 473 (1969).

22. E. B. Kula and A. A. Anctil, J. of Mat. 4(4), 817 (1969).

23. F. L. Carr and F. R. Larson, J. of Mat. 4(4), 865 (1969).

24. C. E. Sims, Trans. AIME 162, 734 (1945).

25. H. W. McQuaid, Trans. ASM 23, 797 (1935).

26. D. Hall and G. H. J. Bennett, JISI 205, 309 (1967).

27. A. S. Kenneford, V. E. Rance and S. Turner, JISI 205, 665 (1967).

28. K. R. Kinsman and H. I. Aaronson, Met. Trans. 4, 959 (1973).

29. R. Oshima and C. M. Wayman, Met. Trans. 3, 2163 (1972).

30. Aluminum in Iron and Steel, S. L. Case and K. R. Van Horn, Eds., John Wiley & Sons, Inc., New York (1953).

31. J. A. Duma, Trans. ASM 27, 149 (1939).

32. E. R. Morgan and V. F. Zackay, Met. Prog. 68(4), 126 (1955).

33. W. Justusson, V. F. Zackay and E. R. Morgan, Trans. ASM 49, 905 (1957).

34. K. Nishida, Trans. ISIJ 8, 156 (1968).

35. A. G. Alten, Discussion of paper by W. S. Owen, Trans. ASM 46, 828 (1954).

36. W. C. Leslie, Met. Trans. 3, 5 (1972).

37. R. L. Miller, Trans. ASM 57, 892 (1964).

38. J. Dumin and R. A. Ridal, JISI 206, 60 (1968).

39. G. Kurdjumov and G. Sachs, Z. Physik 64, 325 (1930).

40. L. Brewer, Private Communication.

41. P. Rocquet, G. Jegaden and J. C. Petit, JISI 205, 437 (1967).

42. Metals Handbook, 8, T. Lyman, Ed., American Society for Metals, Ohio, 1973, p. 306.

43. A. Zyuzin, V. Sadovski and S. Baranchuk, Metallurg. 14, 75 (1939).

44. W. Steven and A. G. Haynes, JISI 183, 349 (1956).

45. P. Payson and C. H. Savage, Trans. ASM 33, 261 (1966).

46. L. A. Carapella, Met. Prog. 46, 108 (1944).

47. K. W. Andrews, JISI 203, 721 (1965).

48. R. A. Grange and H. M. Stewart, Trans. AIME 167, 467 (1946).

49. H. H. Chiswik and A. B. Greninger, Trans. ASM 32, 483 (1944).

50. W. E. Duckworth, Met. Rev. 145 (1968).

51. G. Thomas, Iron and Steel Int. 46, 451 (1973).

52. G. Thomas, Battelle Conf. on Structural Alloy Design, in press Lawrence Berkeley Laboratory Report, LBL-4175, (1975).

53. D. P. Koistinen and R. E. Marburger, Acta. Met. 7, 59 (1959).

54. D. J. Roberts, B. L. Averbach and M. Cohen, Trans. ASM 45, 576 (1953).

55. H. W. King and S. G. Glover, JISI 193, 123 (1959).

56. G. R. Speich, Trans. Met. Soc. AIME 245, 2553 (1969).

57. A. S. Kenneford and T. Williams, JISI 185, 467 (1957).

58. H. W. King and S. G. Glover, JISI 196, 281 (1960).

59. G. V. Kurdjumov, JISI 195, 26 (1960).

60. W. S. Owen, JISI 177, 445 (1954).

61. G. R. Speich and W. C. Leslie, Met. Trans. 3, 1043 (1972).

62. B. S. Lement, B. L. Averbach and Morris Cohen, Trans. ASM 46, 851 (1954).

63. E. Tekin and P. M. Kelly, Precipitation from Iron-Base Alloys, Vol. 28, Met. Soc. of AIME Conference Series, Eds. B. Gilbert, R. Speich and J. B. Clark, Gordon and Breach Science Publ., New York, 1965, p. 173.

65. M. G. H. Wells, Acta. Met. 12, 389 (1964).

66. H. W. Wagenblast and R. Glenn, Met. Trans. 1, 2299 (1970).

67. V. I. Izotov and L. M. Utevskii, Fiz. Metl Metalloved 25, 98 (1968).

68. K. I. Hale and D. McLean, JISI 20, 337 (1963).

69. W. C. Leslie, R. M. Fisher and N. Sen, Acta. Met. 7, 632 (1959).

70. K. H. Jack, JISI 169, 26 (1951).

71. W. C. Leslie, Acta Met. 9, 1004 (1961).

72. H. Ino, T. Mouya, E. Fujita, Y. Maeda, Y. Oni, and Y. Inokuti, J. Phys. Soc. Japan 25, 88 (1968).

73. A. Lutts, Rev. Univ. Mines 19, 325 (1963).

74. D. P. Antia and Morris Cohen, Trans. ASM 32, 363 (1944).

75. R. W. Balluffi, Morris Cohen and B. L. Averbach, 43, 497 (1951).

76. W. S. Owen, Trans. ASM 46, 812 (1954).

77. J. Vajda, J. J. Hauser and C. Wells, Trans. ASM 49, 517 (1957).

78. R. A. Tewari and P. R. Dhar, JISI 208, 87 (1970).

79. R. A. Tewari and P. R. Dhar, Trans. IIM, p. 13 (1970).

80. R. A. Tewari and P. R. Dhar, Trans. IIM, p. 35 (1970).

81. G. Y. Lai, W. E. Wood, E. R. Parker and V. F. Zackay, Lawrence Berkeley Laboratory Report, LBL-2236.

82. E. W. Langer, Met. Sci. J. 2, 59 (1968).

83. P. B. Hirsch, A. Howie, R. B. Nicholson, B. W. Pashly and M. J. Whelan, Electron Microscopy of Thin Crystals, Butterworths, London, 1965, p. 320.

84. A. S. Keh and W. C. Leslie, Materials Science Research 1, Plenum Press, New York, 1963, p. 208.

85. F. H. Laxar, J. W. Frame and D. J. Blickwede, Trans. ASM 53, 683 (1961).

86. V. F. Zackay and E. R. Parker, Lawrence Berkeley Laboratory Report, LBL-2782.

87. D. H. Huang and G. Thomas, Met. Trans. 2, 1587 (1971). Discussions of above paper: D. Kalish, Met. Trans. 3, 341 (1972), D. Huang and G. Thomas, ibid, 3, 343 (1972).

88. A. R. Rosenfeld and A. J. McEvily, AGARD Report, Metallurgical Aspects of Fatigue and Fracture Toughness, Dec. 1973, p. 23.

89. G. E. Pellissier, Eng. Frac. Mech. 1, 55 (1968).

90. Y. H. Liu, Trans. ASM 62, 55 (1969).

91. Y. H. Liu, Trans. ASM 62, 545 (1969).

92. J. H. Bucher, G. W. Powell and J. W. Spretenak, Met. Soc. AIME Conference Series, Vol. 31, Gordon and Breach Science Publ., New York, 1966, p. 323.

93. G. Kohn, Ph.D. Thesis, LBL-5716, University of California, Berkeley, California, 1976.

94. R. Horn, Ph.D. Thesis, LBL-5787, University of California, Berkeley, California, 1976.

95. D. Webster, Met. Trans. 2, 2097 (1971).

96. A. J. Baker, F. J. Lauta and R. P. Wei, ASTM STP No. 370, 1965, p.3.

97. C. P. Sullivan, Welding Research Council Bulletin No. 122, (1967).

98. J. M. Capus, JISI 199, 53 (1963).

99. N. J. Petch, JISI 173, 25 (1953).

100. A. H. Cotrell, Trans. AIME 212, 192 (1958).

101. N. J. Petch, Phil. Mag. 3, 1089 (1958).

102. S. Jin, S. K. Hwang and J. W. Morris, Jr., Met. Trans. 6A, 1721 (1975).

103. R. O. Ritchie, L. C. E. Geniets and J. F. Knott, The Microstructure and Design of Alloys, Proc. Third Int. Conf. on Strength of Metals and Alloys, Inst. of Metals, London, 1973, p. 124.

104. B. V. N. Rao, M.S. Thesis, LBL-3794, University of California, Berkeley, California, 1975.

105. P. C. Maxwell, A. Goldberg and J. C. Shyne, Met. Trans. 5, 1319 (1974).

106. L. J. Klinger, W. J. Barnett, R. P. Frohmberg and A. R. Troiano, Trans. ASM 46, 1557 (1954).

107. Metals Handbook, 9, Howard E. Boyer, Ed. American Society for Metals, Ohio, 1974, p. 64.

108. M. A. Grossman, Trans. AIME 167, 38 (1946).

109. Cobalt-Containing High-Strength Steels, Cobalt Monograph Series, A. Magner et al., eds., Cobalt Information Center, Battelle Memorial Institute, Columbus, Ohio, 1974, p. 69, 114.

110. B. de Mirmon, M. S. Thesis, UCRL-17849, University of California, Berkeley, California, 1967.

111. R. M. Bozorth, Ferromagnetism, D. Van Nostrand Co., New York (1951).

112. R. O. Ritchie, Lawrence Berkeley Laboratory, Berkeley, CA 94720.

Table I. Chemical composition of modified AISI 4340* steels used in this investigation.

Alloy Designation	Chemical Composition (wt. pct)		
	C	Al	Si
4340+1Al	0.38	0.98	-
4340+2Al	0.37	1.95	-
4340+3Al	0.41	2.89	-
4340+.5Al+.5Si	0.40	0.51	0.66
4340+1Al+1Si	0.39	1.00	1.15
4340+1.5Al+1.5Si	0.39	1.51	1.64
4340+2Al+2Si	0.39	1.97	2.10
4340+1Si	0.37	-	1.13
4340+2Si	0.37	-	2.11
4340+3Si	0.38	-	3.15

*Base Steel Composition: C-0.39, Cr-0.81, Mn-0.74, Ni-1.81, Si-0.20, Mo-0.25, Cu-0.18, P-0.007, S-0.003. Folllowing remelting there was a change in C as shown above. The concentration of the other elements did not change appreciably.

Table II. Austenitization temperatures, M_s and M_f temperatures of AISI 4340 and modified AISI 4340 steels.

Alloy Designation	Austenitization Temperature °C	M_s °C	M_f °C	M_s-M_f °C
4340	900	300	170	130
4340+1Al	900	315	225	90
4340+2Al	900	310	200	110
4340+3Al	1100	310	200	110
4340+.5Al+.5Si	900	295	180	115
4340+1Al+1Si	900	295	175	120
4340+1.5Al+1.5Si	950	310	190	120
4340+2Al+2Si	1100	295	150	145
4340+1Si	900	320	235	85
4340+2Si	900	290	190	100
4340+3Si	900	275	145	130

Table III. Mechanical Properties of 4340+Al Steels.

Alloy Designation	Austenitization Temperature (°C)	Tempering Temperature (°C)	Yield Strength (ksi)	Ultimate Strength (ksi)	Total Elongation (%)	K_{Ic} (ksi$\sqrt{in}$)	C_v (ft-lbs)
4340+1Al	900	As-Quenched	204	286	5.9	66.8	-
	"	250	220	258	5.3	77.5	-
	"	300	210	245	5.3	72.4	-
	"	350	198	231	5.3	-	-
	"	400	184	213	6.0	-	-
4340+2Al	900	As-Quenched	215**	290**	9.6*	55	18.2
	"	250	222	262	5.4	80.7	19.0
	"	325	226**	261**	11.7*	75	16.9
	"	375	227**	254**	10.8*	73	17.4
	"	400	218	243	4.8	-	16.9
4340+3Al	1100	As-Quenched	214**	290*	4.5*	63.1	11.9
	"	300	230**	264**	5.9*	81.2	11.0
	"	350	231	257	-	79.2	11.2
	"	400	233**	260**	5.0*	83.9	11.1
	"	450	219	244	-	79.2	8.3

*Total elongations marked with an asterisk were obtained from round tensile specimens. The other values were obtained from results of tests on flat tensile specimens.

**Strength values marked with a double asterisk are average values obtained from results of tests run with flat and round tensile specimens. 1 ksi = 6.89 MPa, 1 ksi$\sqrt{in}$ = 1.098855 MPa$\sqrt{m}$, 1 ft-lb = 1.36J.

Table IV. Mechanical Properties of 4340+Al+Si Steels.

Alloy Desgination	Austenitization Temperature (°C)	Tempering Temperature (°C)	Yield Strength (ksi)	Ultimate Strength (ksi)	Total Elongation (%)	K_{Ic} (ksi$\sqrt{in}$)	C_v (ft-lbs)
4340+.5Al+.5Si	900	As-Quenched	228	307	5.7	58	18
	"	250	233	271	6	80	20
	"	300	232	268	5.8	80	22.4
	"	350	227	259	6	74	17.5
	"	400	207	236	6.8	81	13.3
4340+1Al+1Si	900	As-Quenched	218**	304**	11.5*	43	-
	"	250	233**	276**	12.8*	83	-
	"	300	229	269	5.9	81	-
	"	350	231**	264**	12.7*	81	-
	"	400	225	250	5.6	-	-
4340+2Al+2Si	1100	As-Quenched	230	310	2.7	33.8	-
	"	300	250	290	4.4	81.3	-
	"	350	252	289	-	78.6	-
	"	400	260	288	4.5	74.2	-
	"	450	249	273	-	60.0	-
	"	500	224	248	-	-	-

*Total elongations marked with an asterisk were obtained from round tensile specimens. The other values were obtained from results on flat tensile specimens.

**Strength values marked with a double asterisk are average values obtained from results of tests run with flat and round tensile specimens. 1 ksi = 6.89 MPa, 1 ksi$\sqrt{in}$ = 1.098855 MPa$\sqrt{m}$, 1 ft-lb = 1.36J.

Table V. Mechanical Properties of 4340+1.5Al+1.5Si Steels.

Austenitization Temperature (°C)	Tempering Temperature (°C)	Yield Strength (ksi)	Ultimate Strength (ksi)	Total Elongation (%)	K_{Ic} (ksi$\sqrt{in}$)	C_v (ft-lbs)
950	As-Quenched	229**	318**	9.8*	41.7	-
	250	244**	287**	11.6*	73.3	-
	300	245**	286**	11.0*	80.3	-
	350	250**	288**	11.3*	72.7	-
	400	248**	275**	11.1*	73.3	-
	450	224	252	-	-	
	500	207	232	-	-	
1000	As-Quenched	233	296	-	42.3	12.6
	300	237	279	-	82.5	16.1
	350	240	272	-	74.2	23.3
	400	233	264	-	70.5	15.5
	450	222	251	-	54.0	10.6

*Total elongations marked with an asterisk were obtained from round tensile specimens.

**Strength values marked with a double asterisk are average values obtained from results of tests run with flat and round tensile specimens. 1 ksi = 6.89 MPa, 1 ksi$\sqrt{in}$ = 1.098855 MPa$\sqrt{m}$, 1 ft-lb = 1.36J.

Table VI. Mechanical Properties of 4340+Si Steels.

Alloy Designation	Tempering Temperature (°C)	Yield Strength (ksi)	Ultimate Strength (ksi)	Total Elongation (%)	K_{Ic} (ksi$\sqrt{in}$)	C_v (ft-lbs)
4340+1Si	As-Quenched	230	301	6.2	71.5	22.5
	250	235	280	5.5	79.1	24.3
	300	233	271	5.4	70.3	21.5
	350	226	260	5.7	72.1	20.9
	400	208	234	5.9	60.2	17.1
4340+2Si	As-Quenched	256	340	6.3	56.6	18.2
	250	257	307	5.9	74.8	19.9
	300	246	291	5.6	80.4	20.2
	350	255	289	5.2	80.3	22.8
	400	246	272	4.5	57.8	20.7
4340+3Si	As-Quenched	273	350	5.8	40	14.0
	250	270	319	5.6	75.2	21.1
	300	258	305	5.4	81.6	21.1
	350	264	299	3.5	75.1	19.1
	400	265	293	4.8	78.4	18.3
	450	-	-	-	46.3	9.0

NOTE: The tensile data was taken from the unpublished results of G. Kohn, Lawrence Berkeley Laboratory (1975). Flat tensile specimens were used in the study. The K_{Ic} and C_v data were obtained in this study from a new set of ingots.

Table VII. The Variation in Plane Strain Fracture Toughness (K_{Ic}) with Austenitization Temperature of 4340+1Al and 4340+2Al+2Si Steels.

Alloy Designation	Austenitization Temperature (°C)	Tempering Temperature (°C)	K_{Ic} ($ksi\sqrt{in}$)
4340+1Al	900	As-Quenched	66.8
4340+1Al	1100	"	66.3
4340+1Al	1200	"	71.9
4340+2Al+2Si	1100	As-Quenched	33.8
4340+2Al+2Si	1100	300	81.3
4340+2Al+2Si	1200	As-Quenched	36.0
4340+2Al+2Si	1200	300	83.1

$1\ ksi\sqrt{in} = 1.098855\ MPa \cdot m^{1/2}$

Table VIII. ASTM Grain Size Numbers of the Modified Steels.

Alloy Designation	Austenite Temperature (°C)	ASTM Grain Size No.
4340+1Al	900	7
4340+2Al	900	5
4340+3Al	1100	2
4340+.5Al+.5Si	900	7
4340+1Al+1Si	900	7
4340+1.5Al+1.5Si	950	6
4340+1.5Al+1.5Si	1000	4-5
4340+2Al+2Si	1100	2
4340+1Si	950	6
4340+2Si	950	6
4340+3Si	950	6

FIGURE CAPTIONS

Fig. 1. Schematic diagram showing orientations of specimens in the forged bar.

Fig. 2. Sketch of sheet tensile specimen (Thickness of the specimen was 0.05").

Fig. 3. Sketch of round tensile specimen.

Fig. 4. Sketch of compact tension specimen.

Fig. 5. Sketch of Charpy V-notch specimen.

Fig. 6. Sketch of dilatometer specimen.

Fig. 7. Schematic diagram of the magnetic saturation device.

Fig. 8. Optical micrographs of 4340+3Al steel austenitized at (a) 900°C (b) 1000°C and (c) 1075°C.

Fig. 9. Optical micrographs of 4340+4Al steel austenitized at (a) 900°C (b) 1100°C, (c) 1150°C, (d) 1200°C, and (e) 1300°C.

Fig. 10. Plot of M_s temperature versus weight pct Al added to AISI 4340.

Fig. 11. Plot of Rockwell hardness (R_c) versus tempering temperature for AISI 4340 and 4340+Al steels.

Fig. 12. Plot of Rockwell hardness (R_c) versus tempering temperature for AISI 4340 and 4340+Al+Si steels.

Fig. 13. Plot of ultimate and 0.2 pct offset yield strength versus tempering temperature for AISI 4340 and 4340+Al steels.

Fig. 14. Plot of ultimate and 0.2 pct offset yield strength versus tempering temperature for AISI 4340 and 4340+Al+Si steels.

Fig. 15. Comparison of strength values obtained by testing two different types of specimens of the same steel given the same heat treatment.

Fig. 16. Plot of fracture toughness (K_{Ic}), ultimate tensile strength (UTS) and 0.2 pct. offset yield strength (YS) versus tempering temperature for 4340+1Al steel

Fig. 17. Plot of Charpy impact energy (C_v), fracture toughness (K_{Ic}), ultimate tensile strength (UTS) and 0.2 pct. offset yield strength (YS) versus tempering temperature for 4340+2Al steel.

Fig. 18. Plot of Charpy impact energy (C_v), fracture toughness (K_{Ic}), ultimate tensile strength (UTS) and 0.2 pct. offset yield strength (YS) versus tempering temperature for 4340+3Al steel.

Fig. 19. Plot of Charpy impact energy (C_v), fracture toughness (K_{Ic}), ultimate tensile strength (UTS) and 0.2 pct. offset yield strength (YS) for 4340+.5Al+.5Si steel.

Fig. 20. Plot of fracture toughness (K_{Ic}), ultimate tensile strength (UTS) and 0.2 pct. offset yield strength (YS) for 4340+1Al+1Si steel.

Fig. 21. Plot of fracture toughness (K_{Ic}), ultimate tensile strength (UTS) and 0.2 pct. offset yield strength (YS) for 4340+1.5Al+1.5Si steel austenitized at 950°C.

Fig. 22. Plot of Charpy impact energy (C_v), fracture toughness (K_{Ic}), ultimate tensile strength (UTS) and 0.2 pct offset yield strength (YS) versus tempering temperature for 4340+1.5Al+1.5Si steel austenitized at 1000°C.

Fig. 23. Plot of fracture toughness (K_{Ic}), ultimate tensile strength (UTS) and 0.2 pct. offset yield strength (YS) versus tempering temperature for 4340+2Al+2Si steel.

Fig. 24. Plot of Charpy impact energy (C_v), fracture toughness (K_{Ic}), ultimate tensile strength (UTS) and 0.2 pct. offset yield strength (YS) for 4340+1Si steel.

Fig. 25. Plot of Charpy impact energy (C_v), fracture toughness (K_{Ic}), ultimate tensile strength (UTS) and 0.2 pct. offset yield strength for 4340+2Si steel.

Fig. 26. Plot of Charpy impact energy (C_v) fracture toughness (K_{Ic}), ultimate tensile strength (UTS) and 0.2 pct. offset yield strength for 4340+3Si steel.

Fig. 27. Variation in retained austenite content with tempering temperature and tensile strain in 4340+1Al steel.

Fig. 28. Variation in retained austenite content with tempering temperature and tensile strain in 4340+2Al steel.

Fig. 29. Variation in retained austenite content with tempering temperature and tensile strain in 4340+3Al steel.

Fig. 30. Variation in retained austenite content with tempering temperature and tensile strain in 4340+.5Al+.5Si steel.

Fig. 31. Variation in retained austenite content with tempering temperature and tensile strain in 4340+1Al+1Si steel.

Fig. 32. Variation in retained austenite content with tempering temperature and tensile strain in 4340+1.5Al+1.5Si steel.

Fig. 33. Variation in retained austenite content with tempering temperature and tensile strain in 4340+2Al+2Si steel.

Fig. 34. Scanning electron fractographs of broken compact tension specimens of 4340+2Al steel in (A) as-quenched, quenched and tempered at (B) 250°C, (C) 325°C and (D) 375°C conditions.

Fig. 35. Scanning electron fractographs of broken compact tension specimens of 4340+3Al steel in (A) As-quenched, quenched and tempered at (B) 300°C, (C) 400°C and (D) 450°C conditions.

Fig. 36. Scanning electron fractographs of broken compact tension specimens of 4340+.5Al+.5Si steel in (A) As-quenched, quenched and tempered at (B) 250°C, (C) 300°C and (D) 400°C conditions.

Fig. 37. Scanning electron fractographs of broken compact tension specimens of 4340+1.5Al+1.5Si steel (austenitized at 950°C) in (A) As-quenched, quenched and tempered at (B) 300°C, (C) 350°C and (D) 400°C conditions.

Fig. 38. Scanning electron fractographs of broken compact tension specimens of 4340+1.5Al+1.5Si steel (austenitized at 1000°C) in (A) As-quenched, quenched and tempered at (B) 300°C, (C) 350°C and (D) 450°C conditions.

Fig. 39. Scanning electron fractographs of broken compact tension specimens of 4340+2Al+2Si steel in (A) As-quenched, quenched and tempered at (B) 300°C, (C) 350°C and (D) 450°C conditions.

Fig. 40. Scanning electron fractographs of broken compact tension specimens of 4340+3Si steel in (A) As-quenched, quenched and tempered at (B) 300°C, (C) 400°C and (D) 450°C conditions.

Fig. 41. Scanning electron fractographs of broken compact tension specimens of 4340+2Al+Si steel (austenitized at 1200°C) in (A) as-quenched and (B) quenched and tempered at 300°C conditions.

Fig. 42. Scanning electron fractographs of broken compact tension specimens of as-quenched 4340+1Al steel austenitized at (A) 900°C, (B) 1100°C and (C) 1200°C.

Fig. 43. Scanning electron fractograph of a 4340+3Al specimen showing an inclusion rich is aluminum.

Fig. 44. Scanning electron fractograph of a 4340+1.5Al+1.5Si specimen showing a rounded inclusion rich in aluminum.

Fig. 45. Scanning electron fractograph of a 4340+1.5Al+1.5Si specimen showing a broken plate-like inclusion rich in aluminum.

Fig. 46. Scanning electron fractograph of a 4340+1.5Al+1.5Si specimen showing an inclusion rich in Al, S, Mn and Fe.

Fig. 47. Scanning electron fractographs of a 4340+3Al specimen showing inclusions, the smaller of which contained the elements Mg, Al, S, Mn and Fe.

Fig. 48. Optical micrographs of 4340+2Al steel in (A) As-quenched, quenched and tempered at (B) 250°C, (C) 325°C and (D) 375°C conditions.

Fig. 49. Optical micrographs of 4340+3Al steel in (A) As-quenched, quenched and tempered at (B) 300°C, (C) 400°C and (D) 450°C conditions.

Fig. 50. Optical micrographs of 4340+1Al+1Si steel in (A) As-quenched, quenched and tempered at (B) 300°C, (C) 350°C and (D) 400°C conditions.

Fig. 51. Optical micrographs of 4340+1.5Al+1.5Si steel (austenitized at 950°C) in (A) As-quenched, quenched and tempered at (B) 300°C, (C) 350°C and (D) 400°C conditions.

Fig. 52. Optical micrographs of 4340+2Al+2Si steel (austenitized at 1100°C) in (A) As-quenched, quenched and tempered at (B) 350°C (C) 400°C and (D) 450°C conditions.

Fig. 53. Optical micrographs of 4340+2Al+2Si steel (austenitized at 1200°C) in (A) As-quenced and (B) Quenched and tempered at 300°C conditions.

Fig. 54. Optical micrographs of 4340+3Si steel in (A) As-quenched, quenched and tempered at (B) 250°C, (C) 300°C and (D) 400°C conditions.

Fig. 55. Transmission electron micrographs obtained from as-quenched 4340+3Al steel showing a bright field-dark field pair of pictures. The dark field was obtained with an austenite reflection.

Fig. 56. Transmission electron micrograph obtained from as-quenched 4340+2Al steel showing a high dislocation density (A), some microtwinning (B), and wavy precipitates (C).

Fig. 57. Transmission electron micrographs obtained from 4340+3Al steel in the quenched and tempered at 300°C condition showing carbide precipitation in two directions. Shown on the

micrograph are six directions, three of which are the major crystallographic directions $[002]_M$, $[0\bar{1}\bar{1}]_M$ and $[011]_M$ for the $(100)_M$ orientation. The second set of directions marked 1, 2 and 3 correspond to the streak directions observed in the diffraction pattern.

Fig. 58. Transmission electron micrographs obtained from 4340+3Al steel in the quenched and tempered at 300°C condition showing carbide precipitation. The dark field was obtained using a carbide spot.

Fig. 59. Trace analysis results of Figs. 57 and 58 showing a possible carbide habit plane.

Fig. 60. Transmission electron micrograph of the same area as in Fig. 58, but at a higher magnification.

Fig. 61. Transmission electron micrograph obtained from 4340+3Al steel in the quenched and tempered at 400°C condition. The foil orientation was close to $(100)_M$ and the three crystallographic directions are shown. Also shown are the two streak directions corresponding to the streaks in the diffraction pattern.

Fig. 62. Transmission electron micrograph obtained from 4340+1.5Al+1.5Si steel in the as-quenched condition. The dark field picture was taken with an austenite reflection.

Fig. 63. Transmission electron micrograph obtained from 4340+1.5Al+1.5Si steel in the as-quenched condition showing wavy autotempered carbides.

Fig. 64. Transmission electron micrograph obtained from 4340+1.5Al+1.5Si steel in the quenched and tempered at 300°C condition showing carbides in a lath of martensite.

Fig. 65. Plot of ultimate tensile strength and 0.2 pct. offset yield strength versus tempering temperature for 4340+1Al, 4340+1.5Al+1.5Si, and 4340+1Si steels.

Fig. 66. Plot of ultimate tensile strength and 0.2 pct. offset yield strength versus tempering temperature for 4340+2Al, 4340+1Al+1Si, and 4340+2Si steels.

Fig. 67. Plot of ultimate tensile strength and 0.2 pct. offset yield strength versus tempering temperature for 4340+3Al, 4340+1.5Al+1.5Si, and 4340+3Si steels.

Fig. 68. Optical micrograph of as-quenched 4340+1.5Al+1.5Si steel austenitized at 950°C showing the presence of some blocky ferrite (light etching phase).

Fig. 69. Plot of fracture toughness (K_{Ic}), ultimate tensile strength, and 0.2 pct. offset yield strength versus tempering temperature for 4340 and 4340+1.5Al+1.5Si steels. (The data for 4340 was obtained from Ref. 3).

Fig. 70. Plot of fracture toughness (K_{Ic}), ultimate tensile strength, and 0.2 pct. offset yield strength versus tempering temperature for 300-M and 4340+1.5Al+1.5Si steels. (The data for 300-M steel was obtained from Ref. 3, 112)

Fig. 71. Plot of retained austenite content in 300-M steel as a function of tempering temperature and tensile strain. (This figure was obtained from Ref. 94.)

Fig. 72. Plot of fracture toughness (K_{Ic}) versus 0.2 pct offset yield strength for the experimental 4340+Al and 4340+Al+Si steels in the quenched and tempered condition, and for the 18NiCoMo maraging alloys (Ref. 109), AISI 4340 (Ref. 3), and 300-M (Ref. 3, 112) steels.

Fig. 73. Plot of fracture toughness (K_{Ic}) versus ultimate tensile strength for the experimental 4340+Al and 4340+Al+Si steels in the quenched and tempered conditions, and for the 18NiCoMo maraging alloys (Ref. 109), AISI 4340 (Ref. 3), and 300-M (Ref. 3, 112) steels.

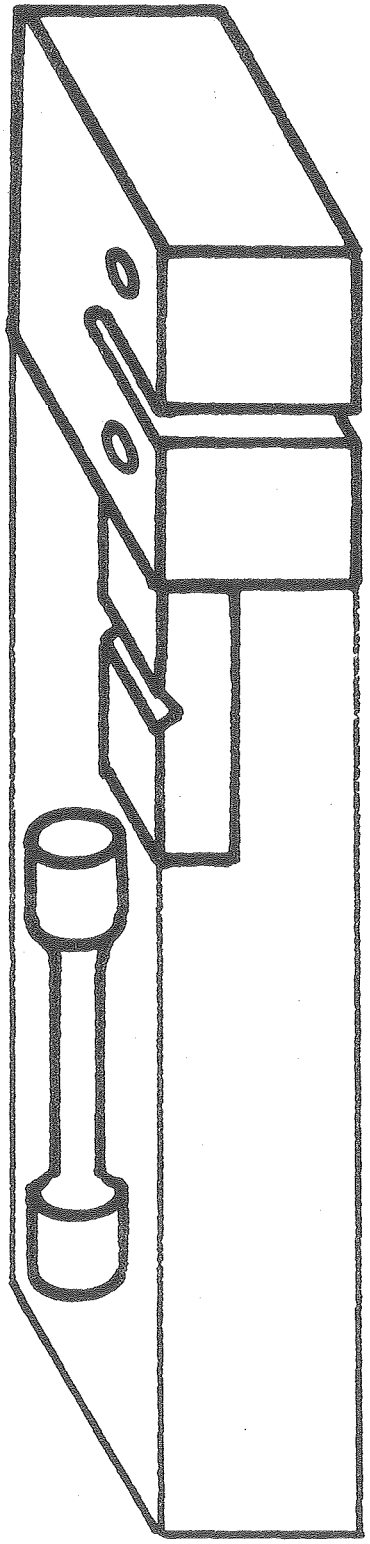

XBL 7612-10410A

Fig. 1.

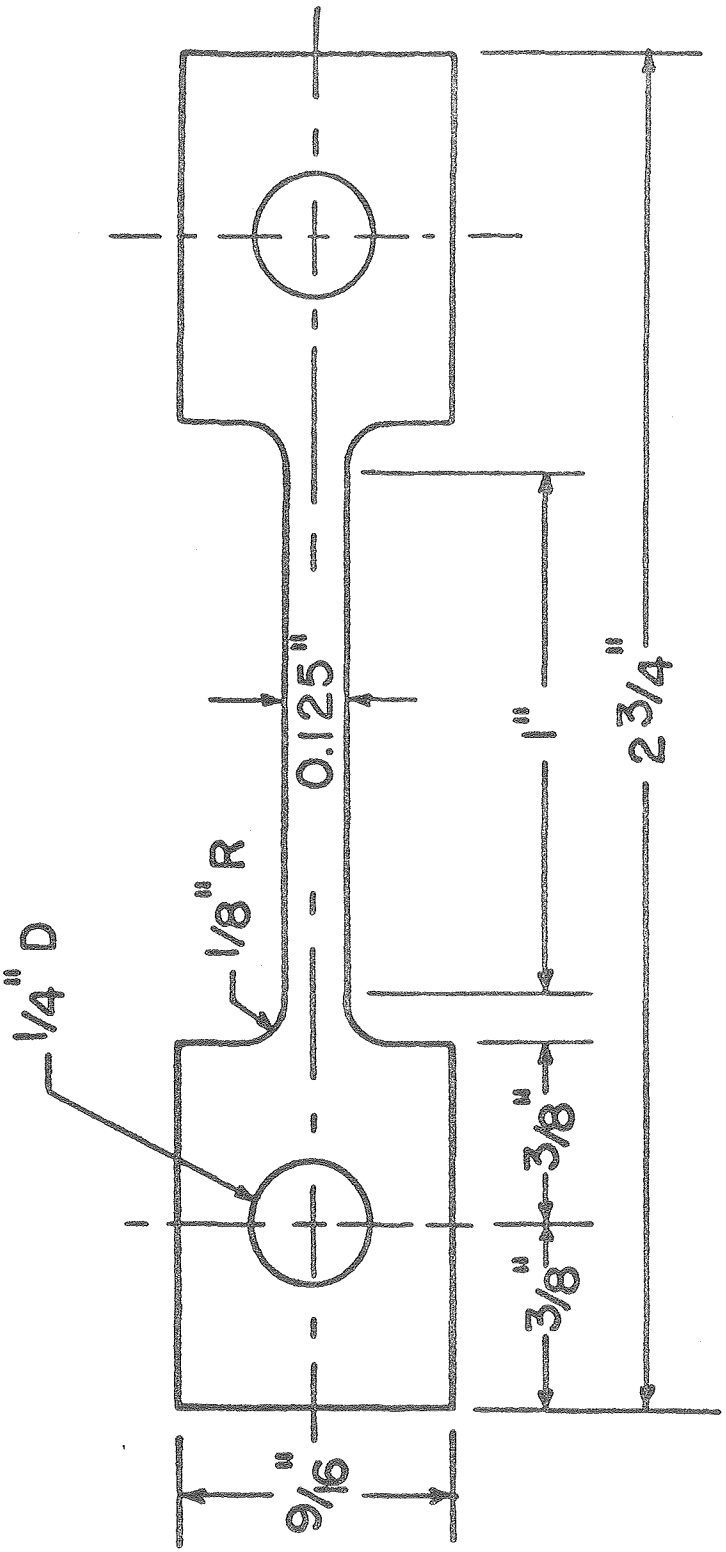

XBL 7612-10410B

Fig. 2.

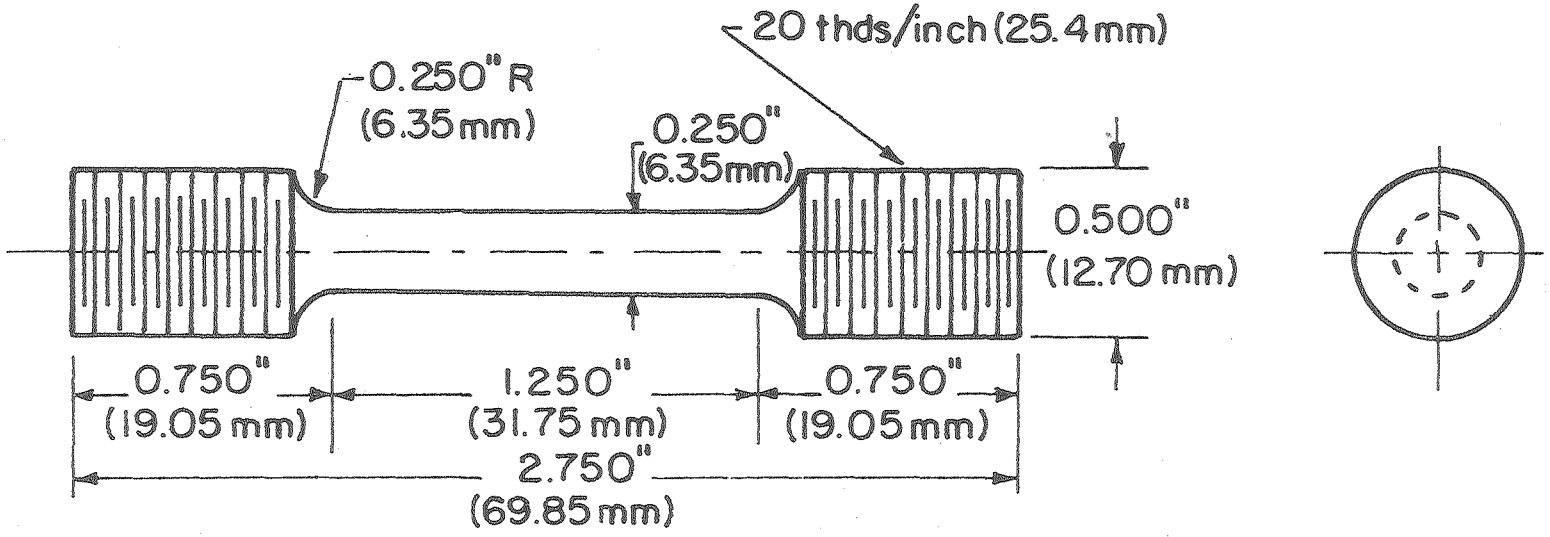

Fig. 3.

XBL 736-6280B

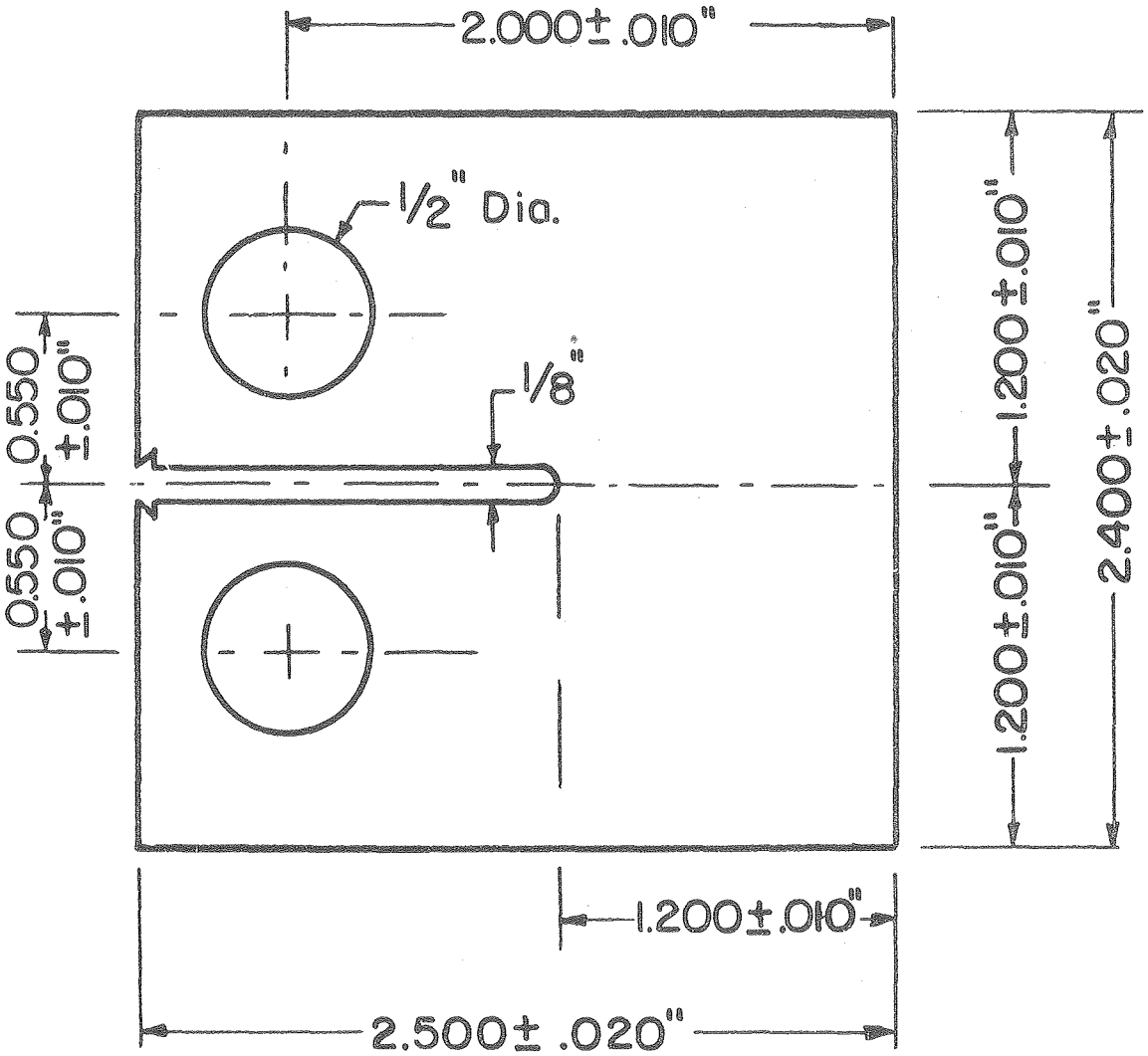

XBL 7612-10410C

Fig. 4.

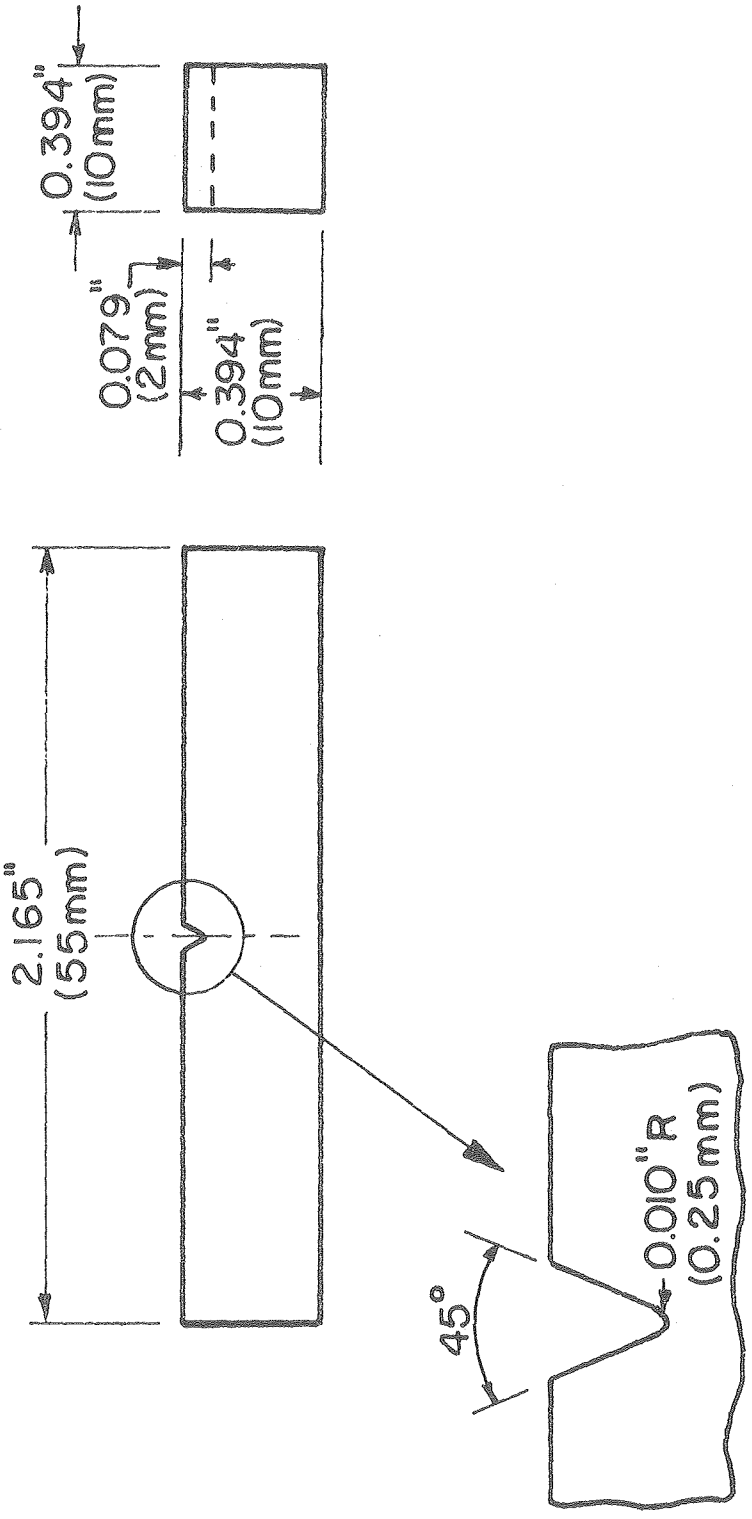

XBL 736-6280A

Fig. 5.

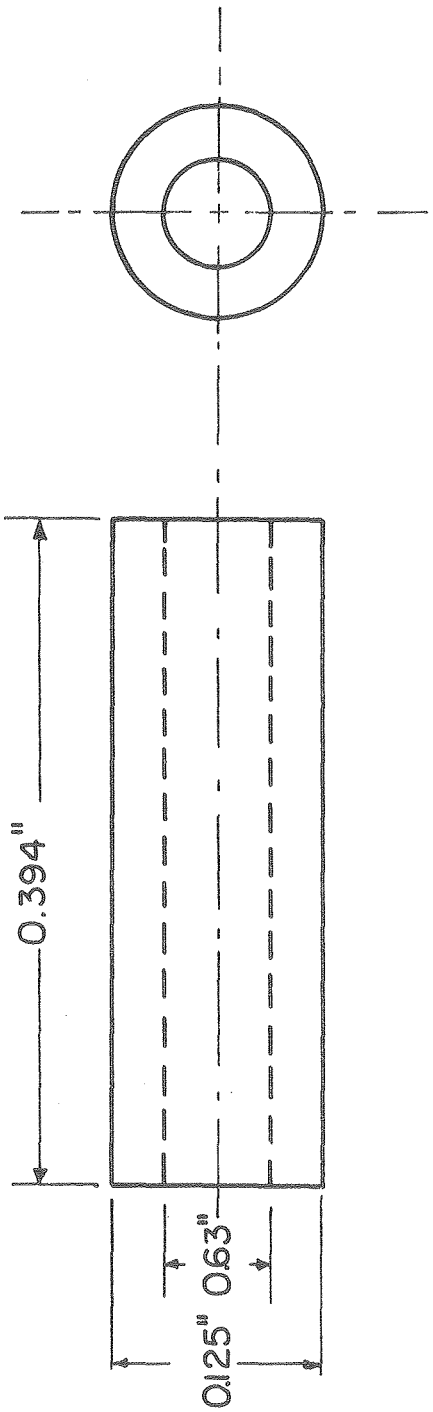

XBL 7612-10,996

Fig. 6.

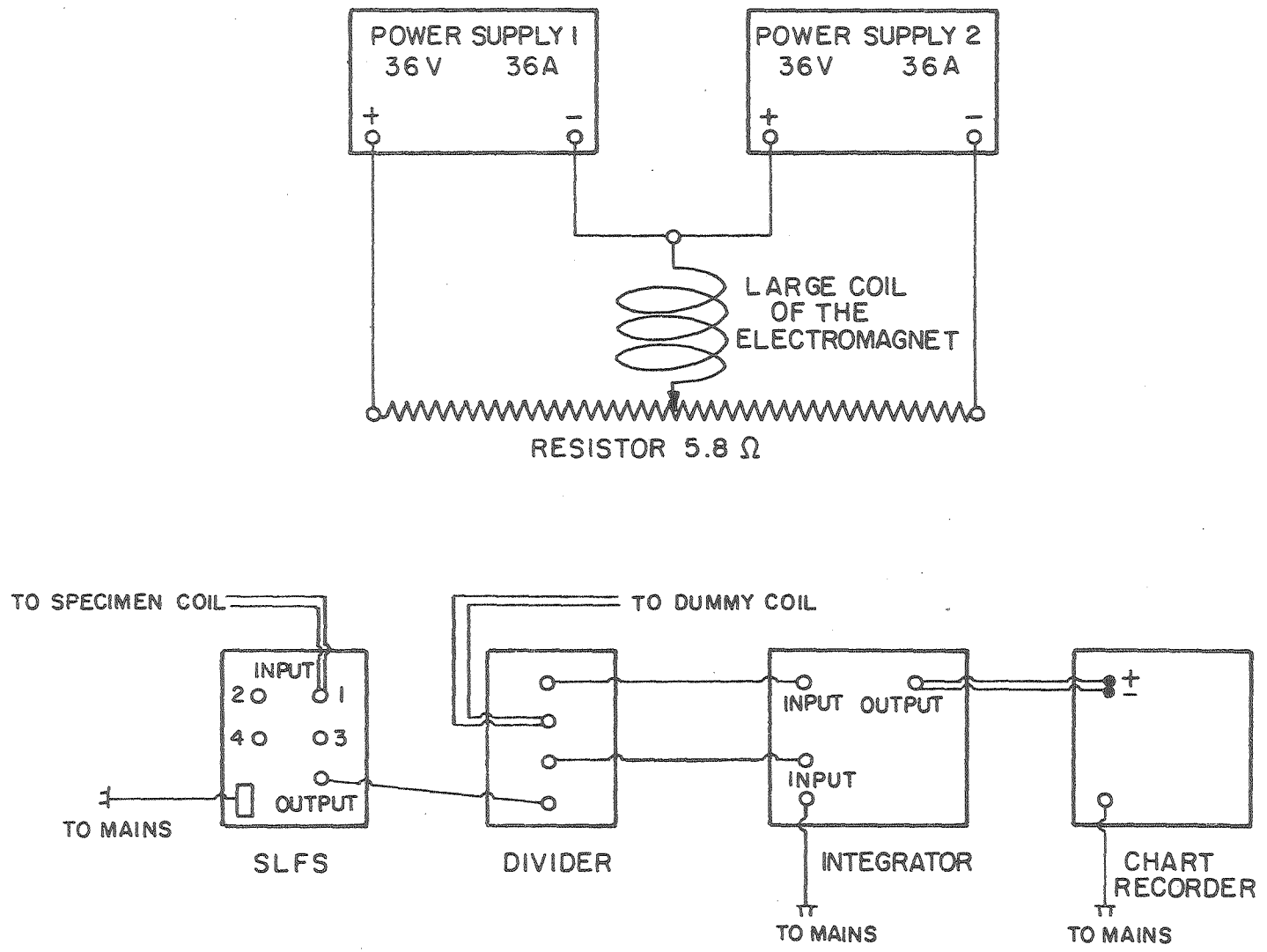

Fig. 7.

XBL771-4917

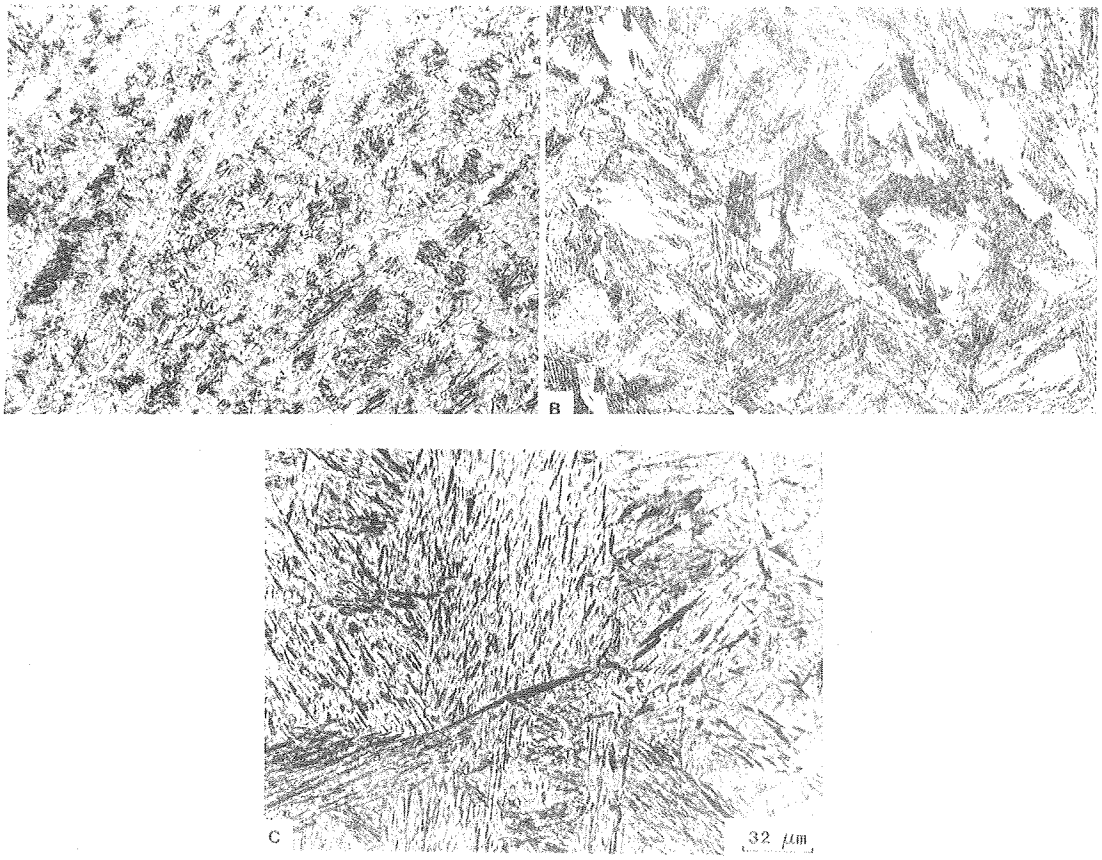

Fig. 8.

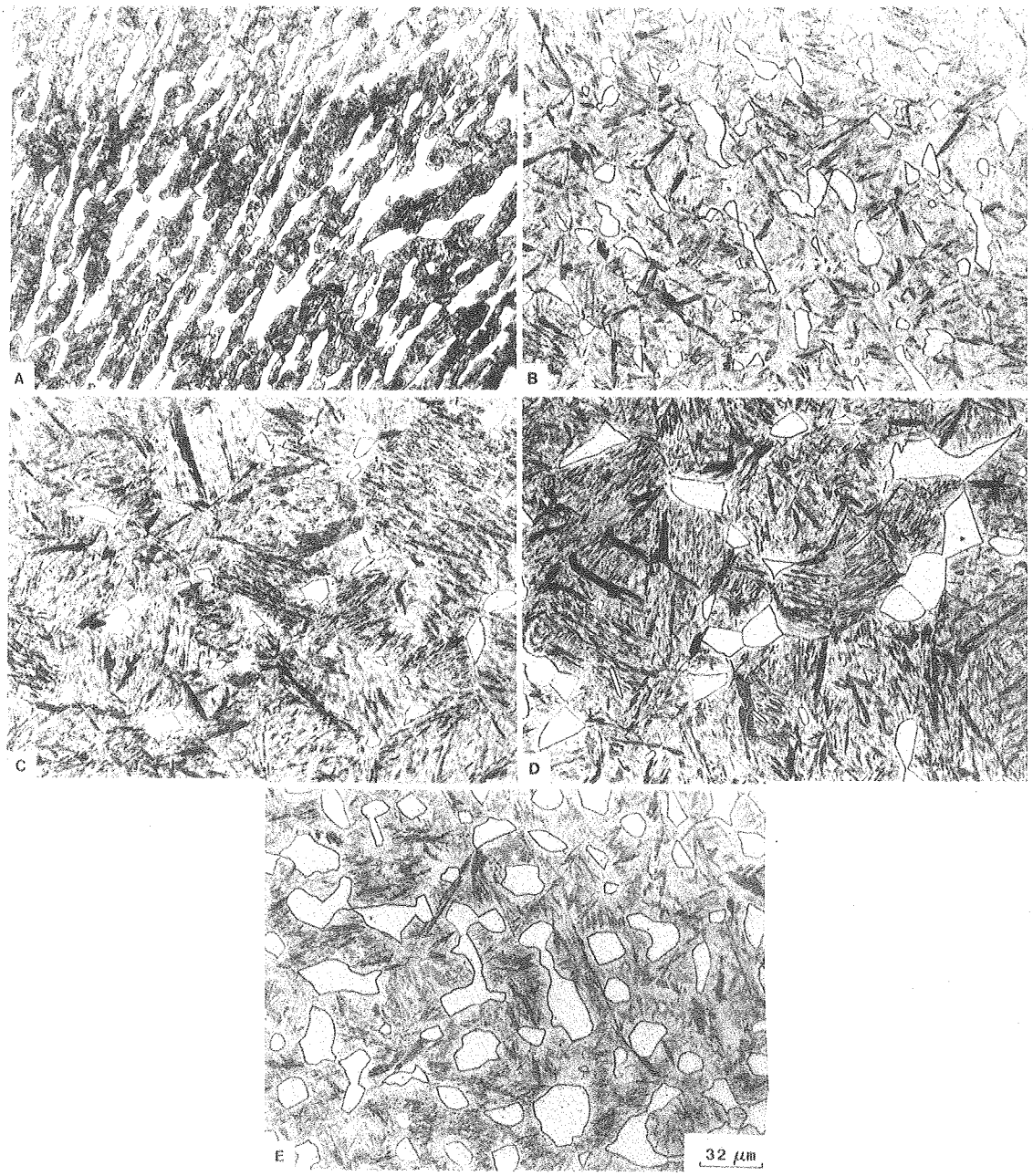

XBB 760-11124

Fig. 9.

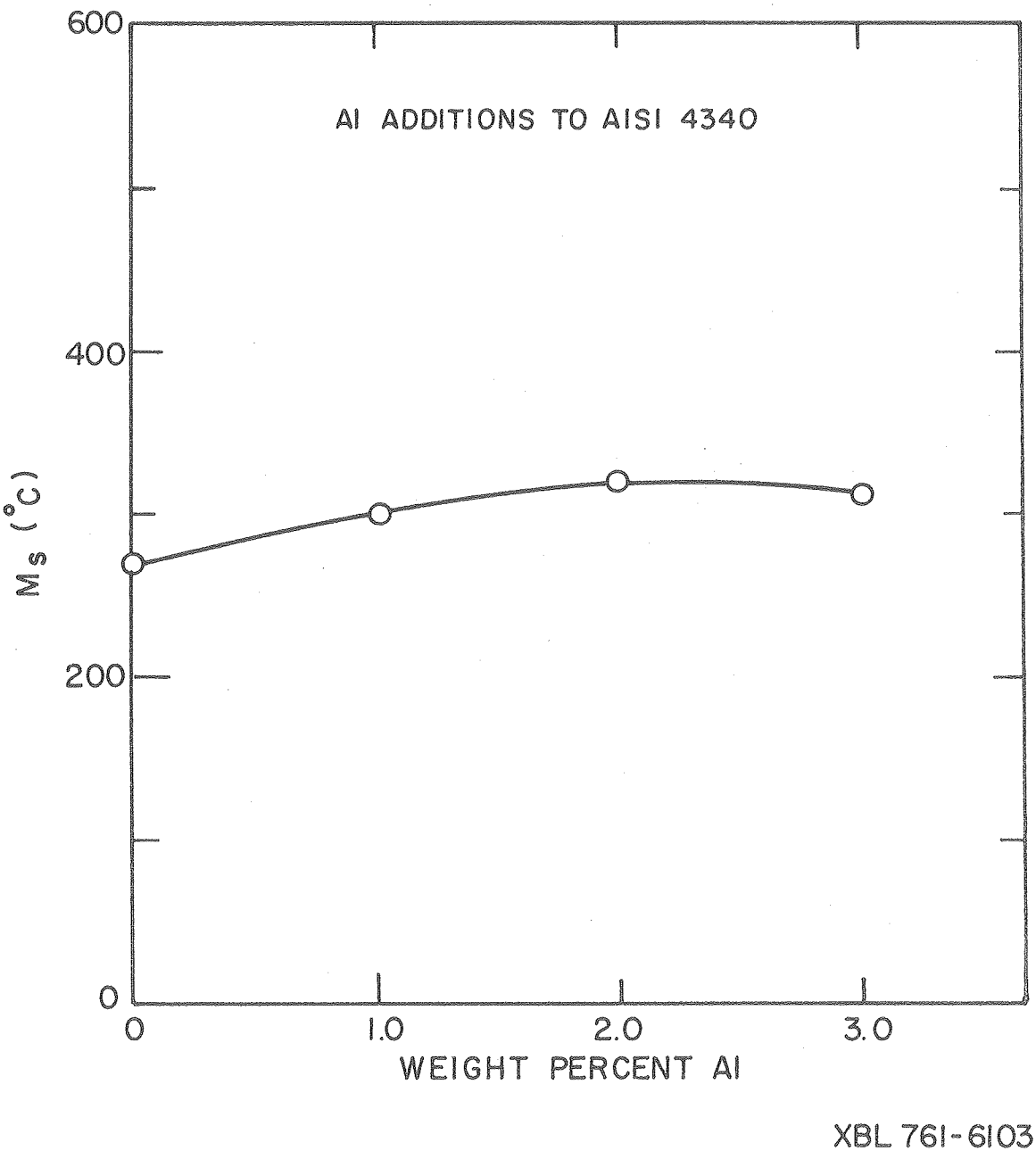
Al ADDITIONS TO AISI 4340
600
400
200
0
Ms (°C)
0
1.0
2.0
3.0
WEIGHT PERCENT Al
XBL 761-6103

Fig. 10.

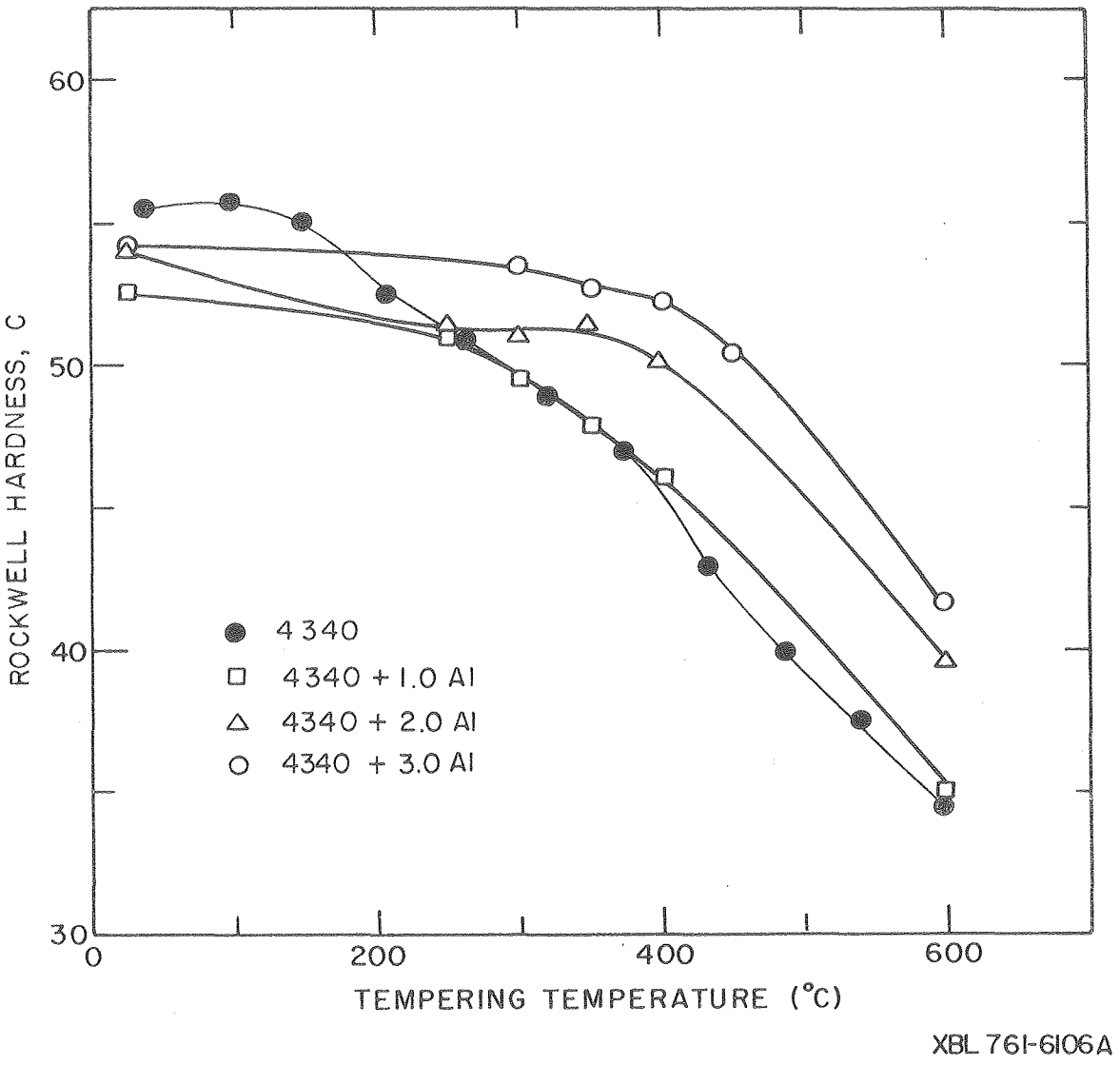

Fig. 11.

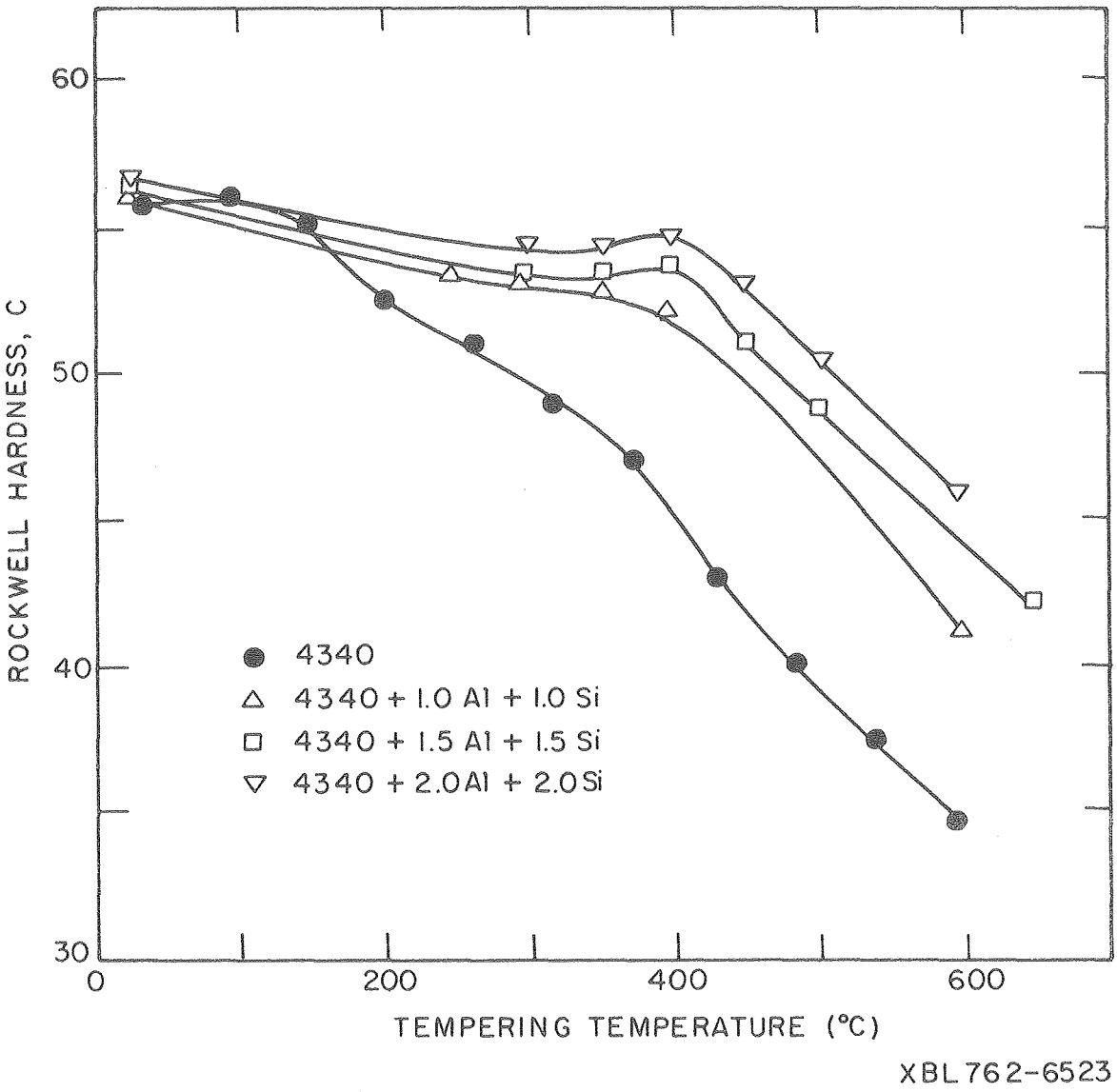
60
50
40
30
0
200
400
600
ROCKWELL HARDNESS, C
TEMPERING TEMPERATURE (°C)
4340
4340 + 1.0 Al + 1.0 Si
4340 + 1.5 Al + 1.5 Si
4340 + 2.0Al + 2.0Si
XBL762-6523

Fig. 12.

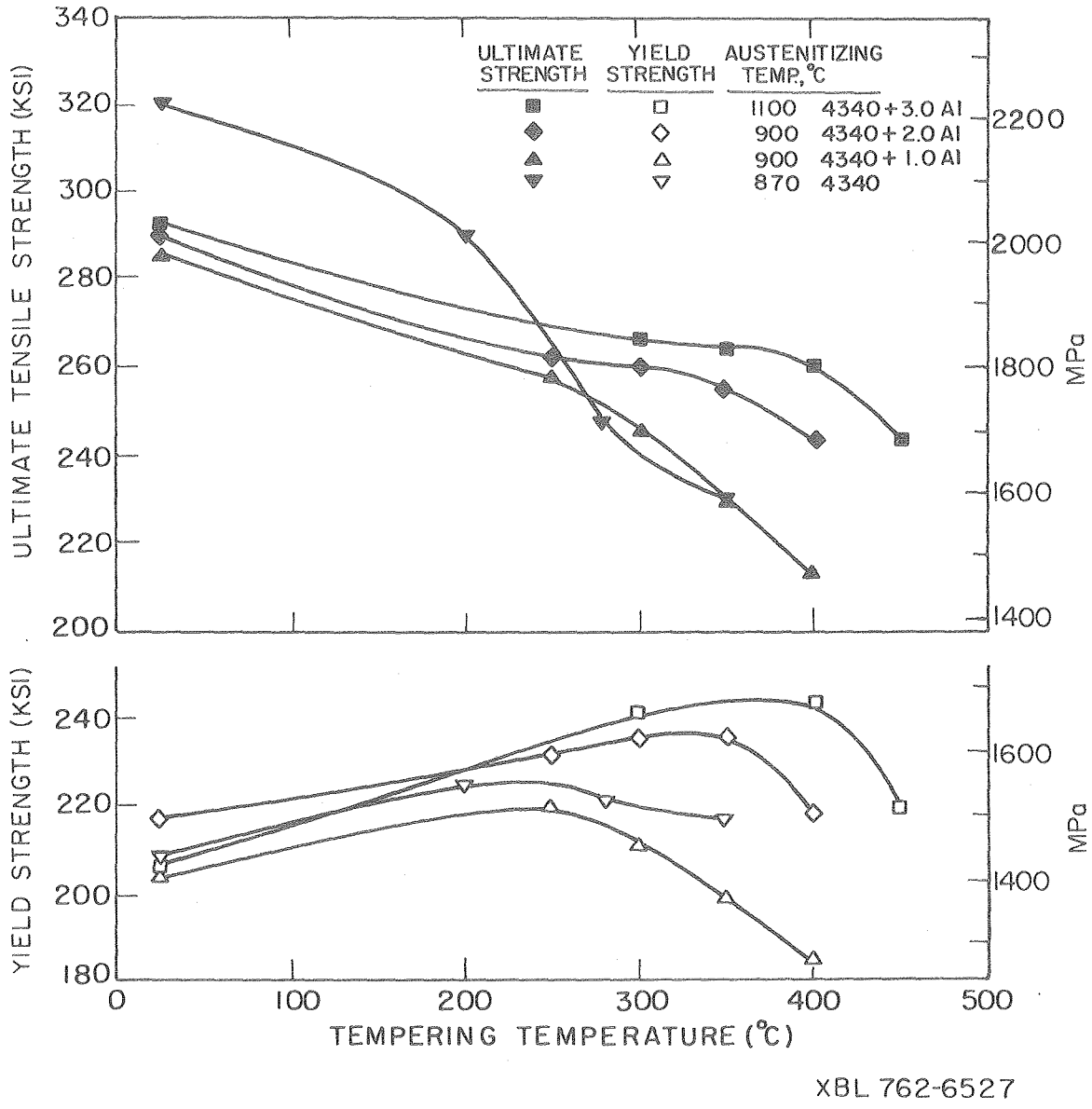
ULTIMATE STRENGTH
YIELD STRENGTH
AUSTENITIZING TEMP, °C
1100 4340+3.0 Al
900 4340+2.0 Al
900 4340+1.0 Al
870 4340
ULTIMATE TENSILE STRENGTH (KSI)
YIELD STRENGTH (KSI)
MPa
TEMPERING TEMPERATURE (°C)
XBL 762-6527

Fig. 13.

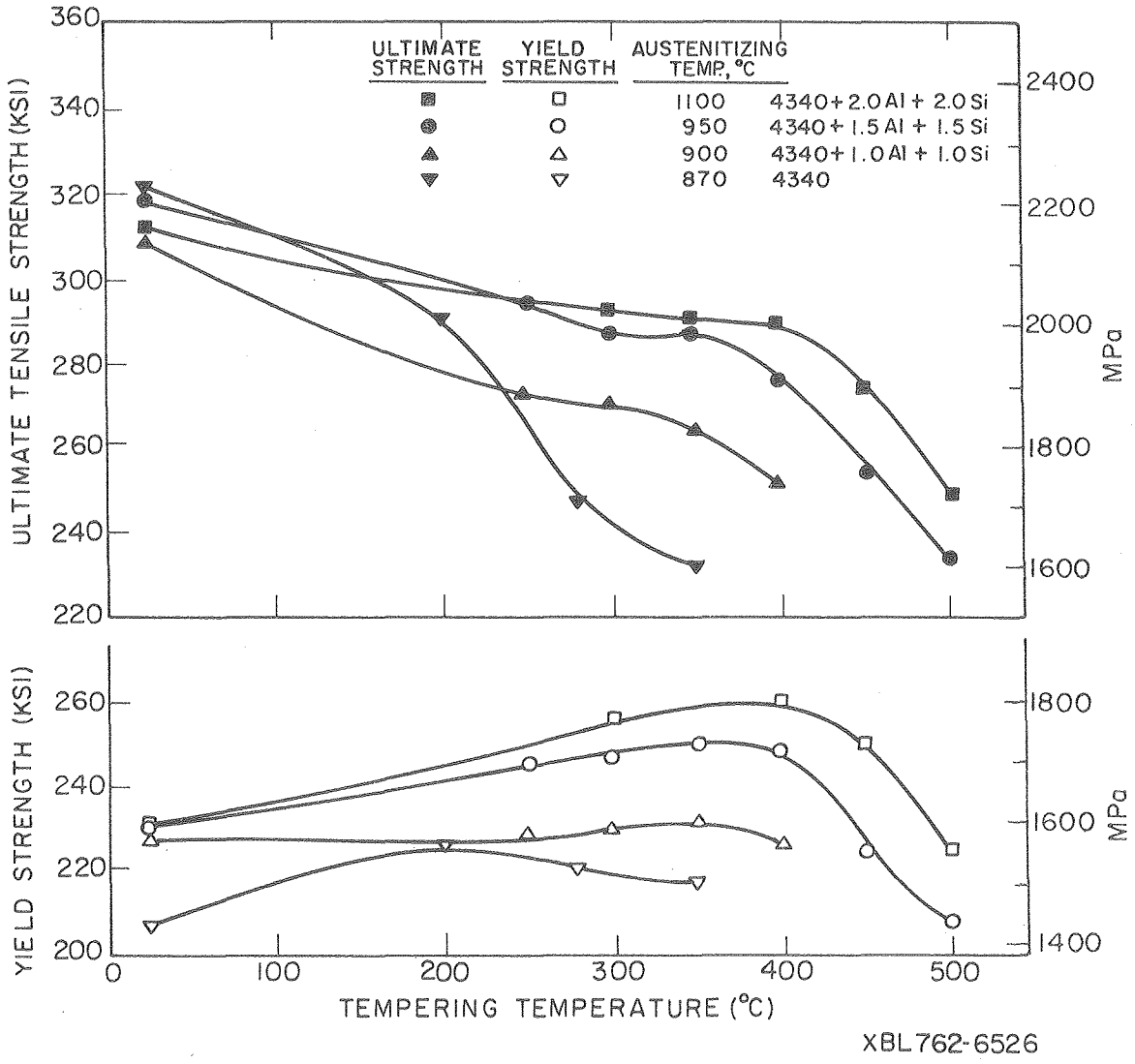
ULTIMATE STRENGTH
YIELD STRENGTH
AUSTENITIZING TEMP., °C
1100 4340+2.0Al+2.0Si
950 4340+1.5Al+1.5Si
900 4340+1.0Al+1.0Si
870 4340
ULTIMATE TENSILE STRENGTH (KSI)
YIELD STRENGTH (KSI)
MPa
TEMPERING TEMPERATURE (°C)
XBL762-6526

Fig. 14.

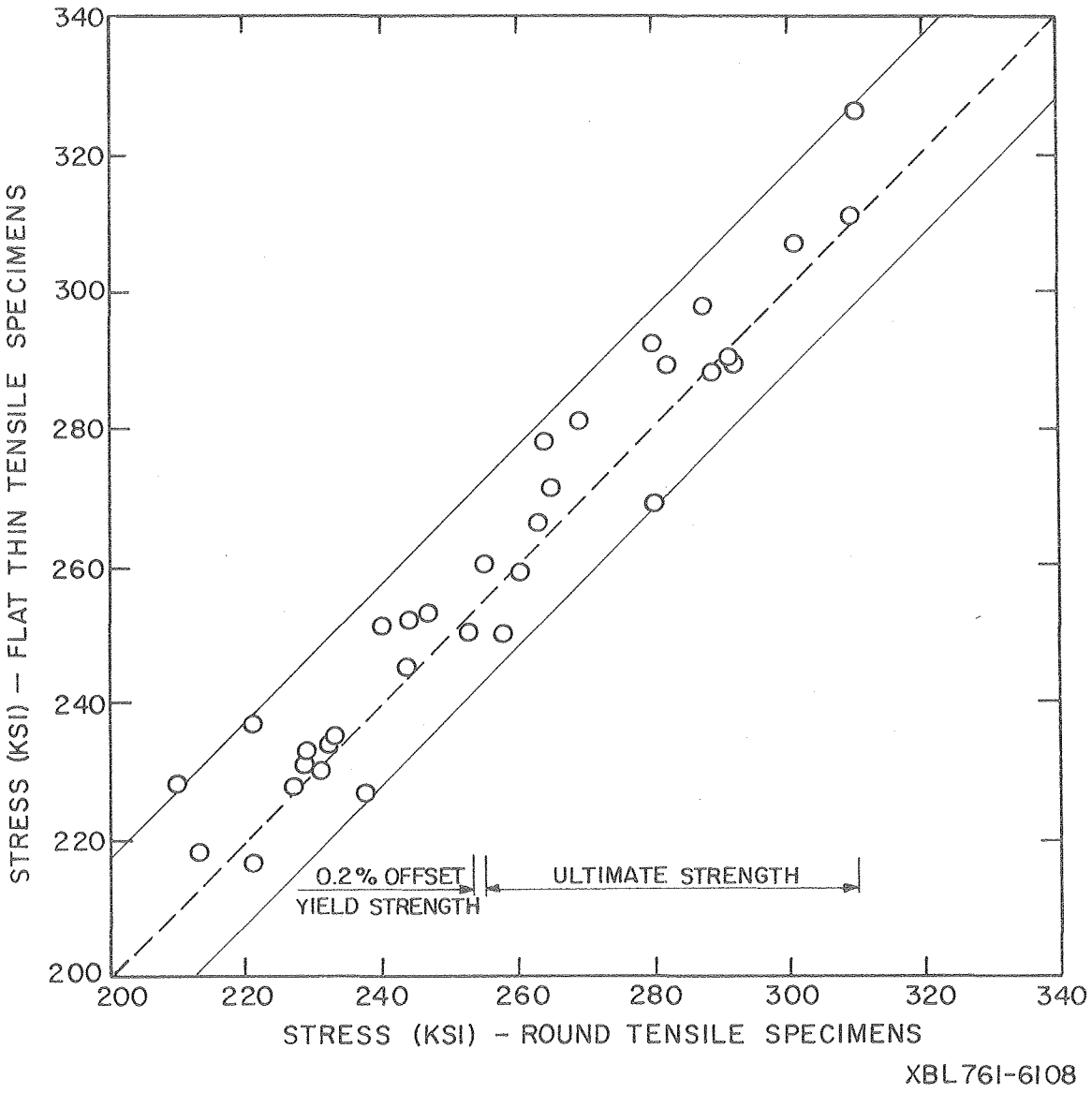

Fig. 15.

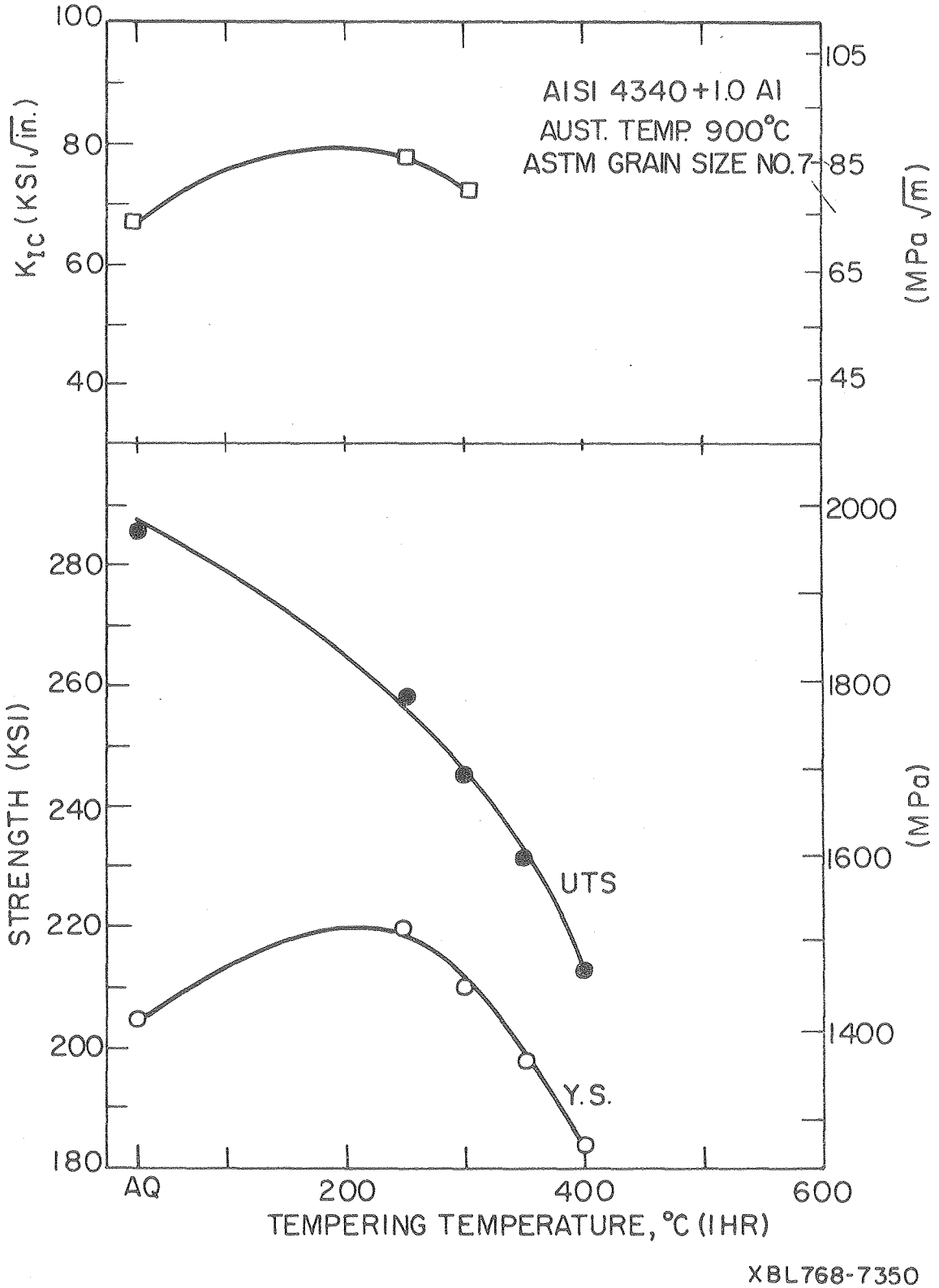
AISI 4340+1.0 Al
AUST. TEMP. 900°C
ASTM GRAIN SIZE NO.7
K_{IC} (KSI$\sqrt{in.}$)
(MPa$\sqrt{m}$)
STRENGTH (KSI)
(MPa)
UTS
Y.S.
AQ
200
400
600
TEMPERING TEMPERATURE, °C (1HR)
XBL768-7350

Fig. 16.

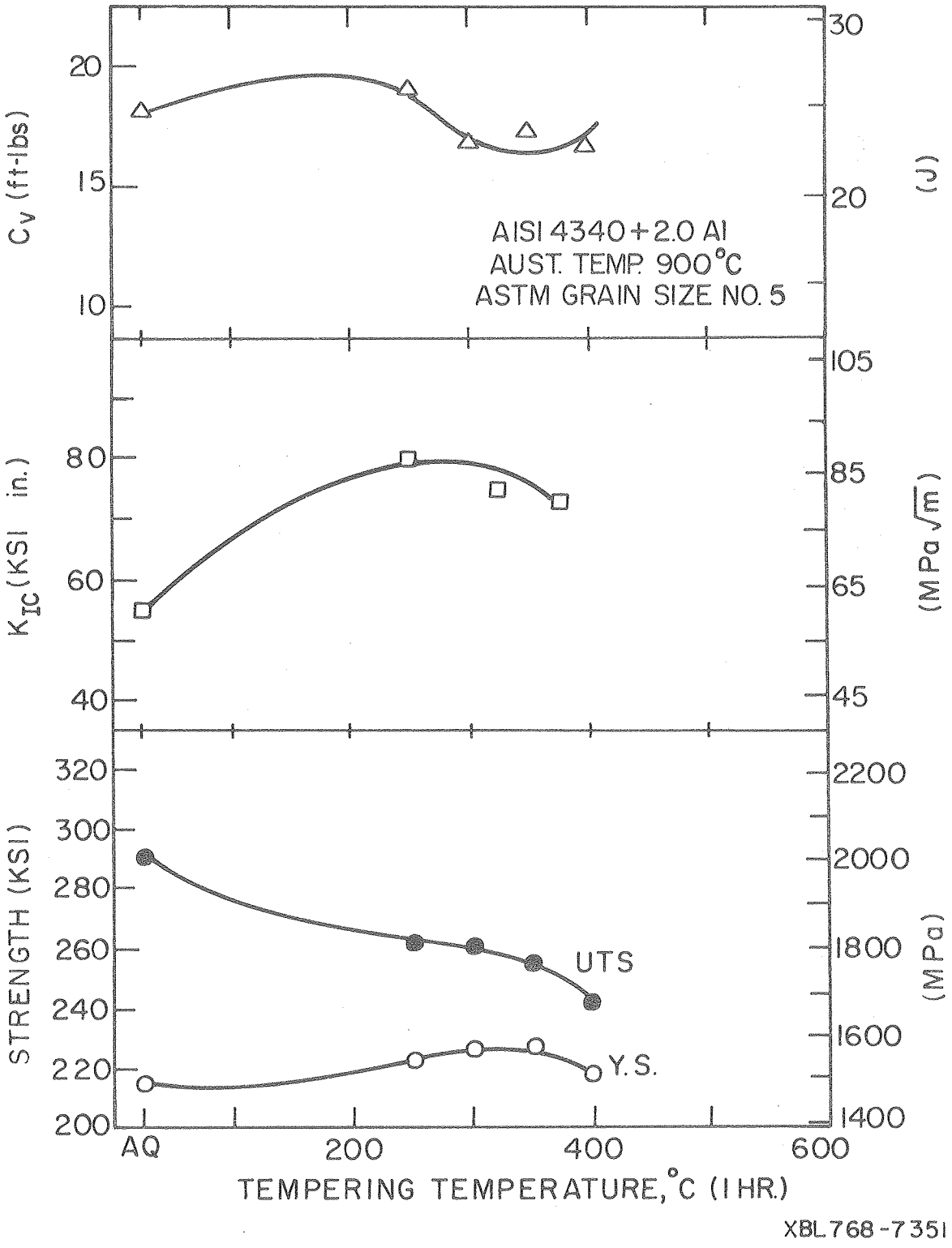

Fig. 17.

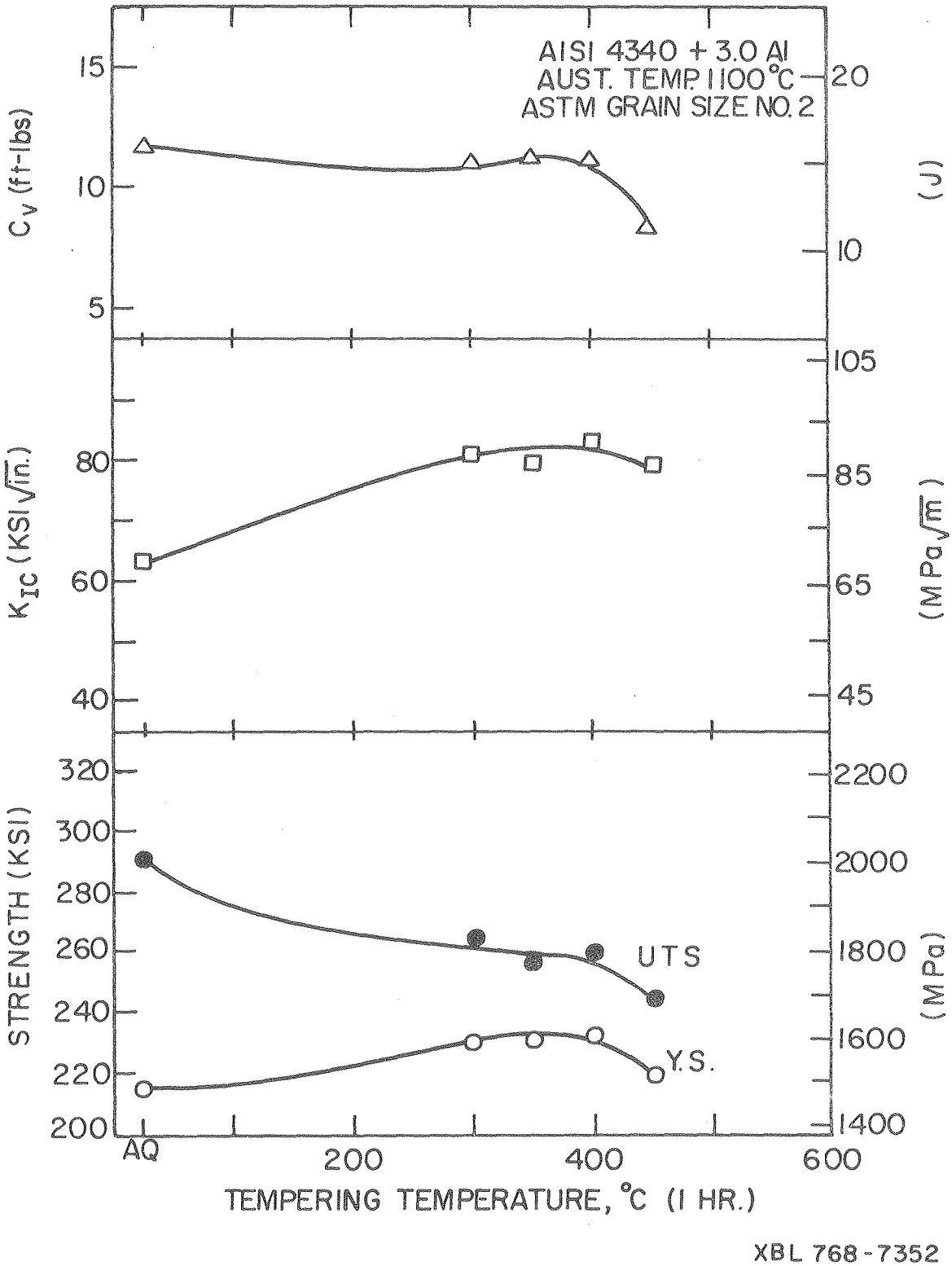
AISI 4340 + 3.0 Al
AUST. TEMP. 1100°C
ASTM GRAIN SIZE NO. 2
C_V (ft-lbs)
(J)
K_{IC} (KSI $\sqrt{in.}$)
(MPa $\sqrt{m}$)
STRENGTH (KSI)
(MPa)
UTS
Y.S.
AQ
TEMPERING TEMPERATURE, °C (1 HR.)
XBL 768-7352

Fig. 18.

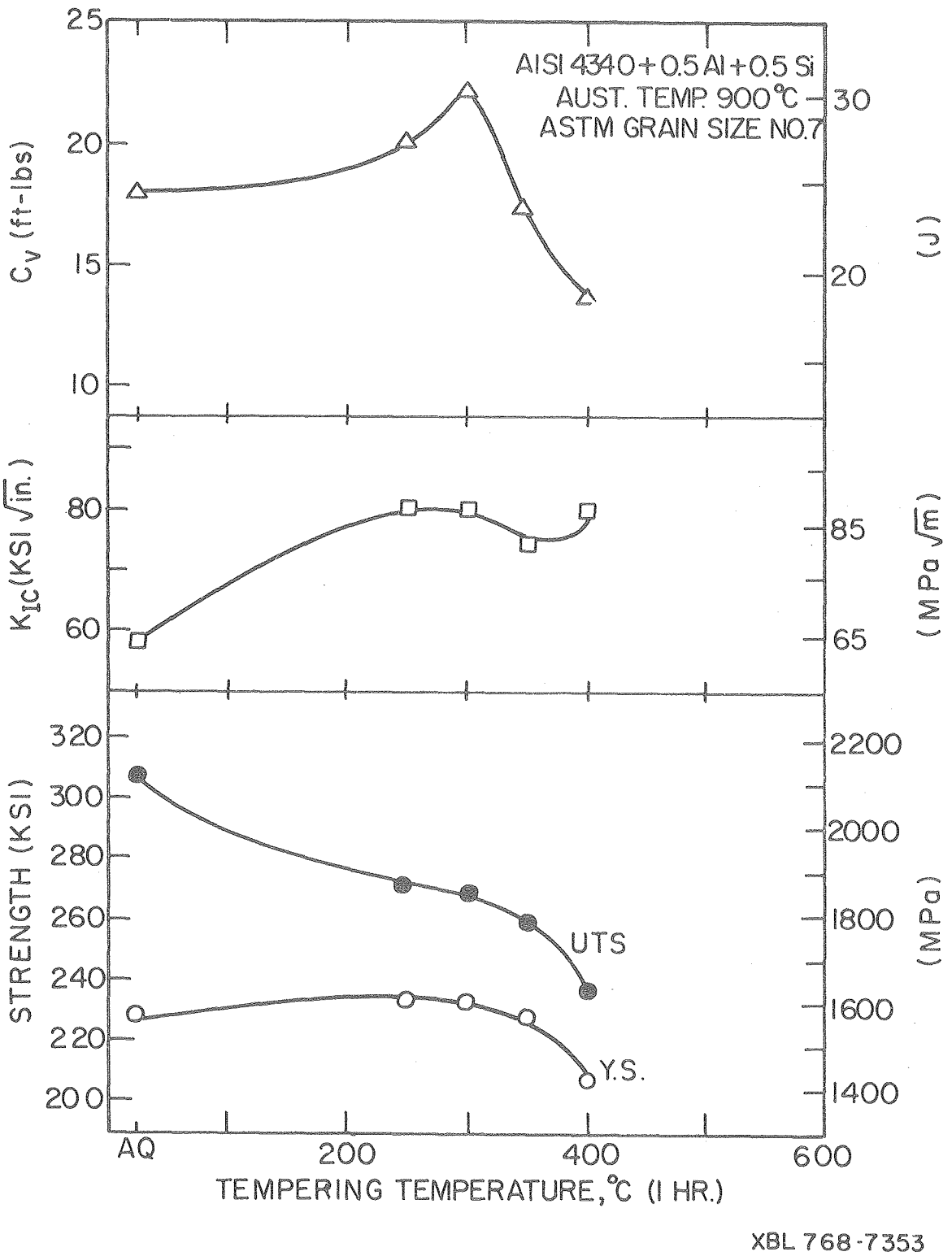

Fig. 19.

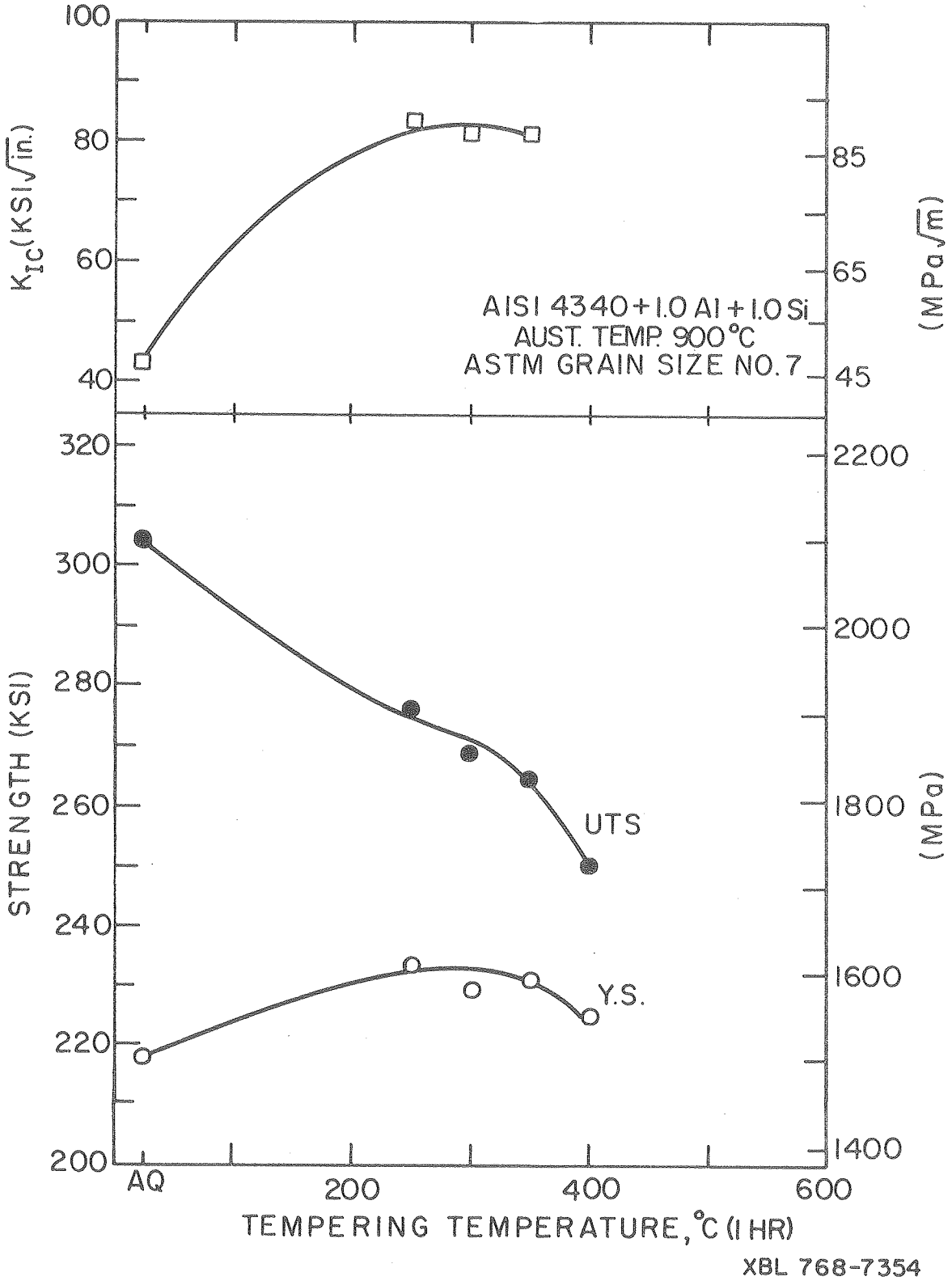
100
80
60
40
K_{IC}(KSI$\sqrt{in.}$)
85
65
45
(MPa$\sqrt{m}$)
AISI 4340+1.0 Al+1.0 Si
AUST. TEMP. 900°C
ASTM GRAIN SIZE NO. 7
320
300
280
260
240
220
200
STRENGTH (KSI)
2200
2000
1800
1600
1400
(MPa)
UTS
Y.S.
AQ
200
400
600
TEMPERING TEMPERATURE, °C (1 HR)
XBL 768-7354

Fig. 20.

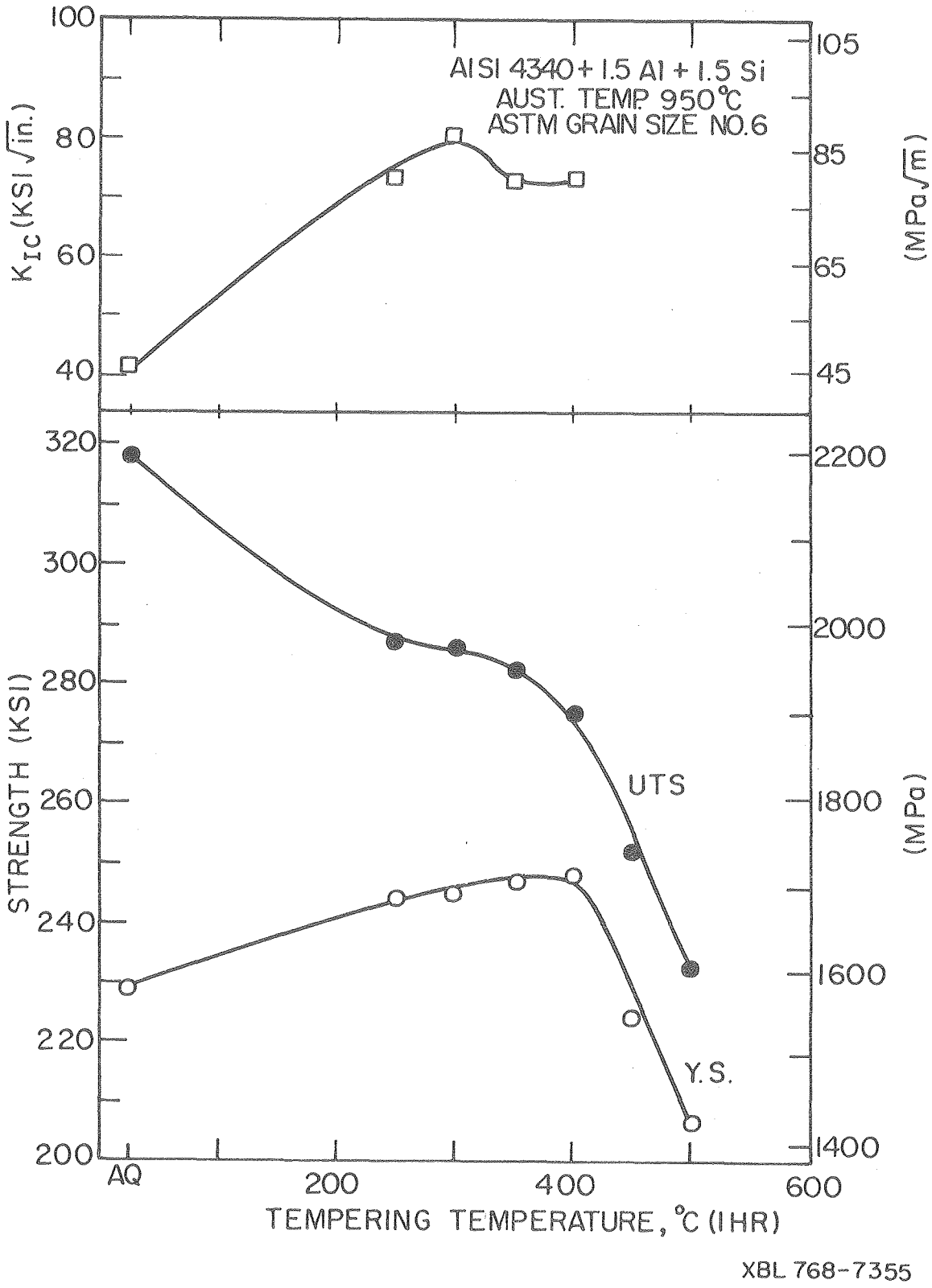

Fig. 21.

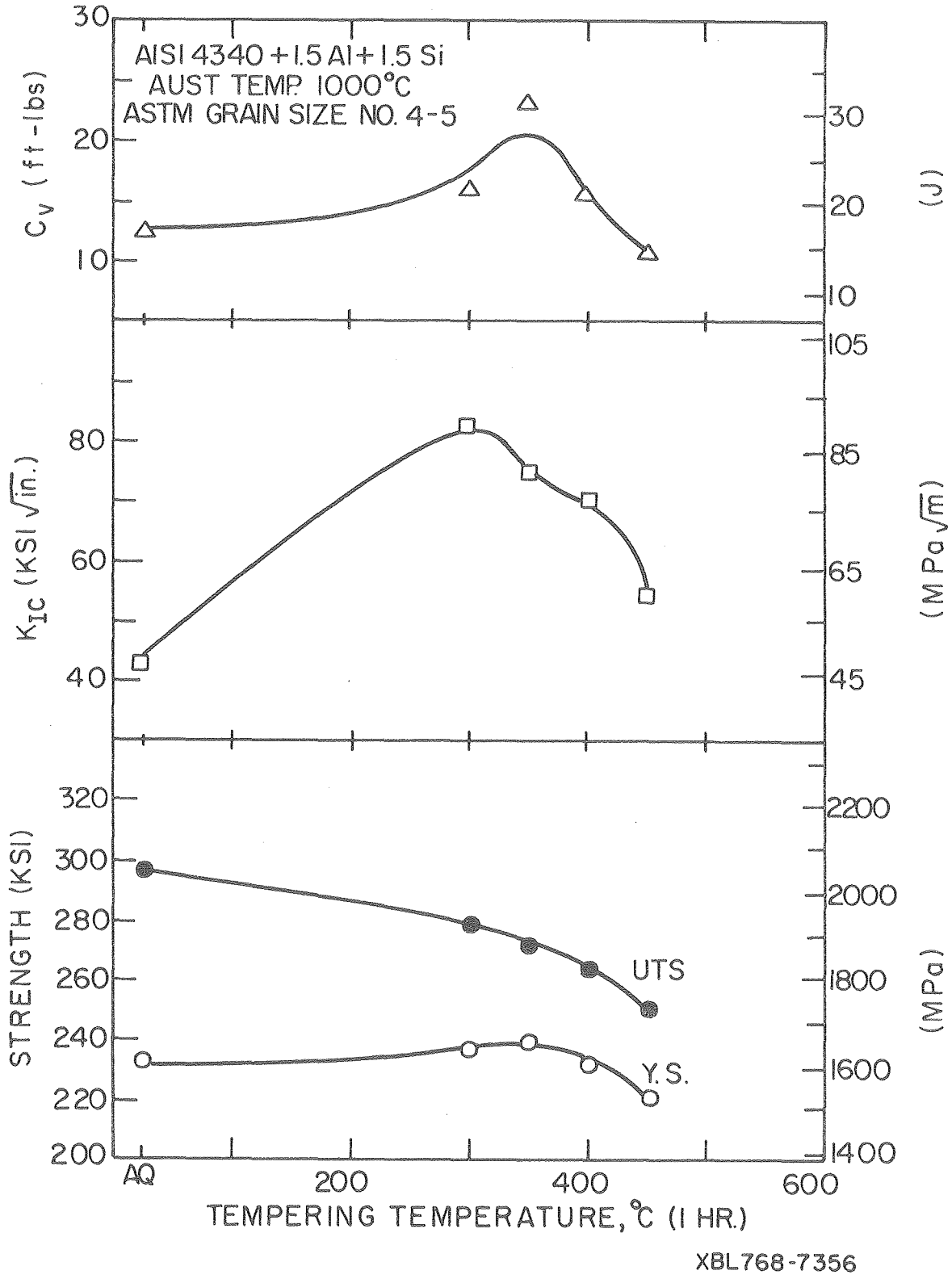
AISI 4340 + 1.5 Al + 1.5 Si
AUST TEMP. 1000°C
ASTM GRAIN SIZE NO. 4-5
C_V (ft-lbs)
(J)
K_{IC} (KSI $\sqrt{in.}$)
(MPa $\sqrt{m}$)
STRENGTH (KSI)
(MPa)
UTS
Y.S.
AQ
TEMPERING TEMPERATURE, °C (1 HR.)
XBL768-7356

Fig. 22.

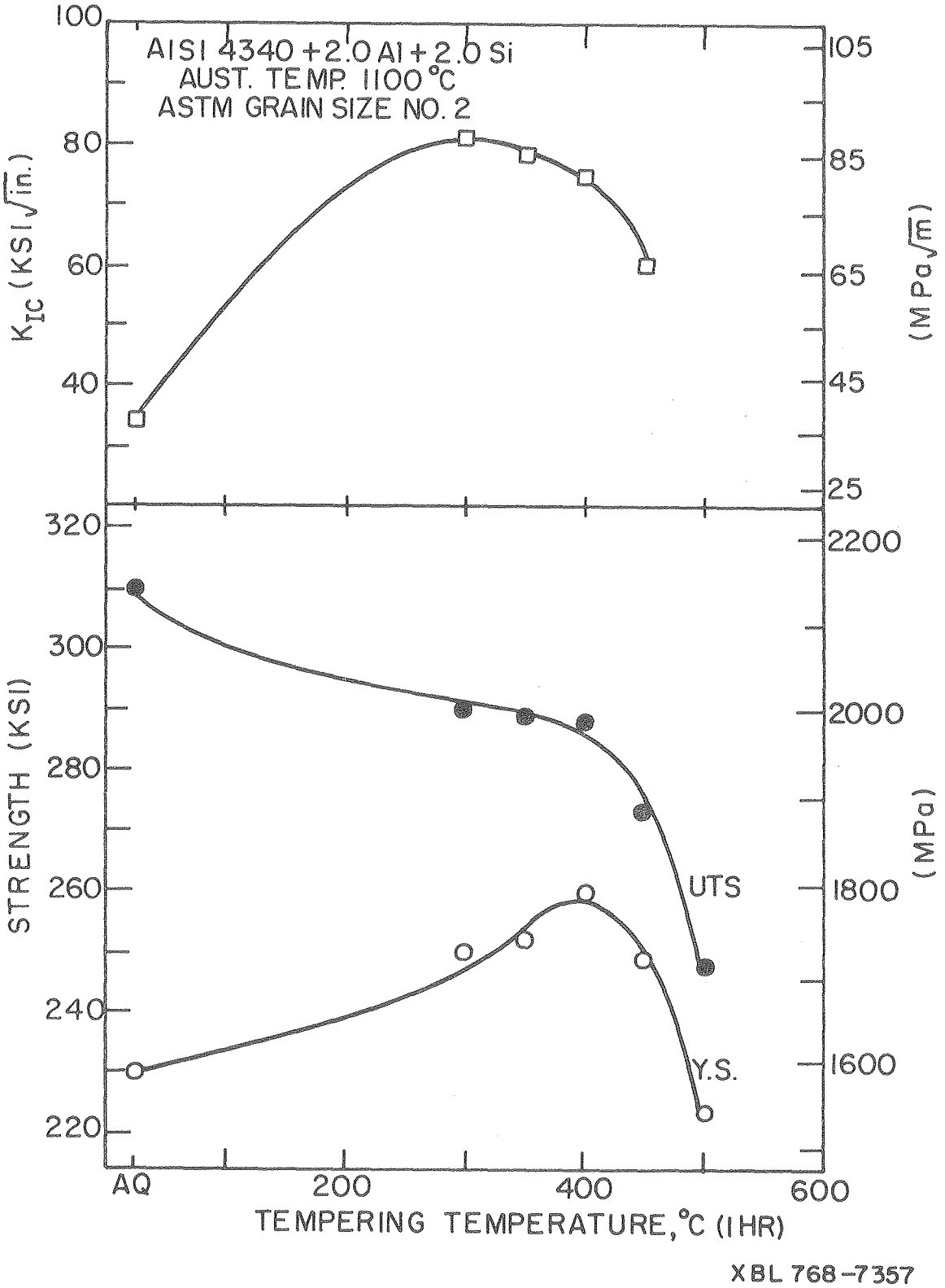

Fig. 23.

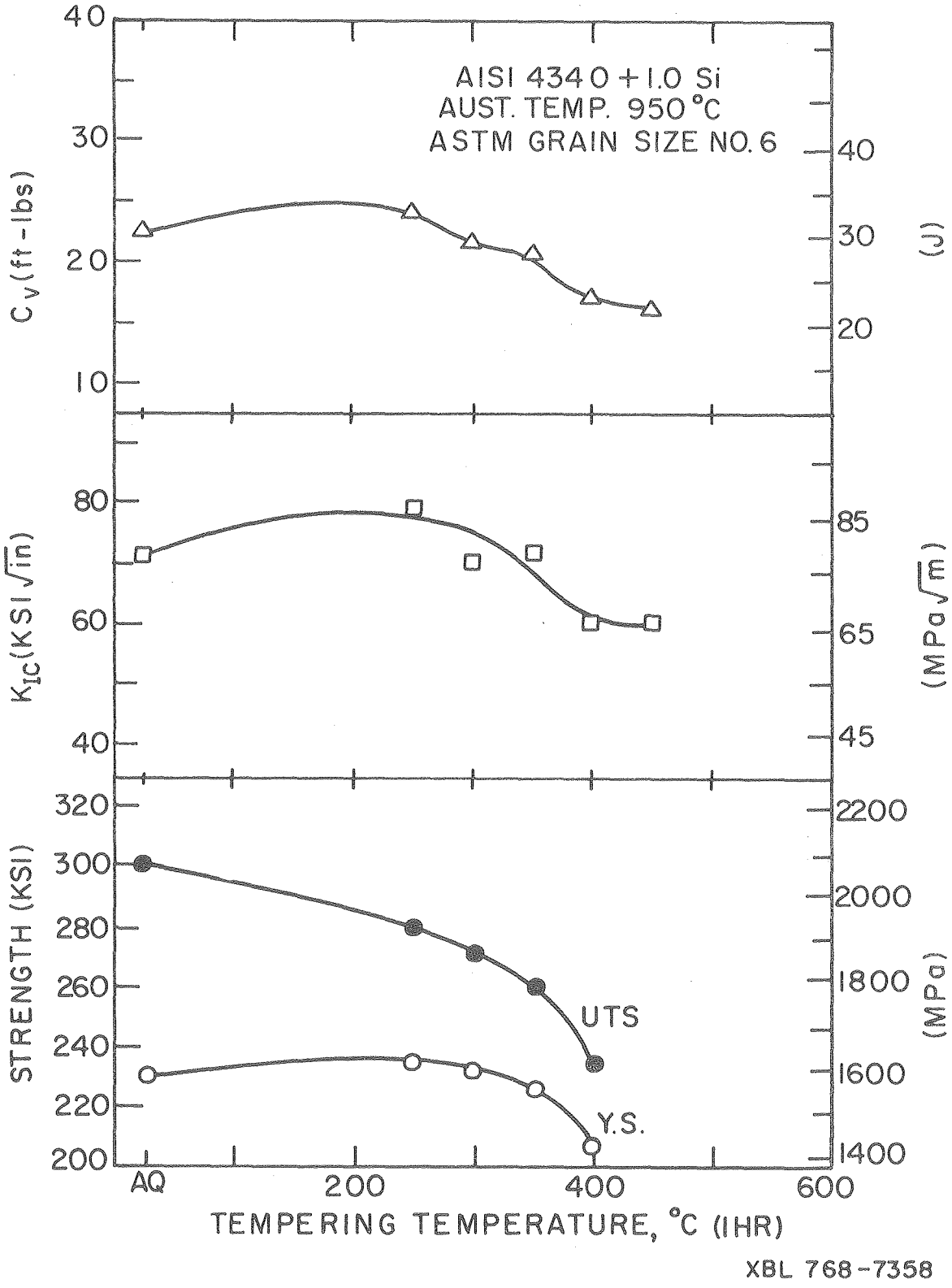
AISI 4340 + 1.0 Si
AUST. TEMP. 950°C
ASTM GRAIN SIZE NO. 6
C_v (ft-lbs)
(J)
K_{IC} (KSI $\sqrt{in}$)
(MPa $\sqrt{m}$)
STRENGTH (KSI)
(MPa)
UTS
Y.S.
AQ
200
400
600
TEMPERING TEMPERATURE, °C (1HR)
XBL 768-7358

Fig. 24.

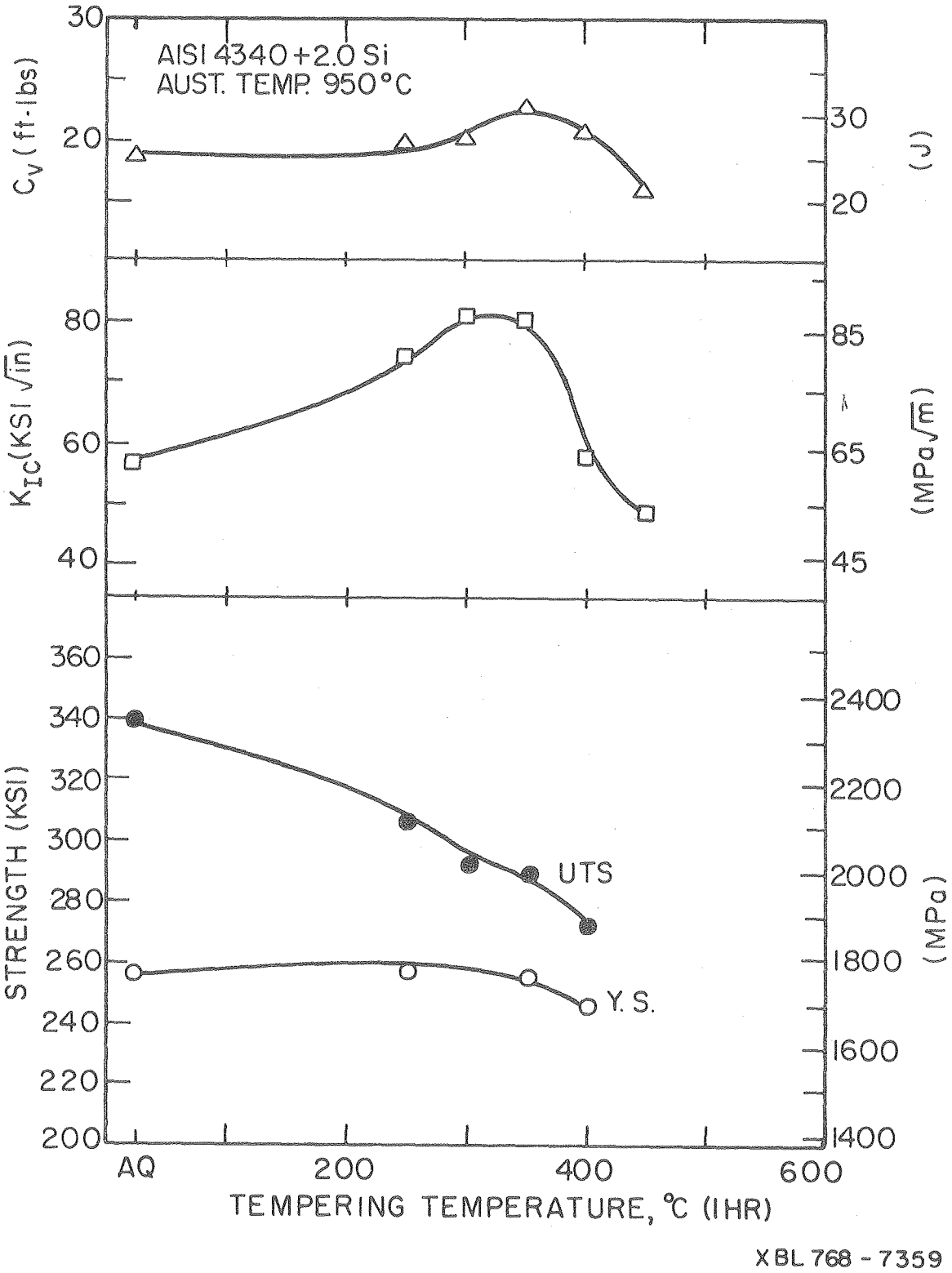

Fig. 25.

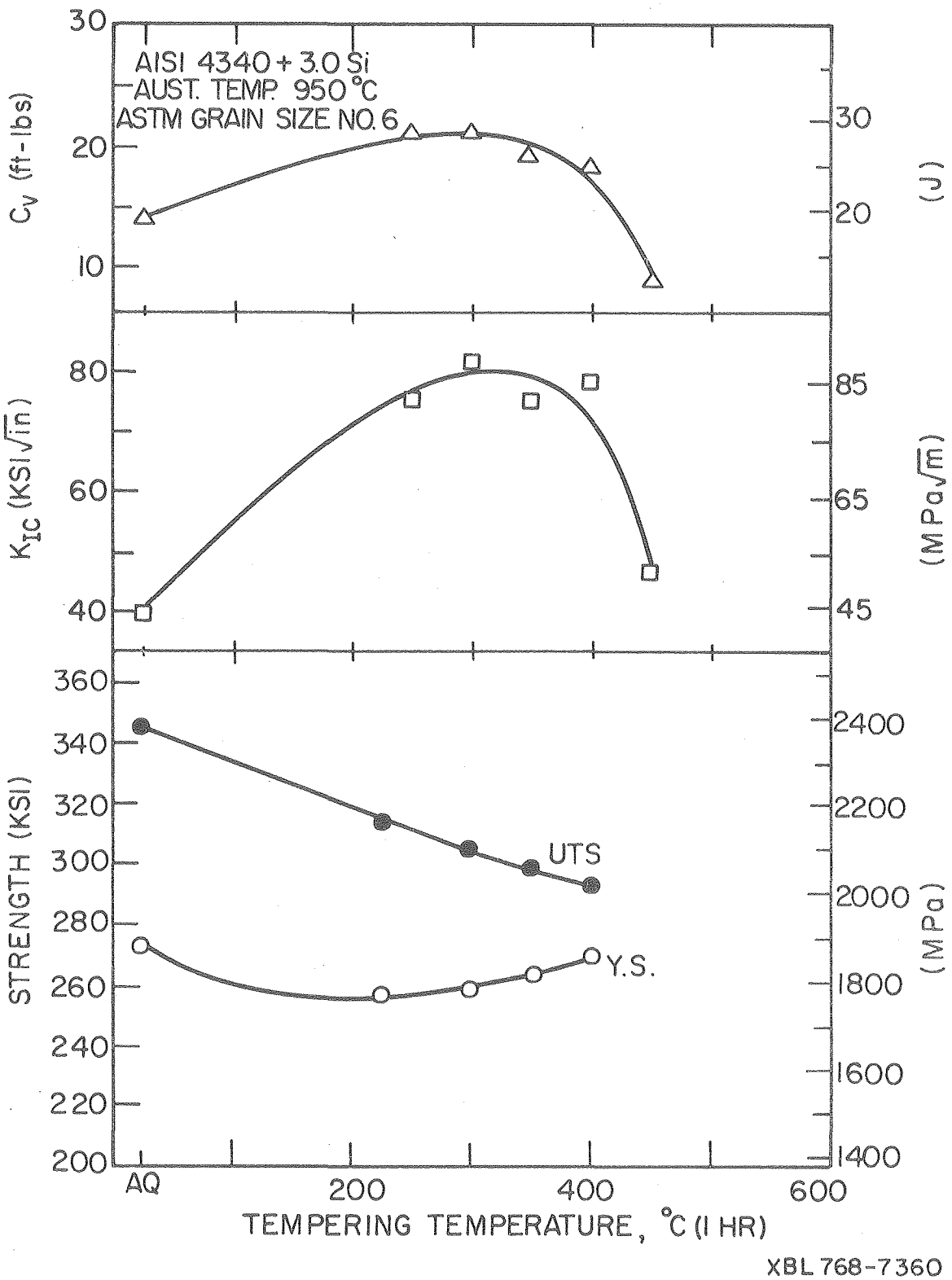
AISI 4340 + 3.0 Si
AUST. TEMP. 950°C
ASTM GRAIN SIZE NO. 6
C_V (ft-lbs)
(J)
K_{IC} (KSI$\sqrt{in}$)
(MPa$\sqrt{m}$)
STRENGTH (KSI)
(MPa)
UTS
Y.S.
AQ
TEMPERING TEMPERATURE, °C (1 HR)
XBL 768-7360

Fig. 26.

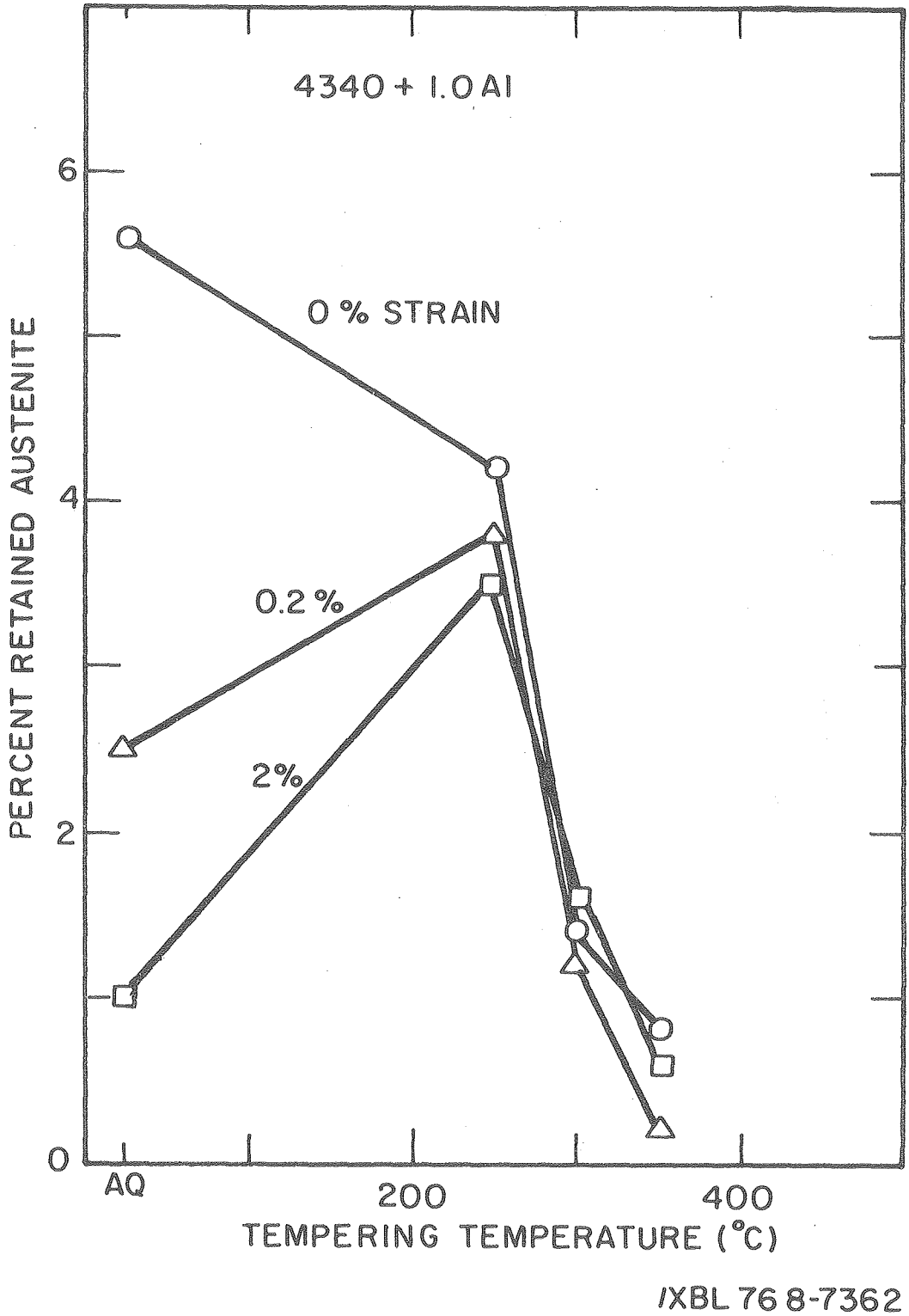

Fig. 27.

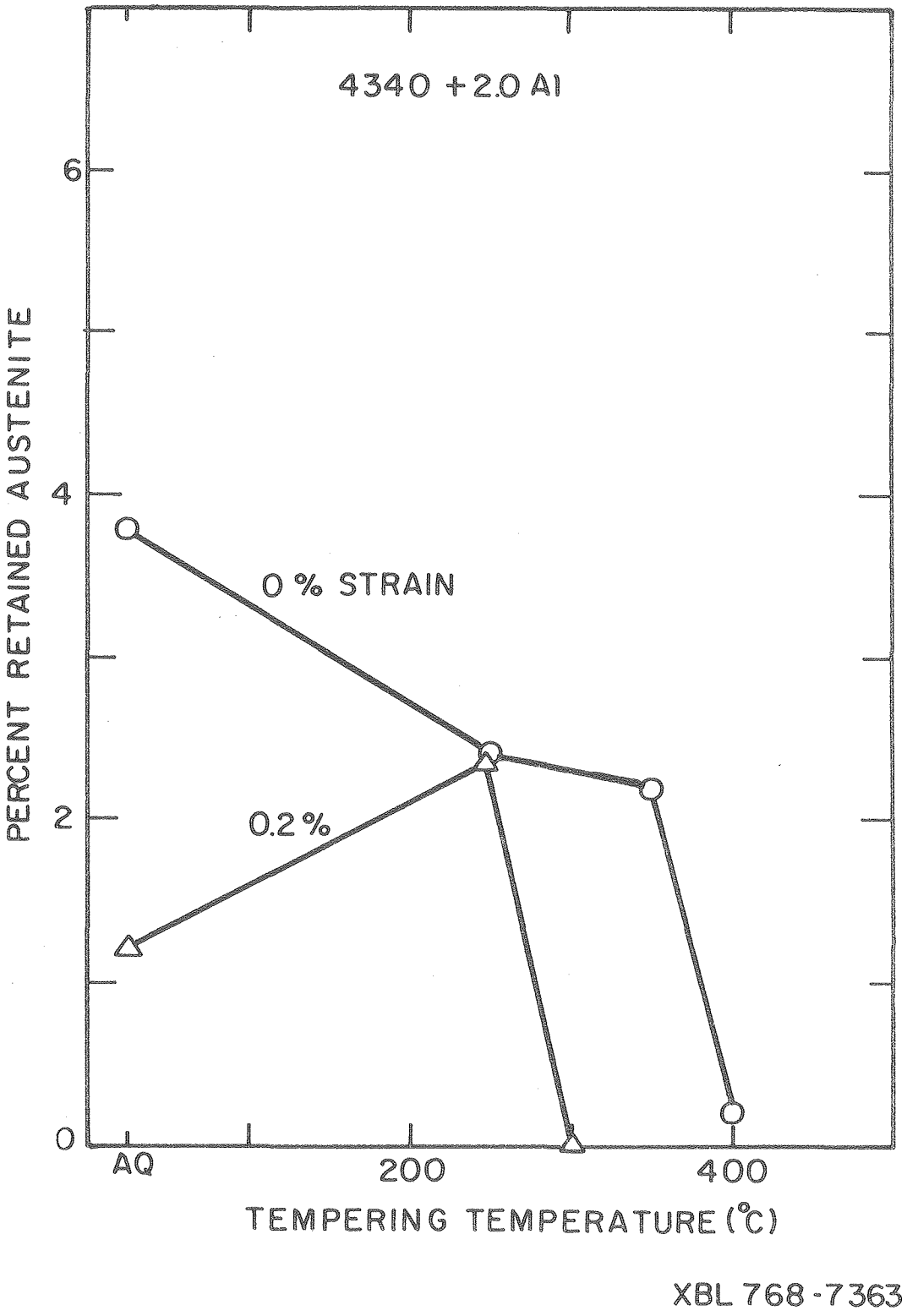
4340 + 2.0 Al
PERCENT RETAINED AUSTENITE
6
4
2
0
0 % STRAIN
0.2 %
AQ
200
400
TEMPERING TEMPERATURE (°C)
XBL 768-7363

Fig. 28.

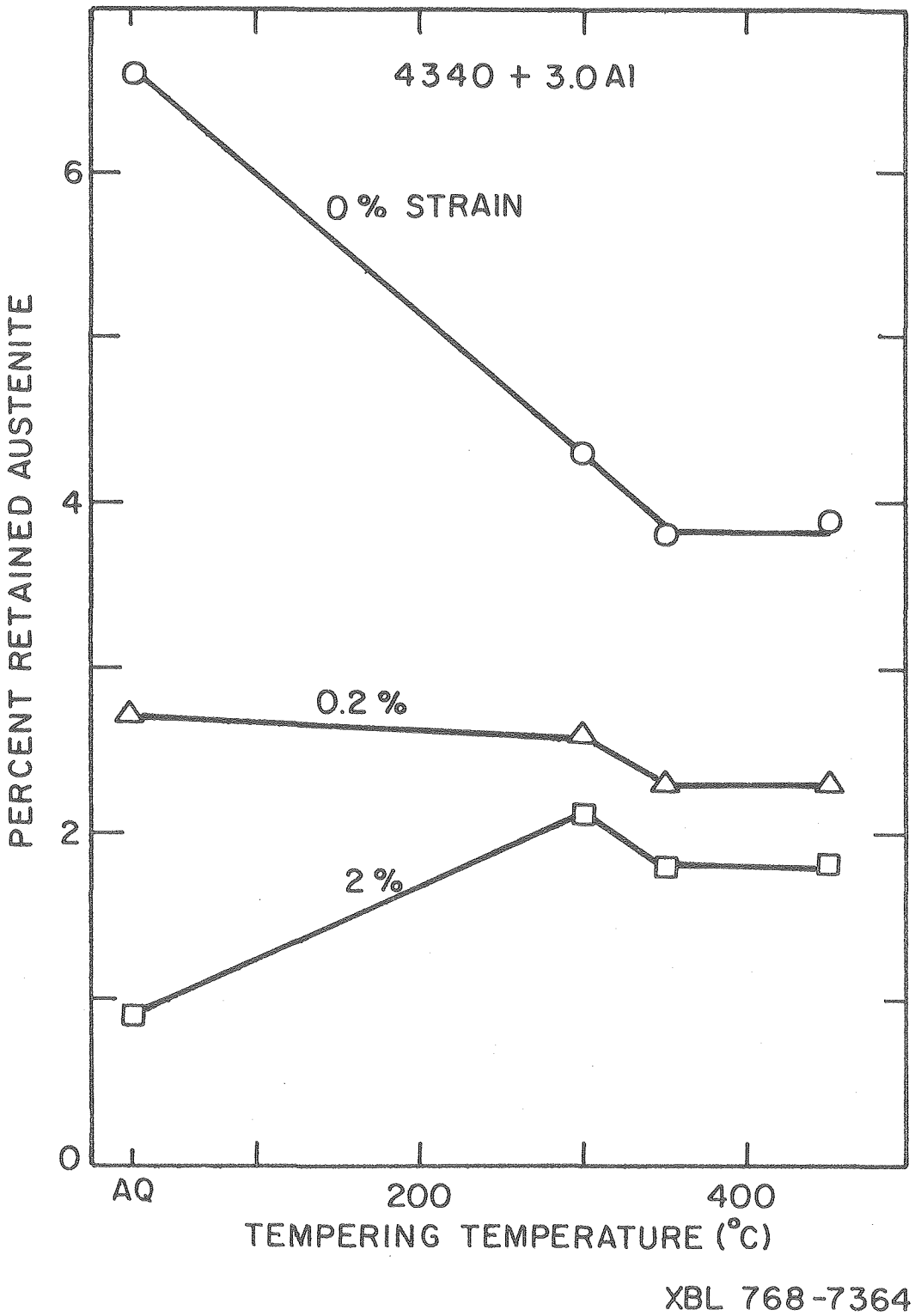

Fig. 29.

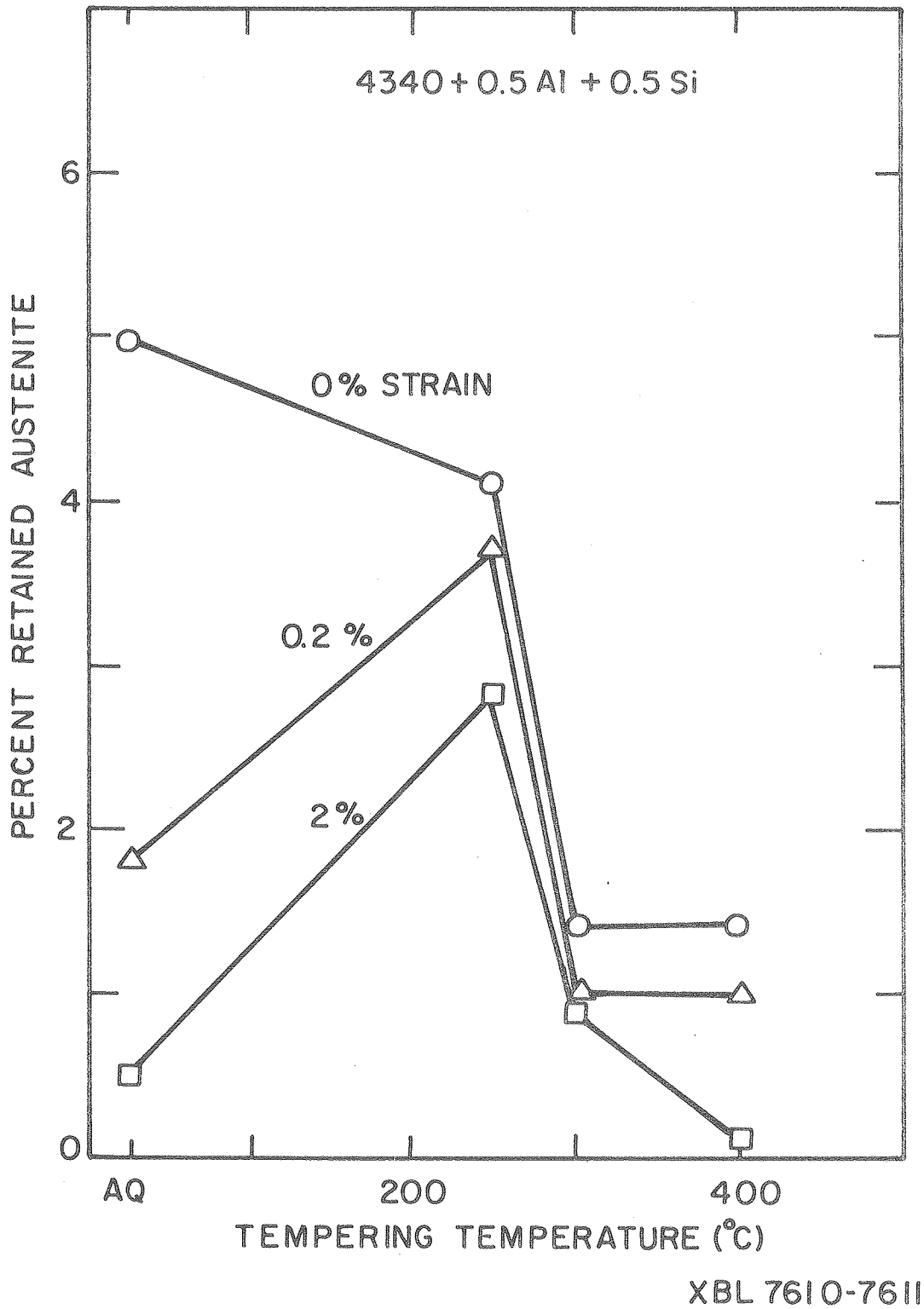
4340 + 0.5 Al + 0.5 Si
PERCENT RETAINED AUSTENITE
0
2
4
6
0% STRAIN
0.2 %
2%
AQ
200
400
TEMPERING TEMPERATURE (°C)
XBL 7610-7611

Fig. 30.

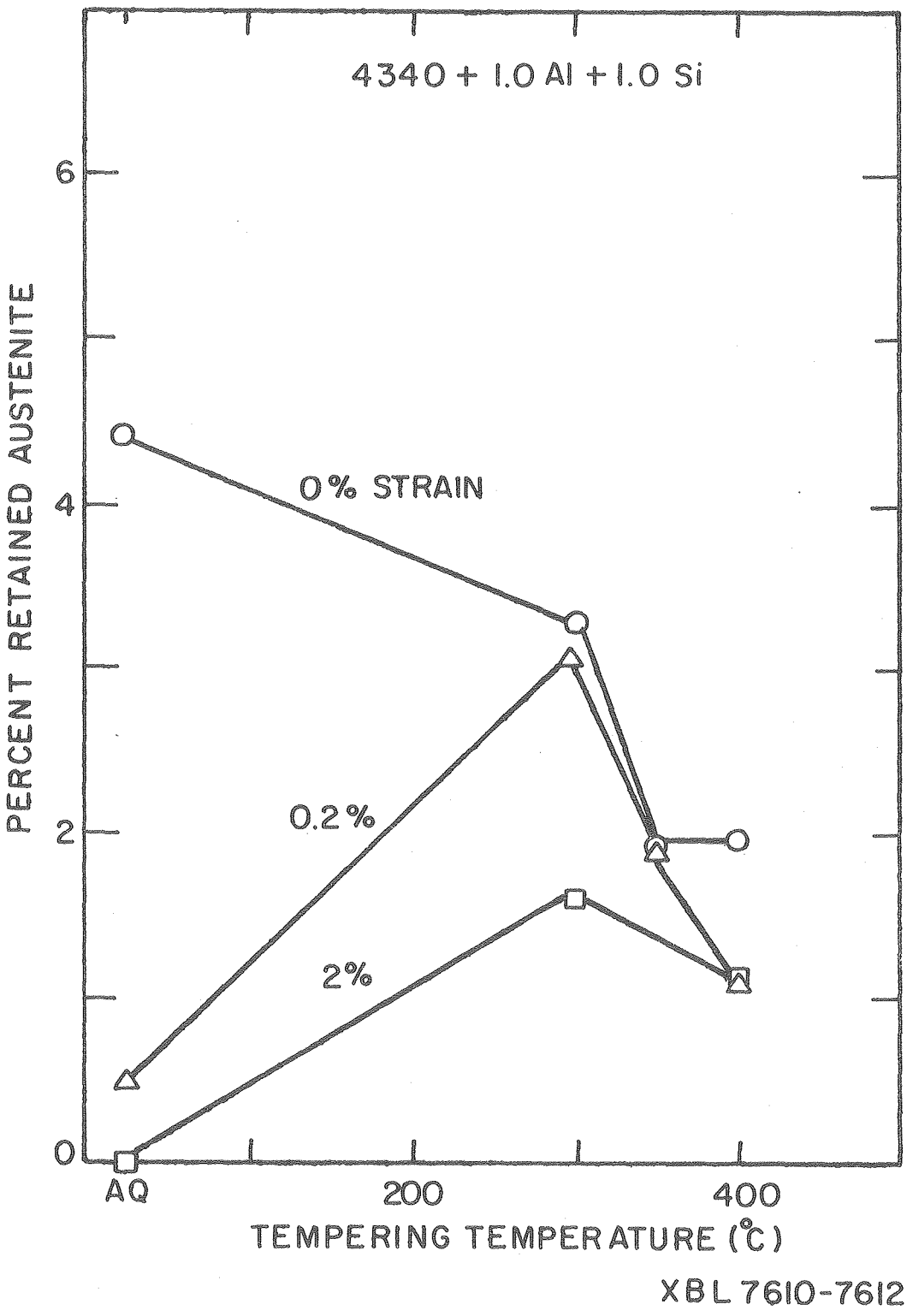

Fig. 31.

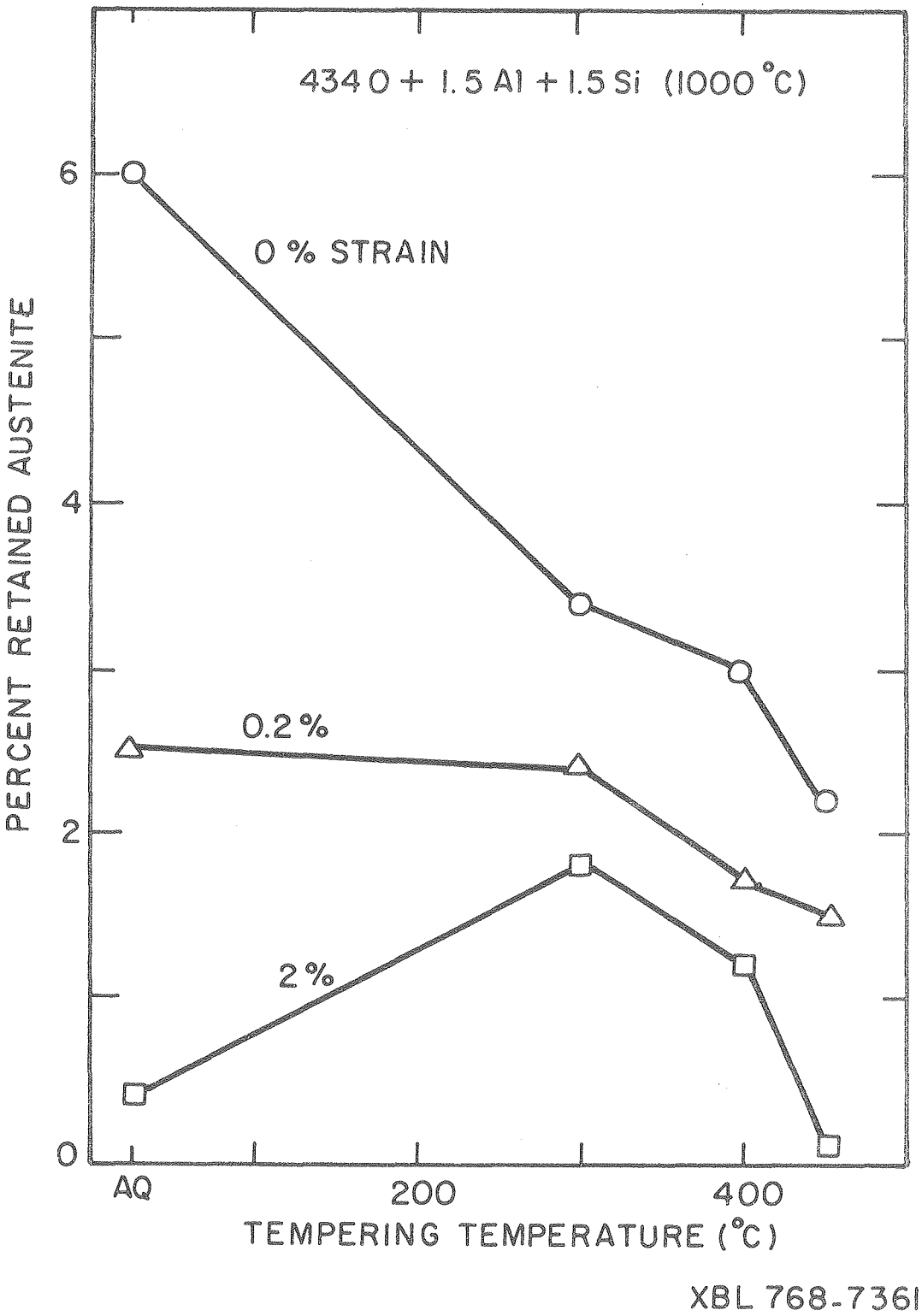
4340 + 1.5 Al + 1.5 Si (1000 °C)
0 % STRAIN
0.2 %
2 %
PERCENT RETAINED AUSTENITE
0
2
4
6
AQ
200
400
TEMPERING TEMPERATURE (°C)
XBL 768-7361

Fig. 32.

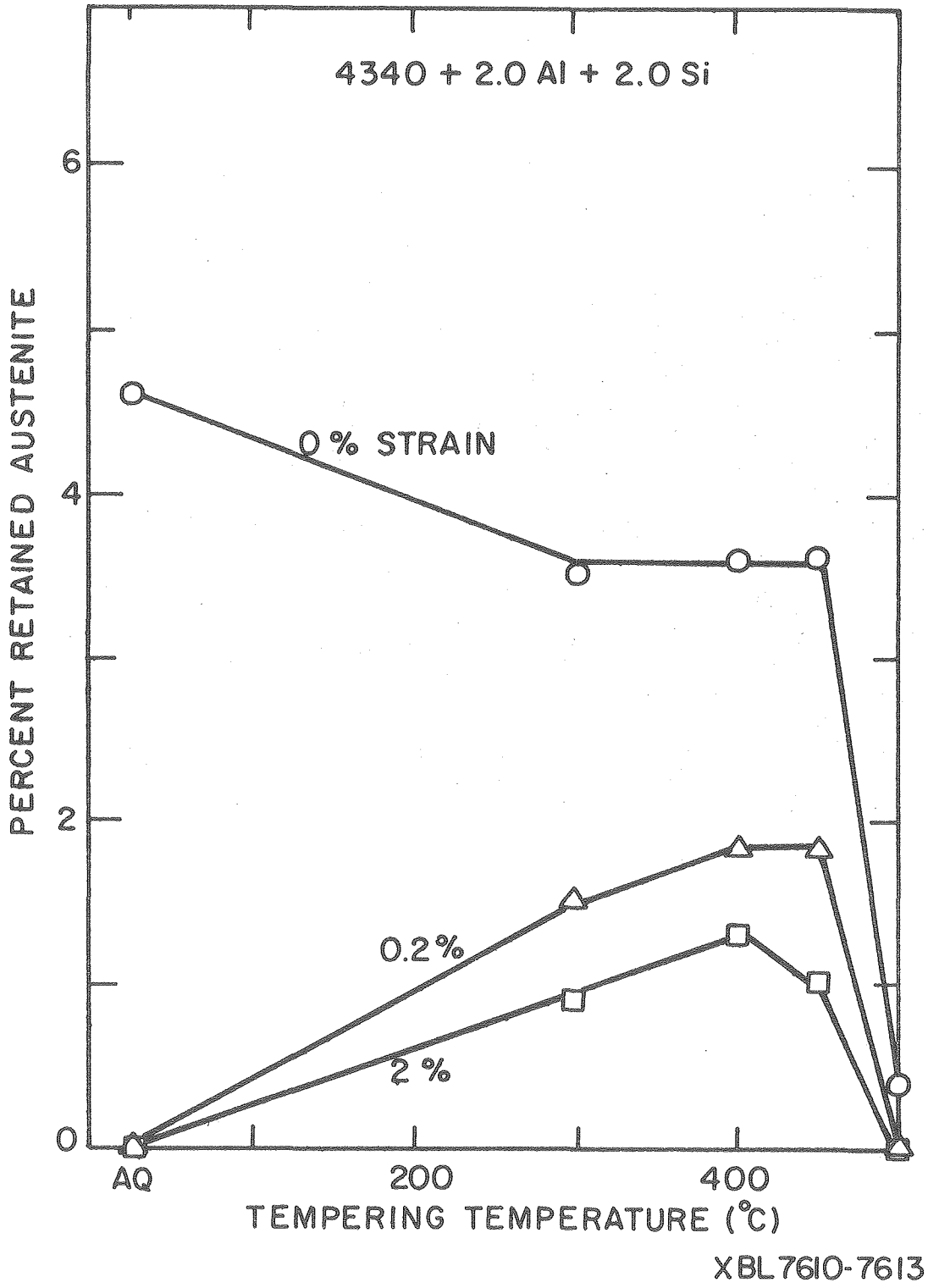

Fig. 33.

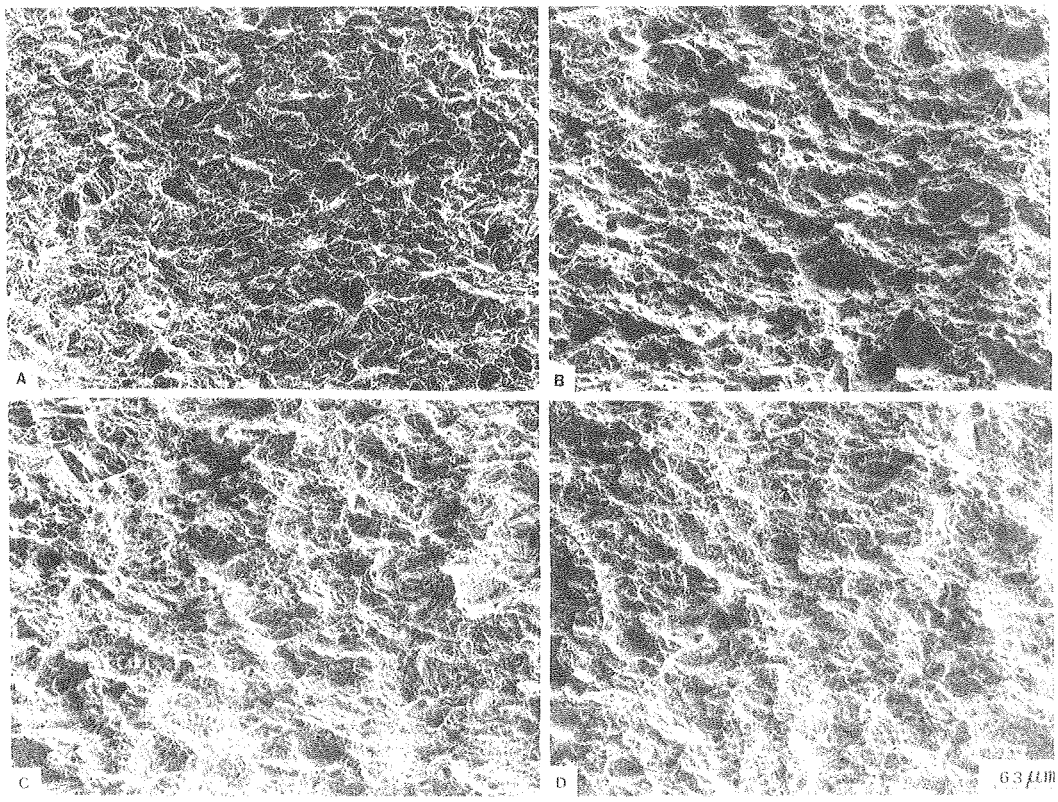

XBB 760-11027

Fig. 34.

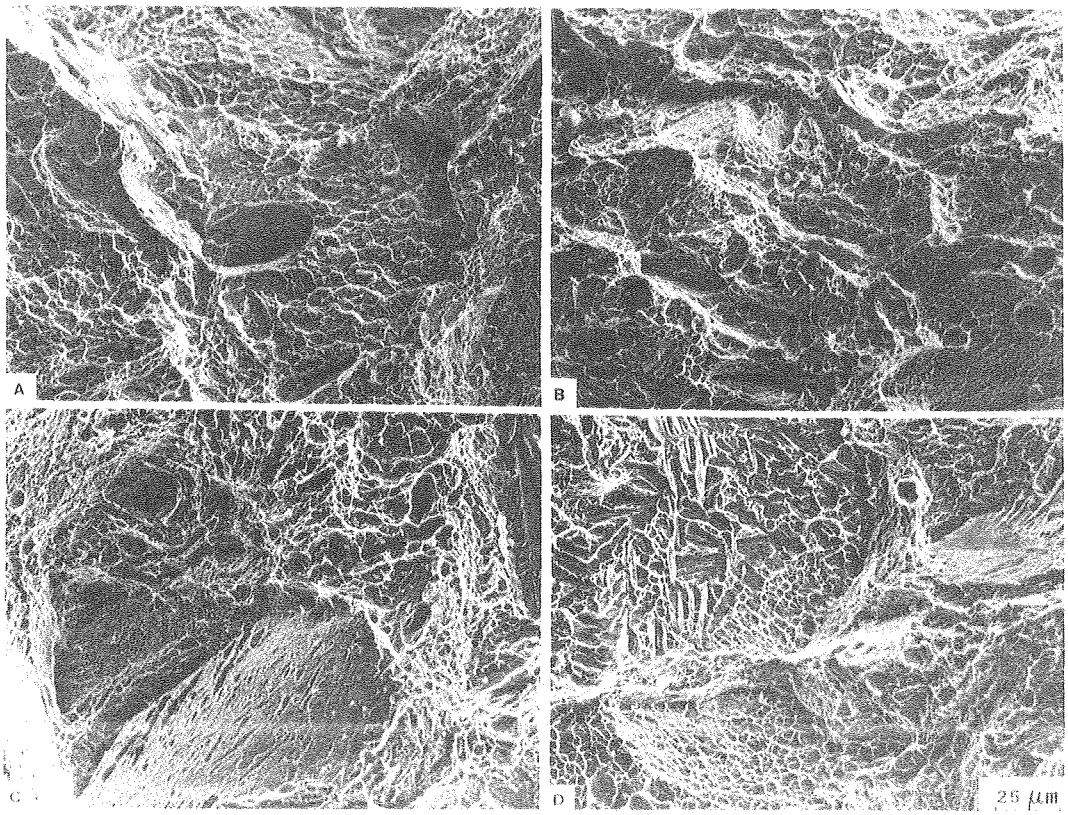

XBB 760-11014

Fig. 35.

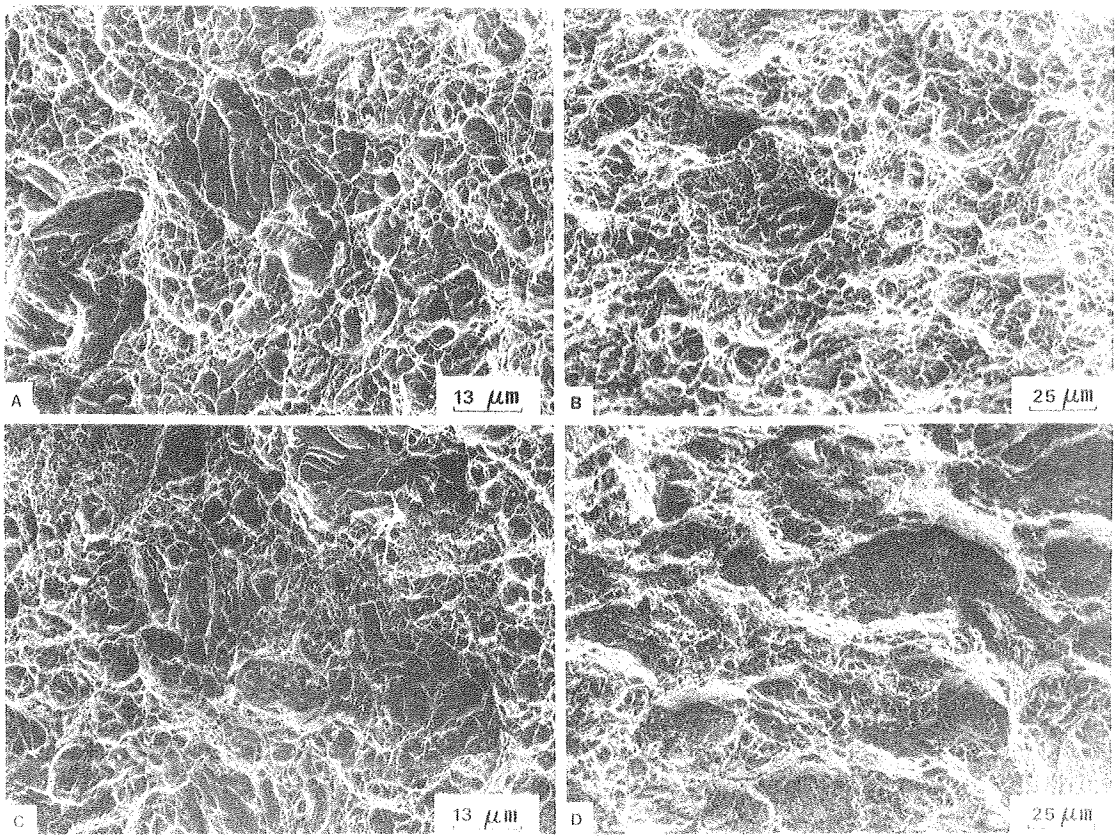

XBB 760-11025

Fig. 36.

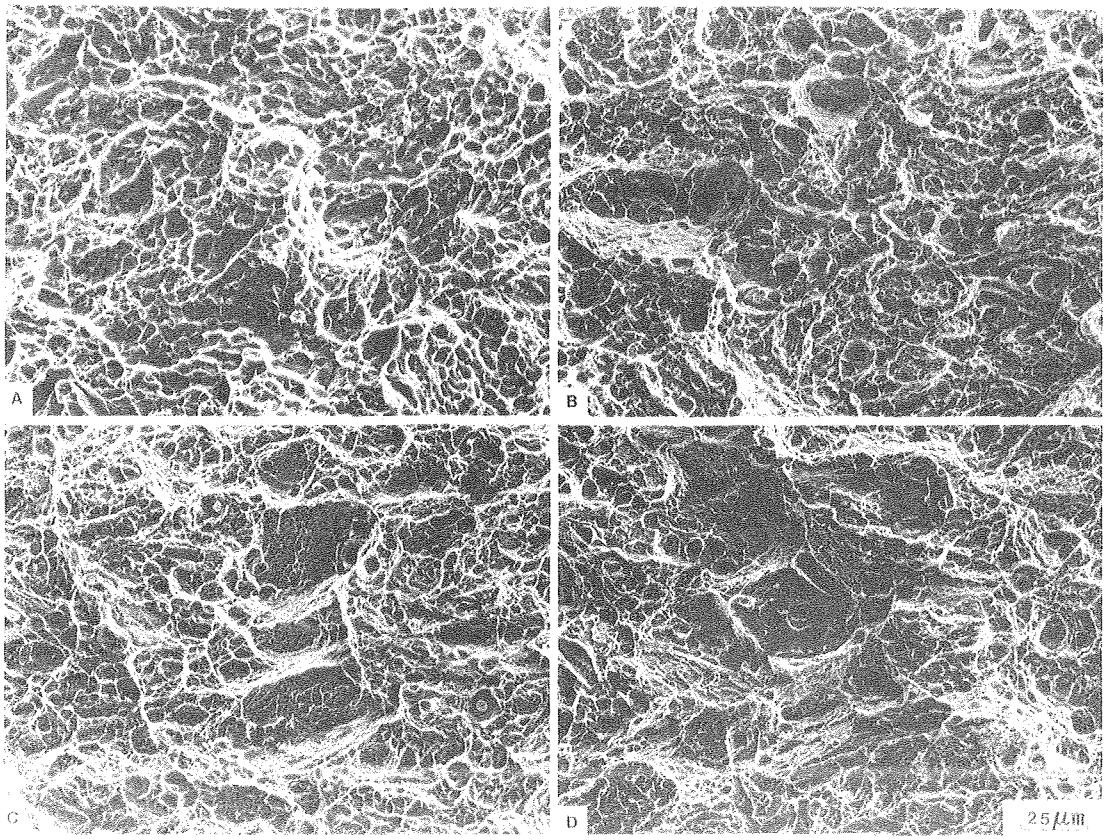

XBB 760-11026

Fig. 37.

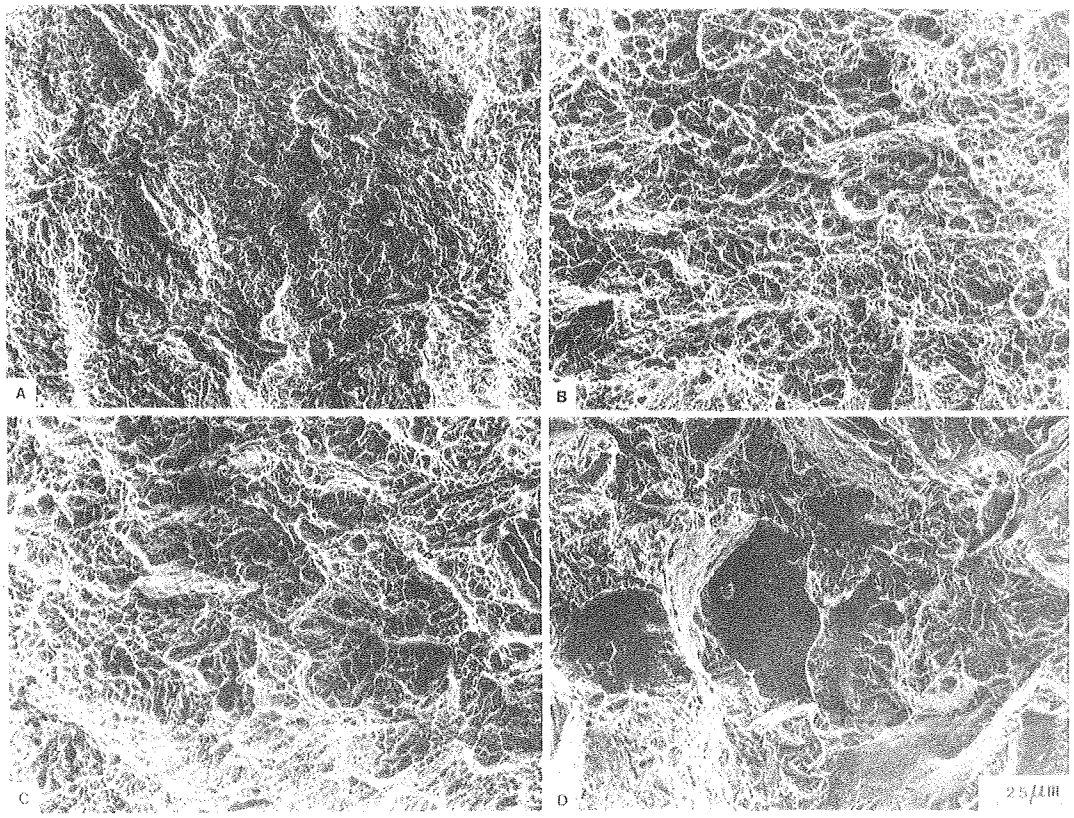

Fig. 38.

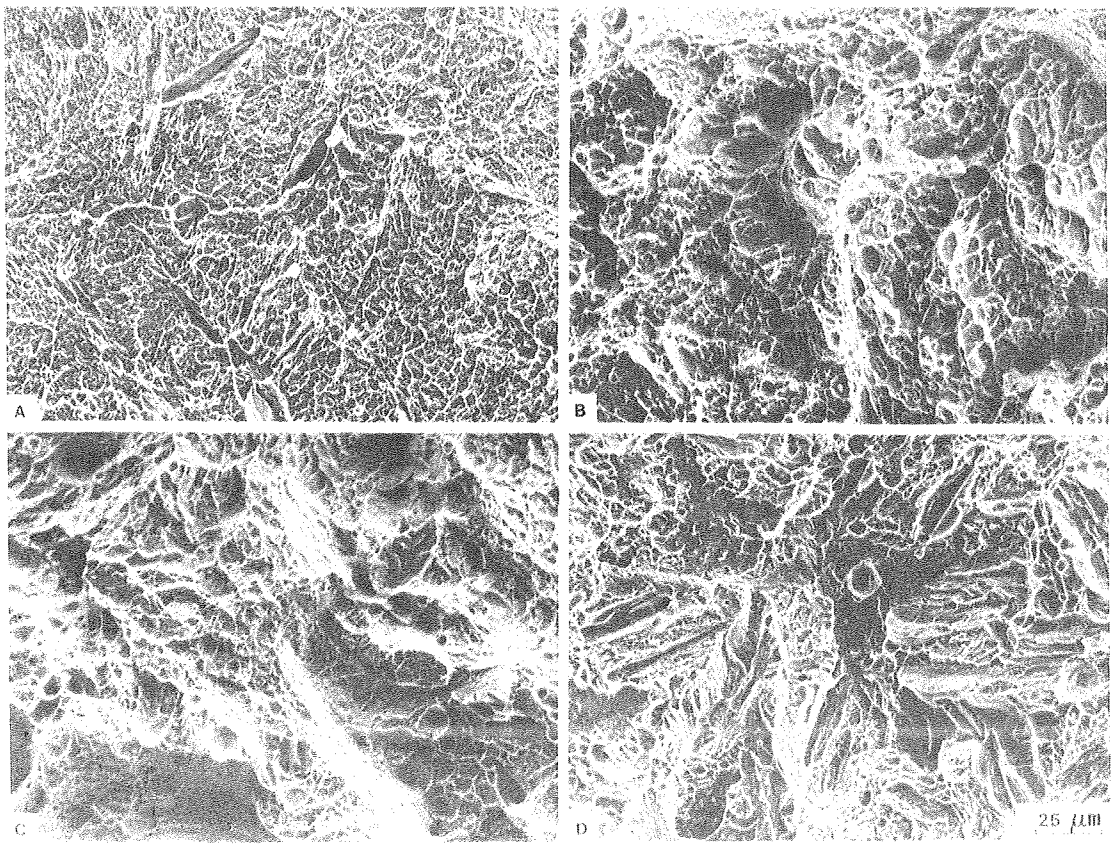

Fig. 39.

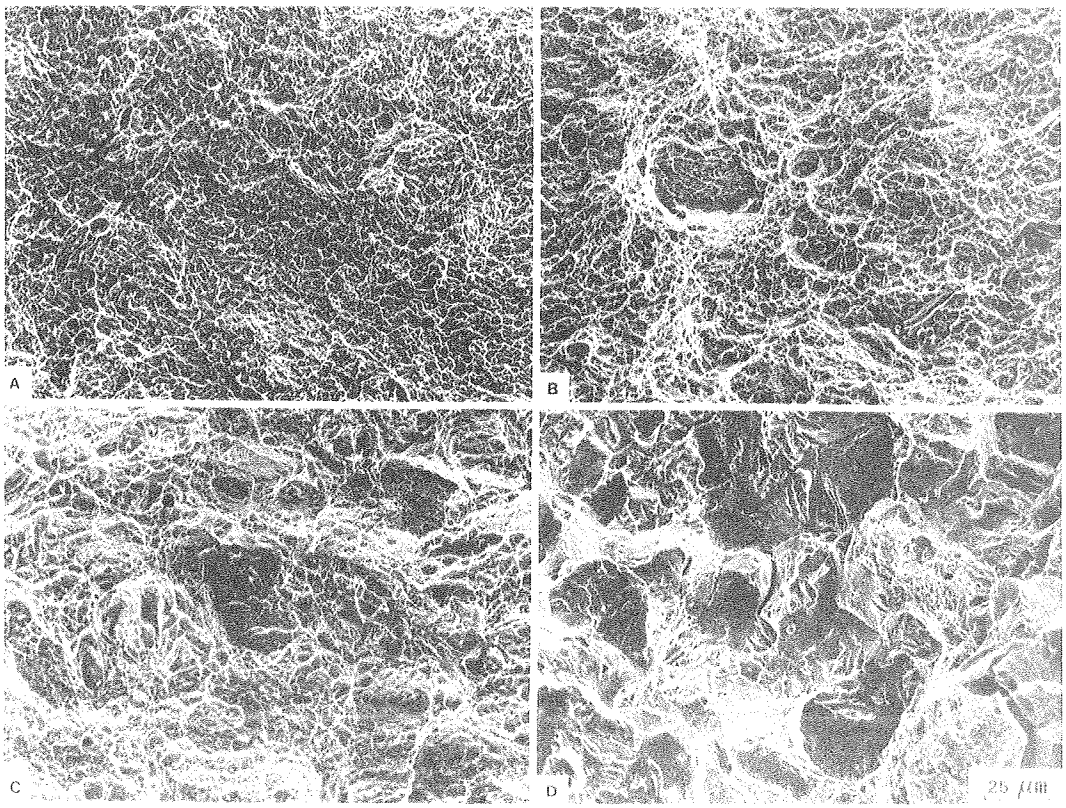

Fig. 40.

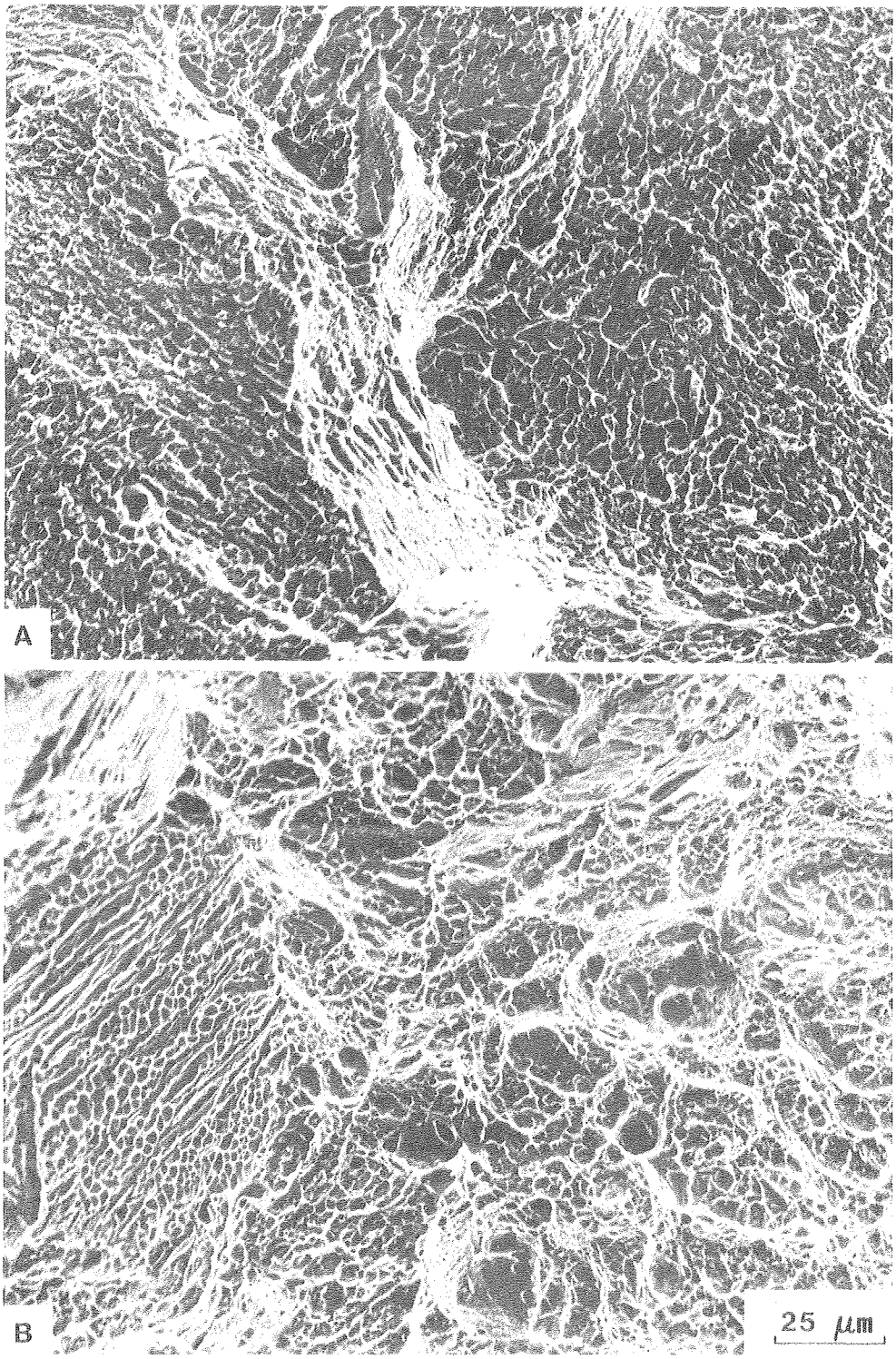

Fig. 41.

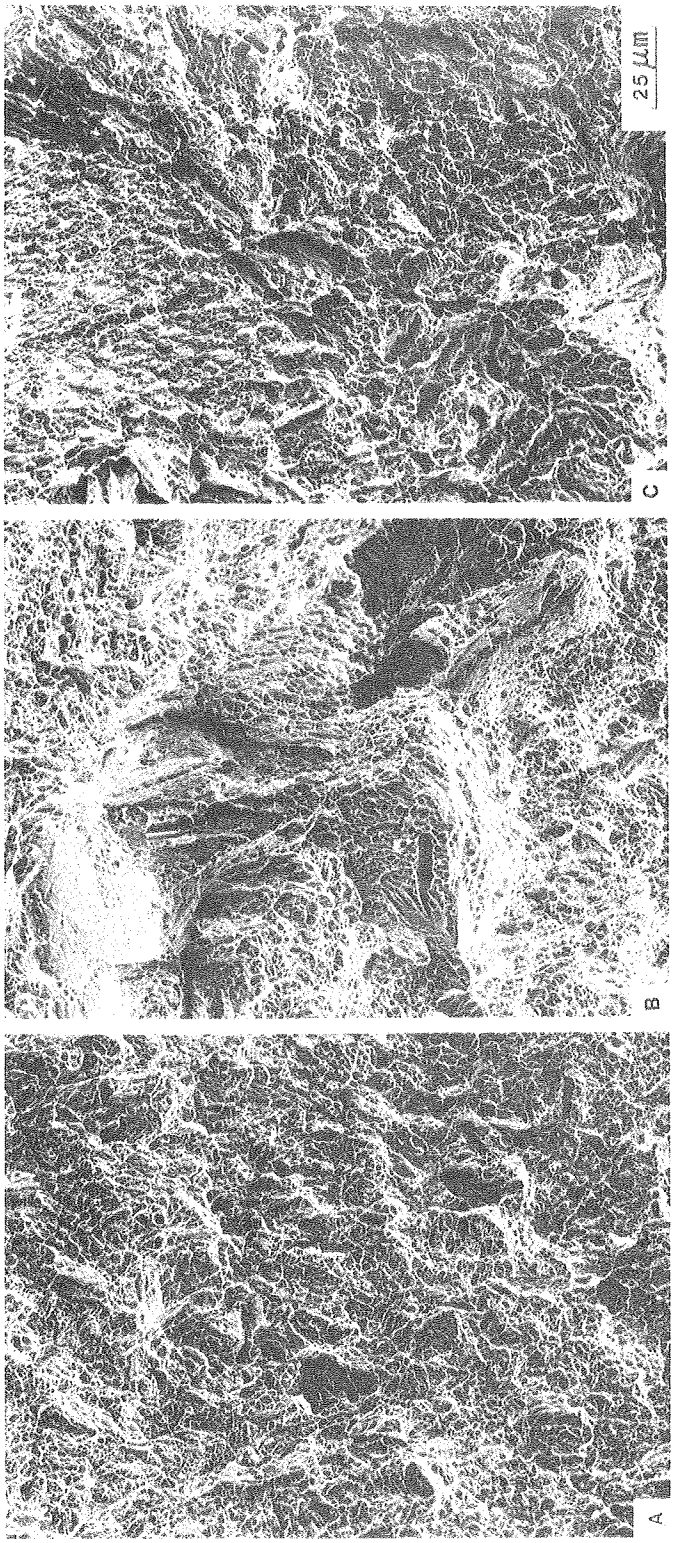

Fig. 42.

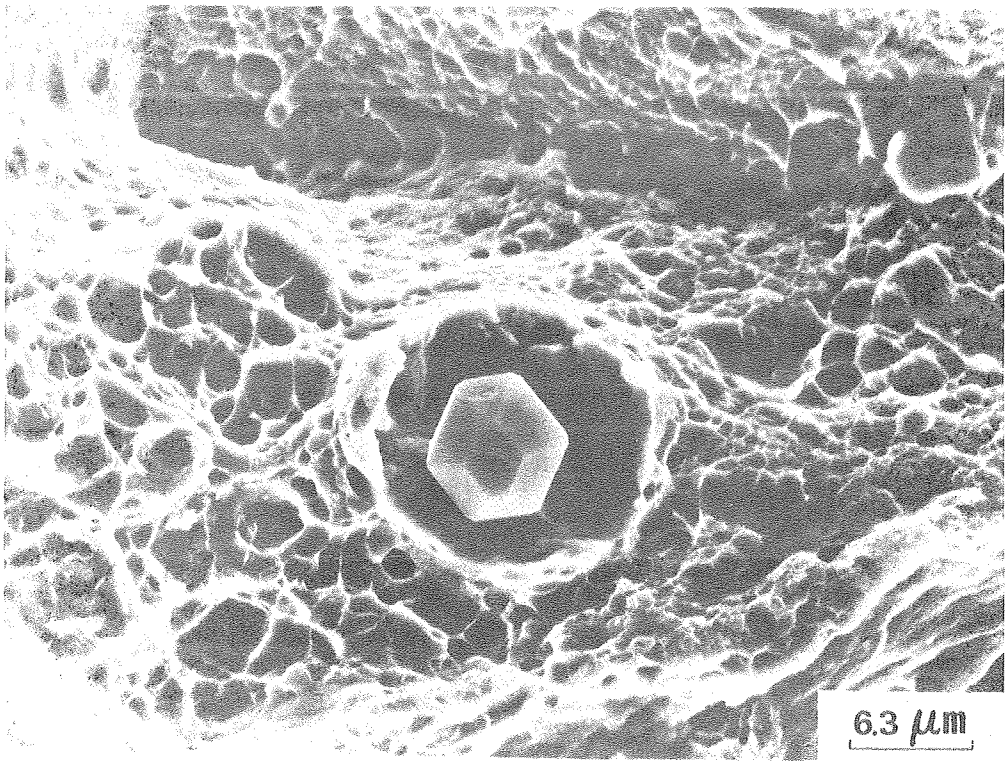

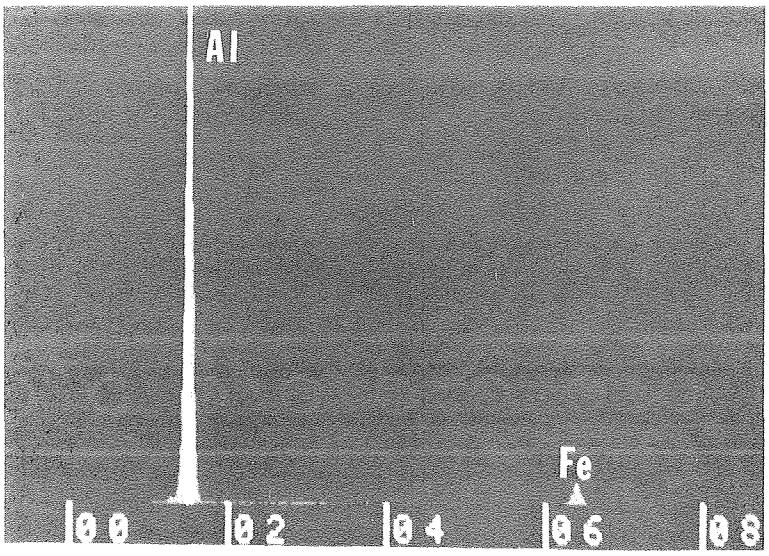

XBB 760-11018

Fig. 43.

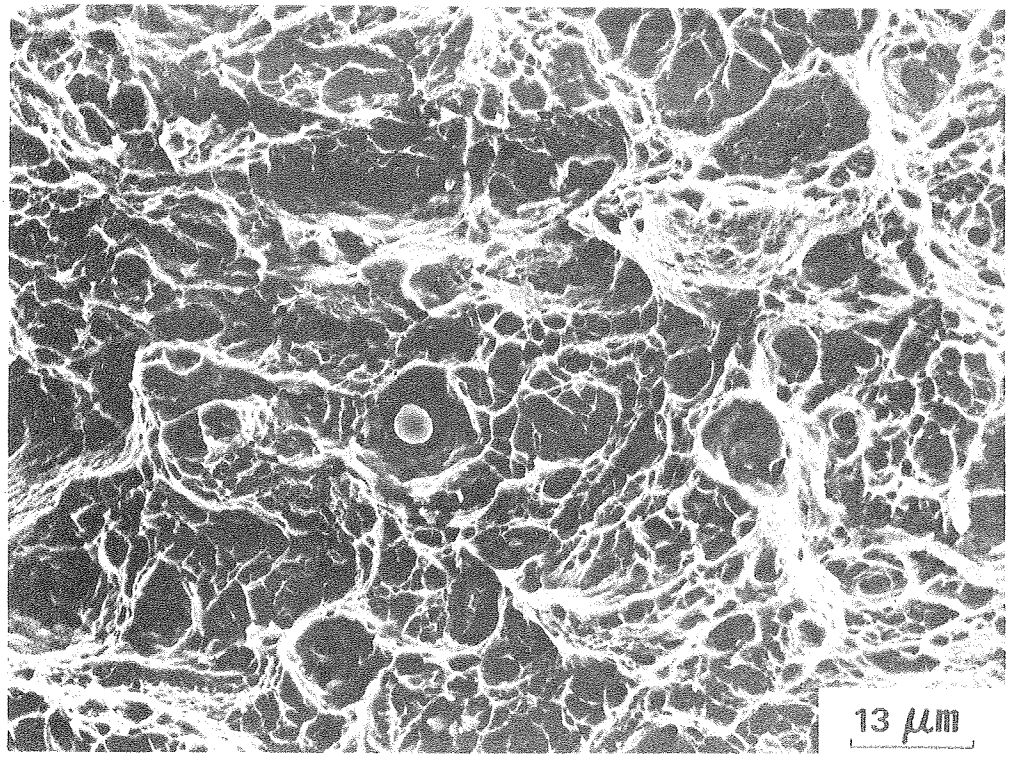

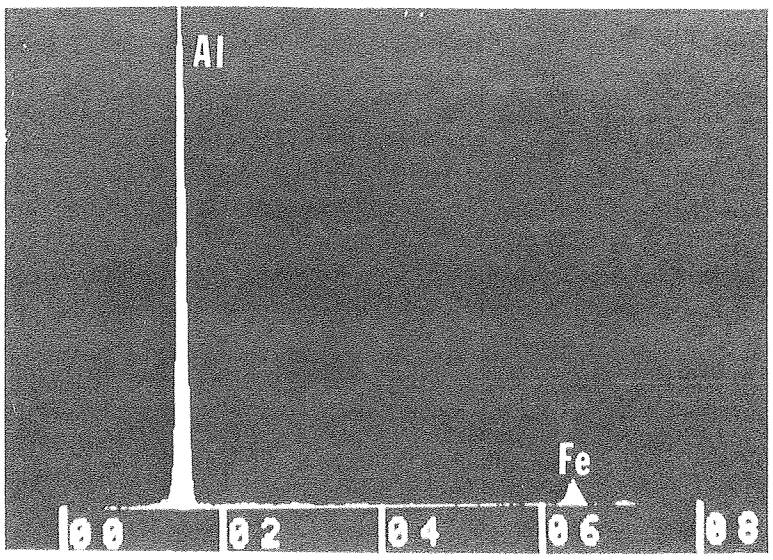

XBB 760-11016

Fig. 44.

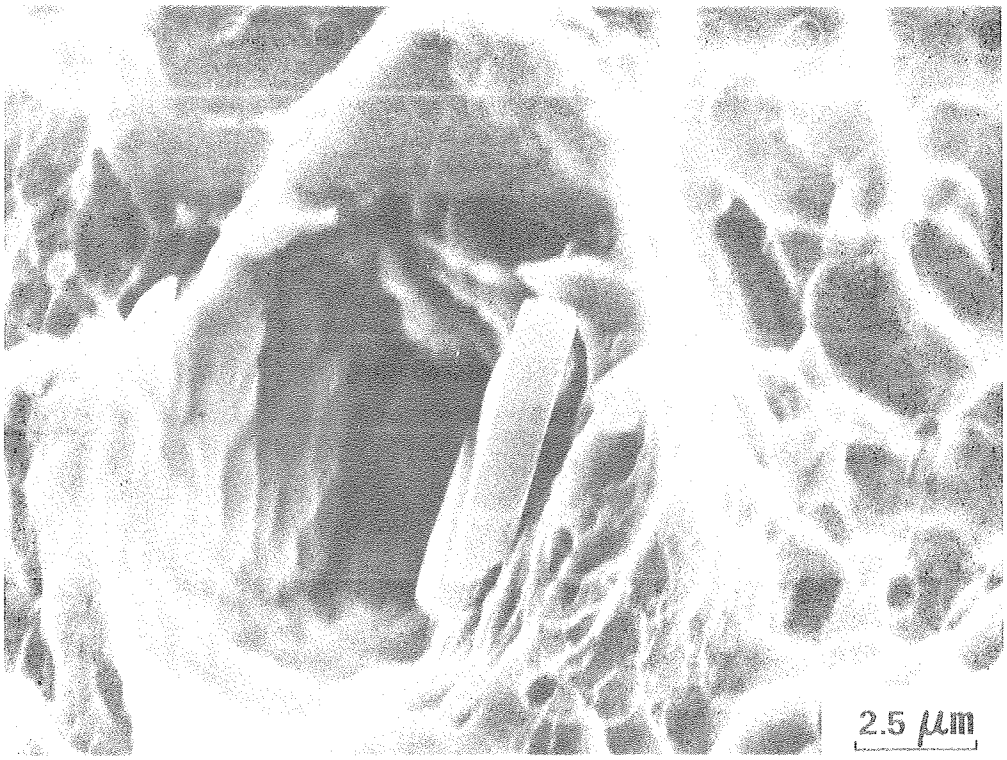

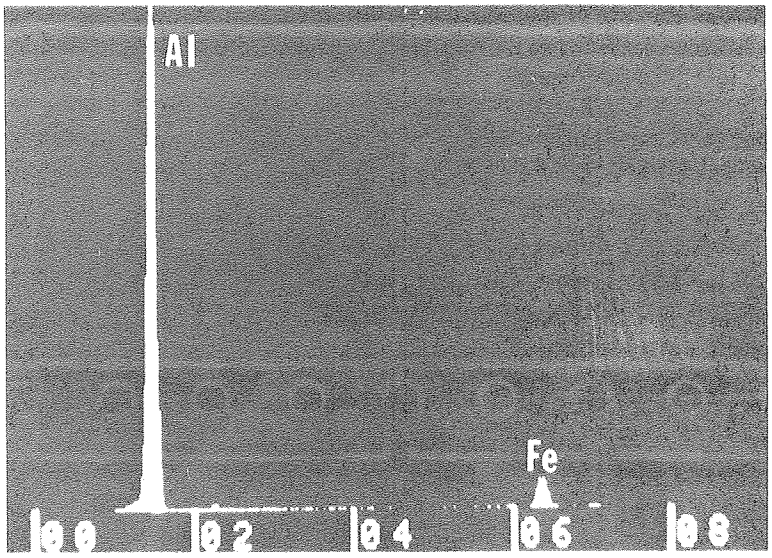

XBB 760-11017

Fig. 45.

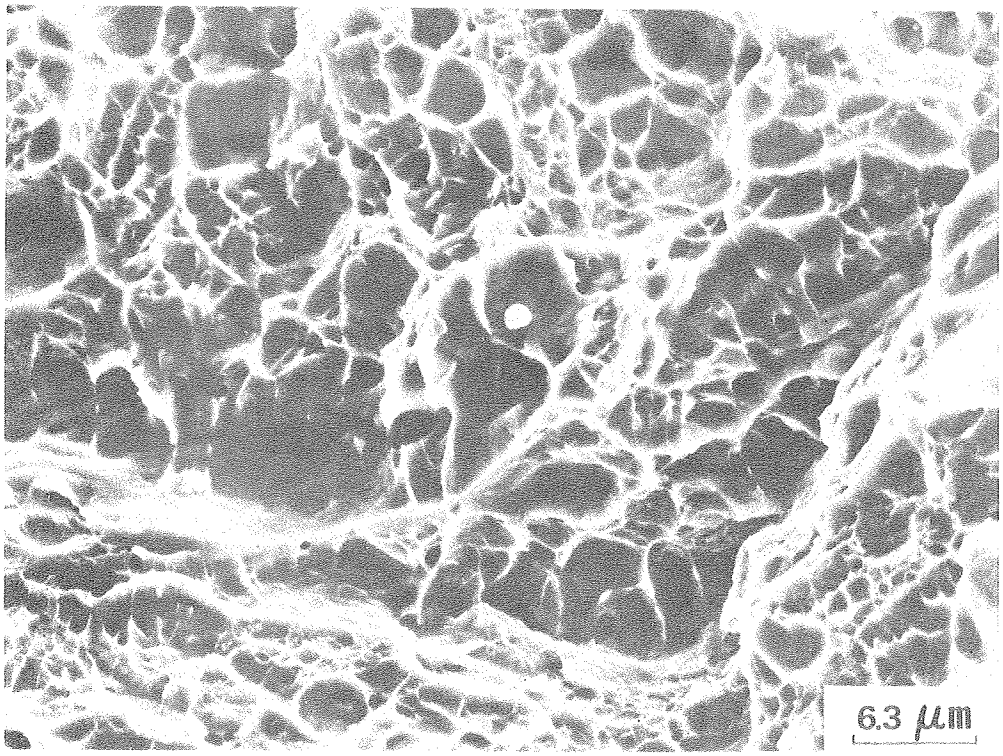

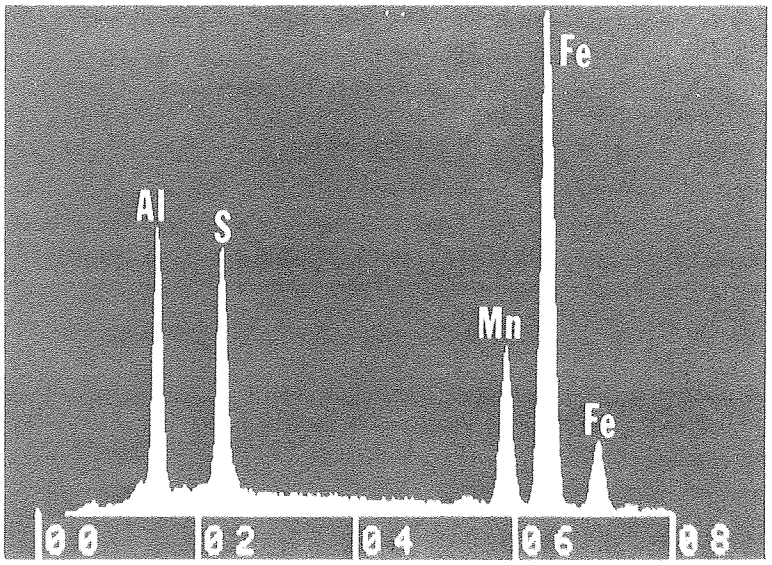

XBB 760-11019

Fig. 46.

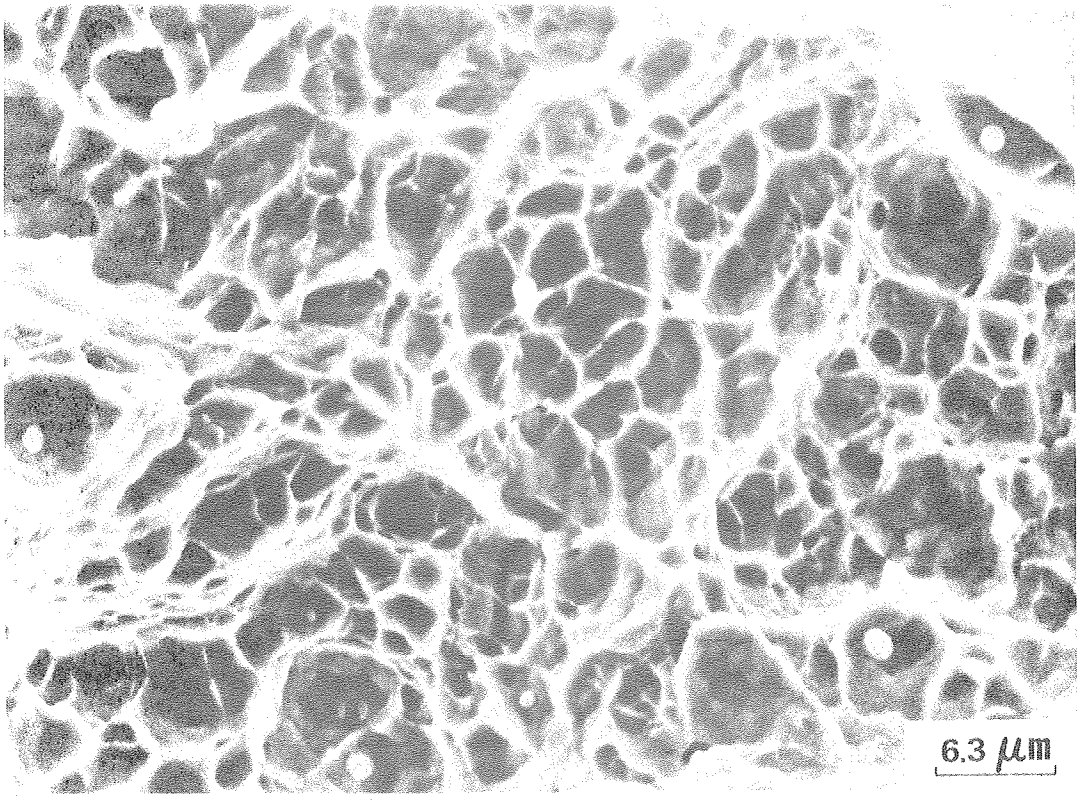

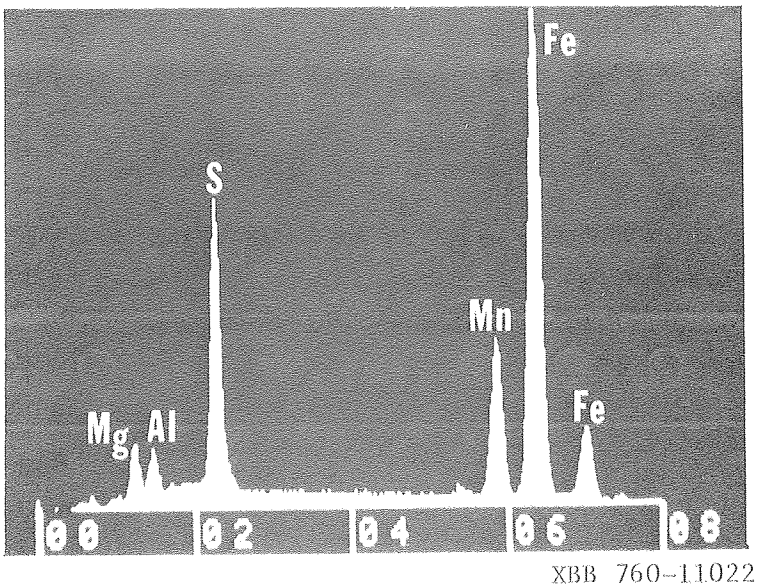

XBB 760-11022

Fig. 47.

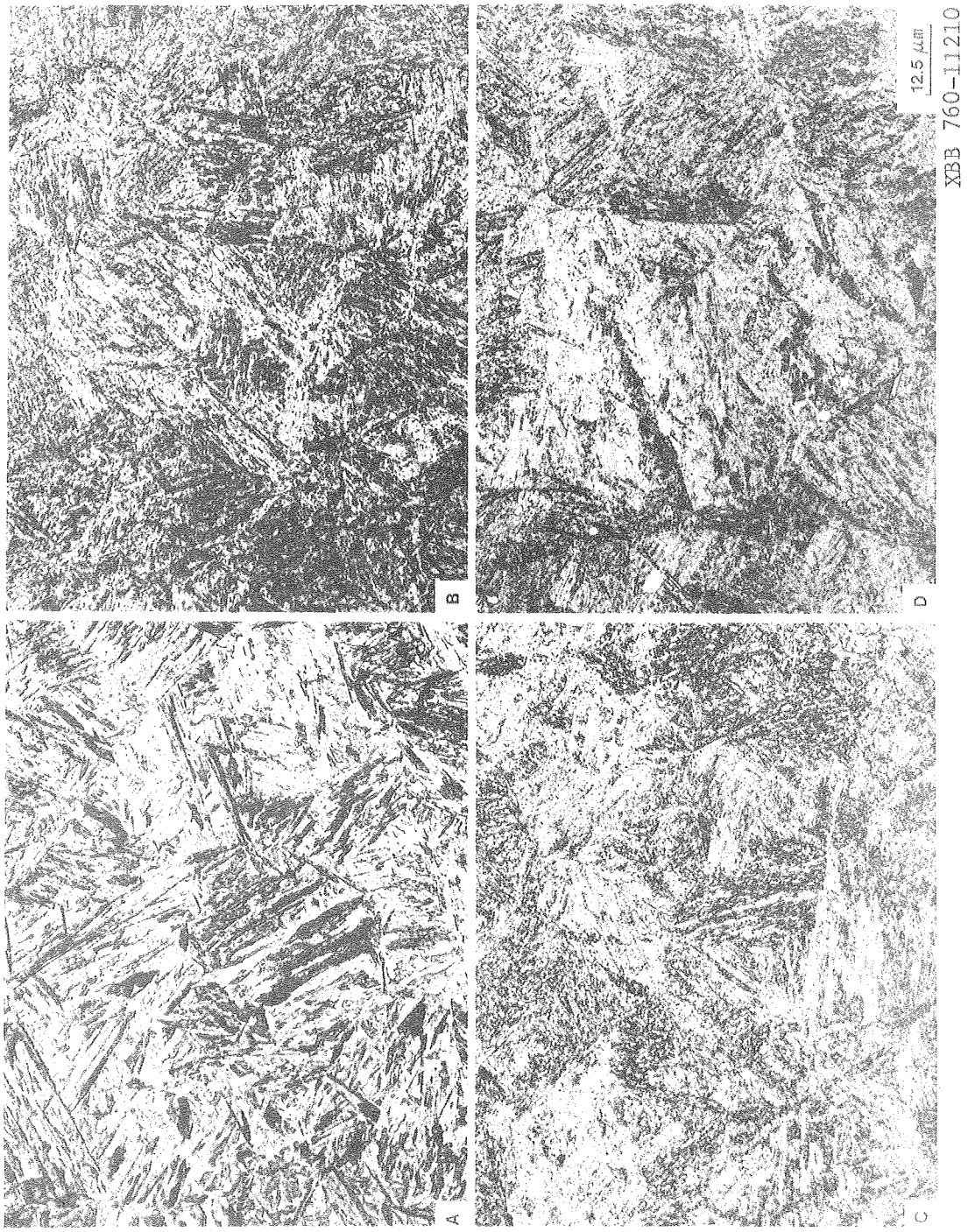
A
B
C
D
12.5 μm
XBB 760-11210

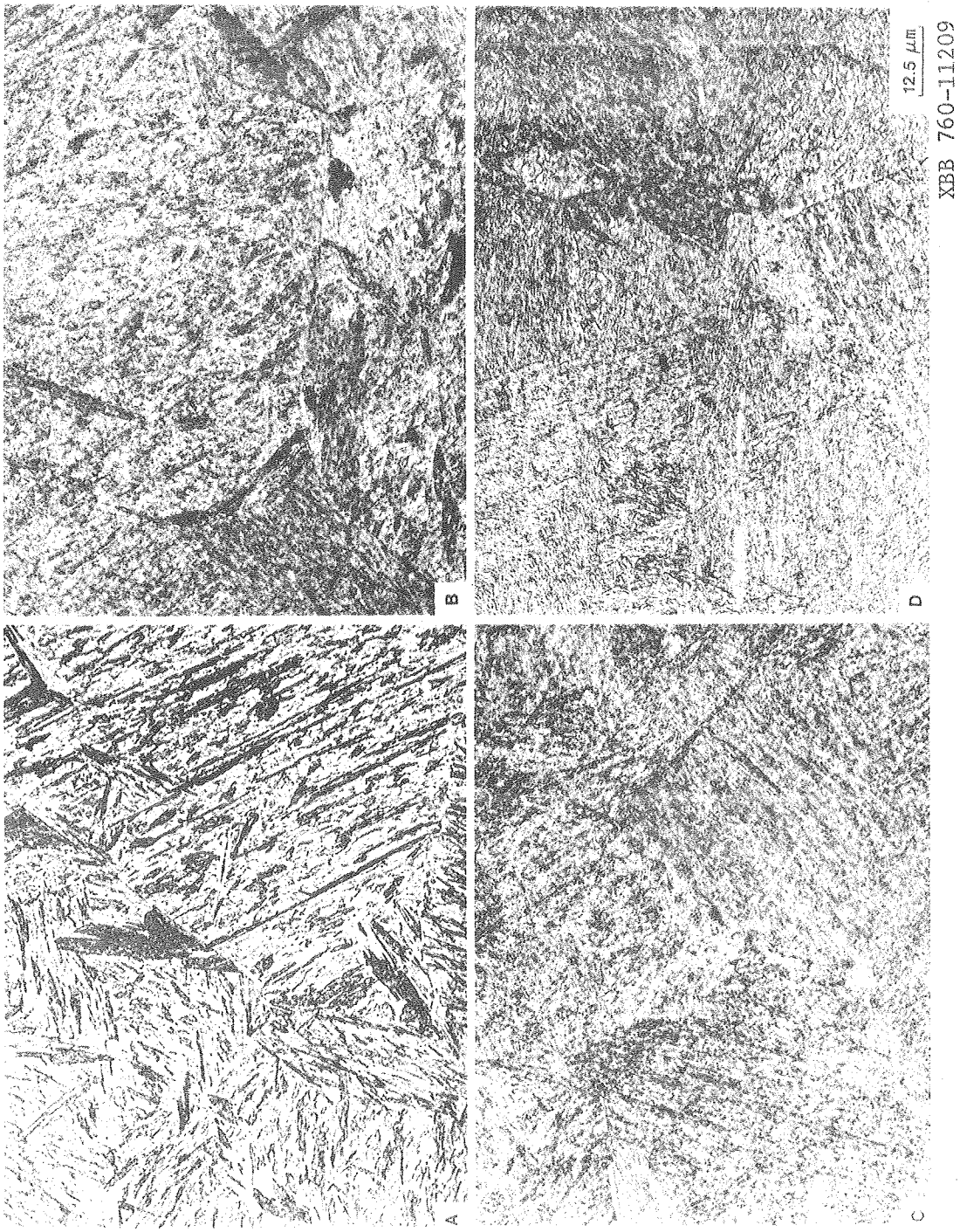

Fig. 49.

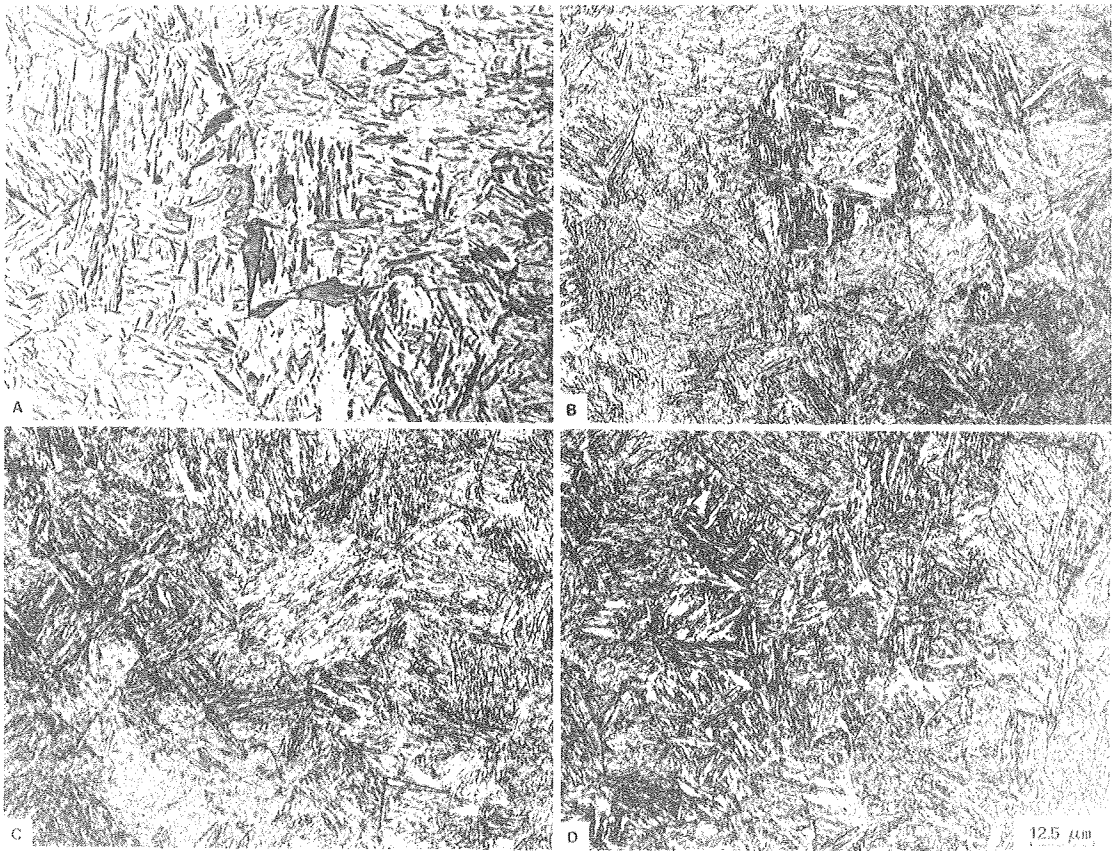

XBB 760-11127

Fig. 50.

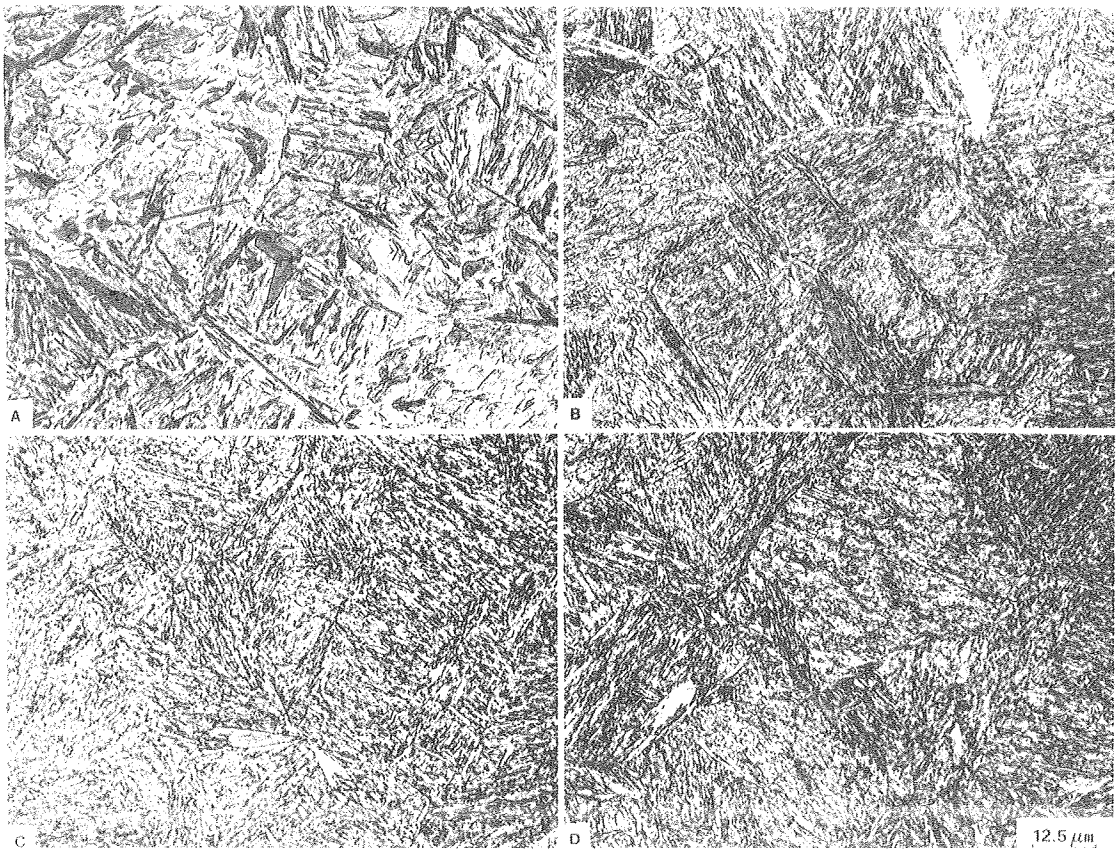

XBB 760-11123

Fig. 51.

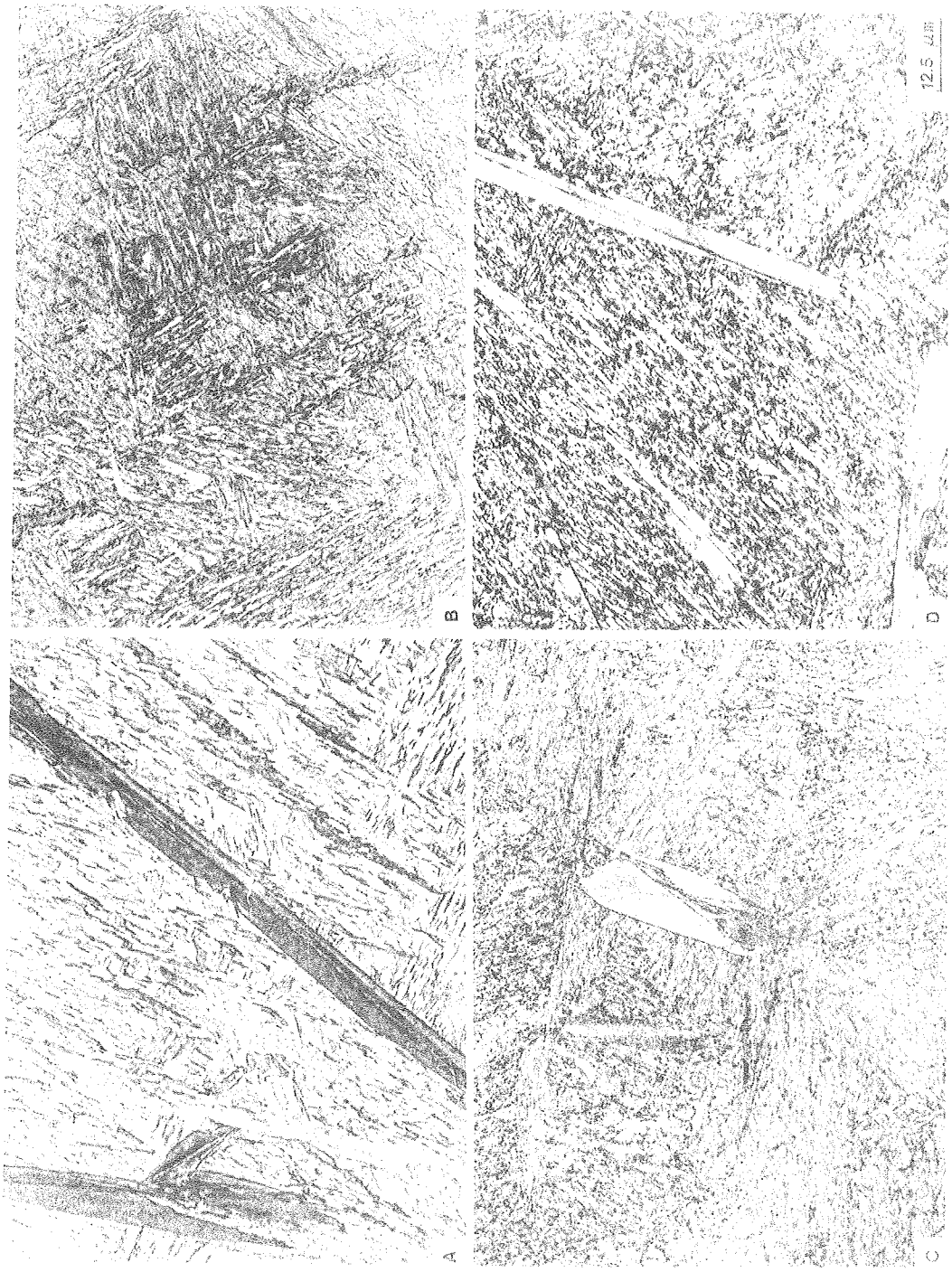

Fig. 52.

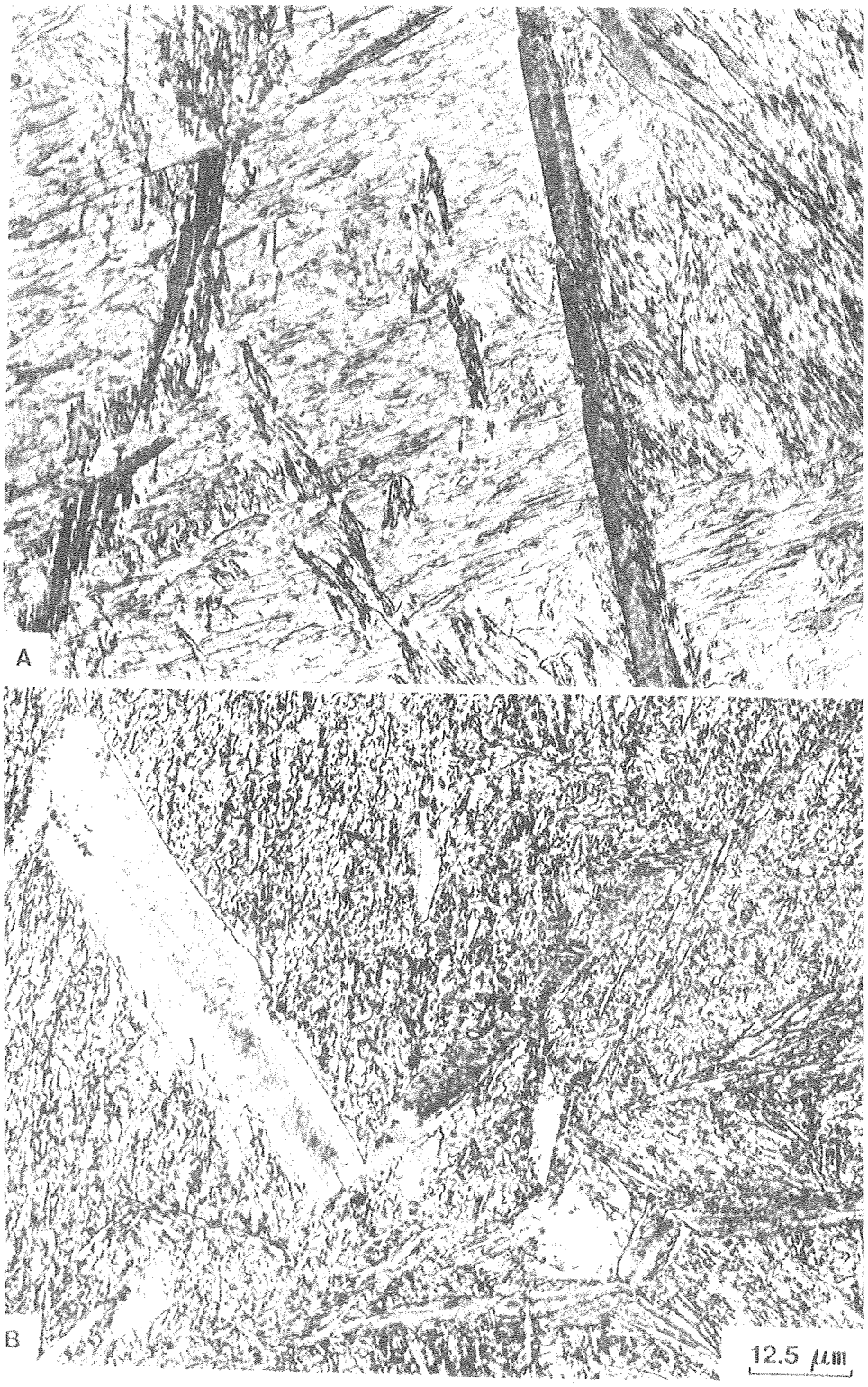

XBB 760-11128

Fig. 53.

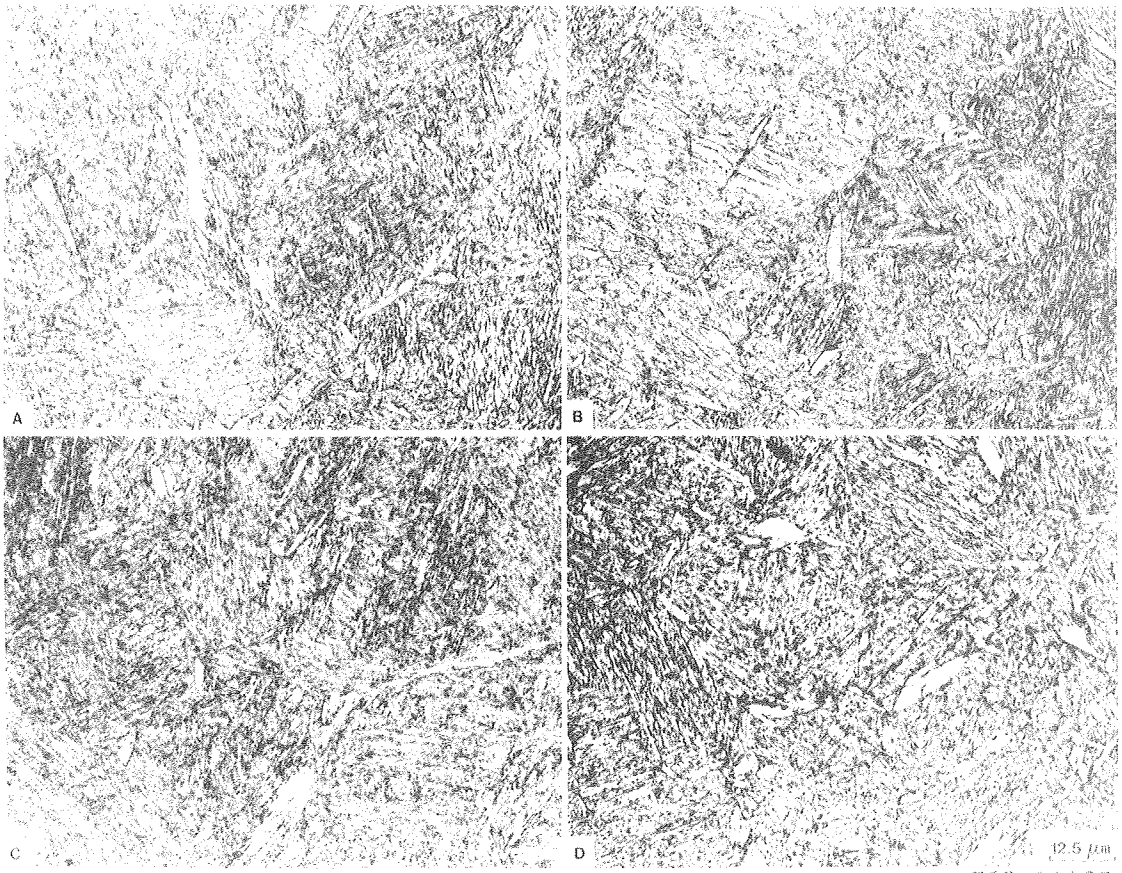

Fig. 54.

XBB 767-6376A

Fig. 55.

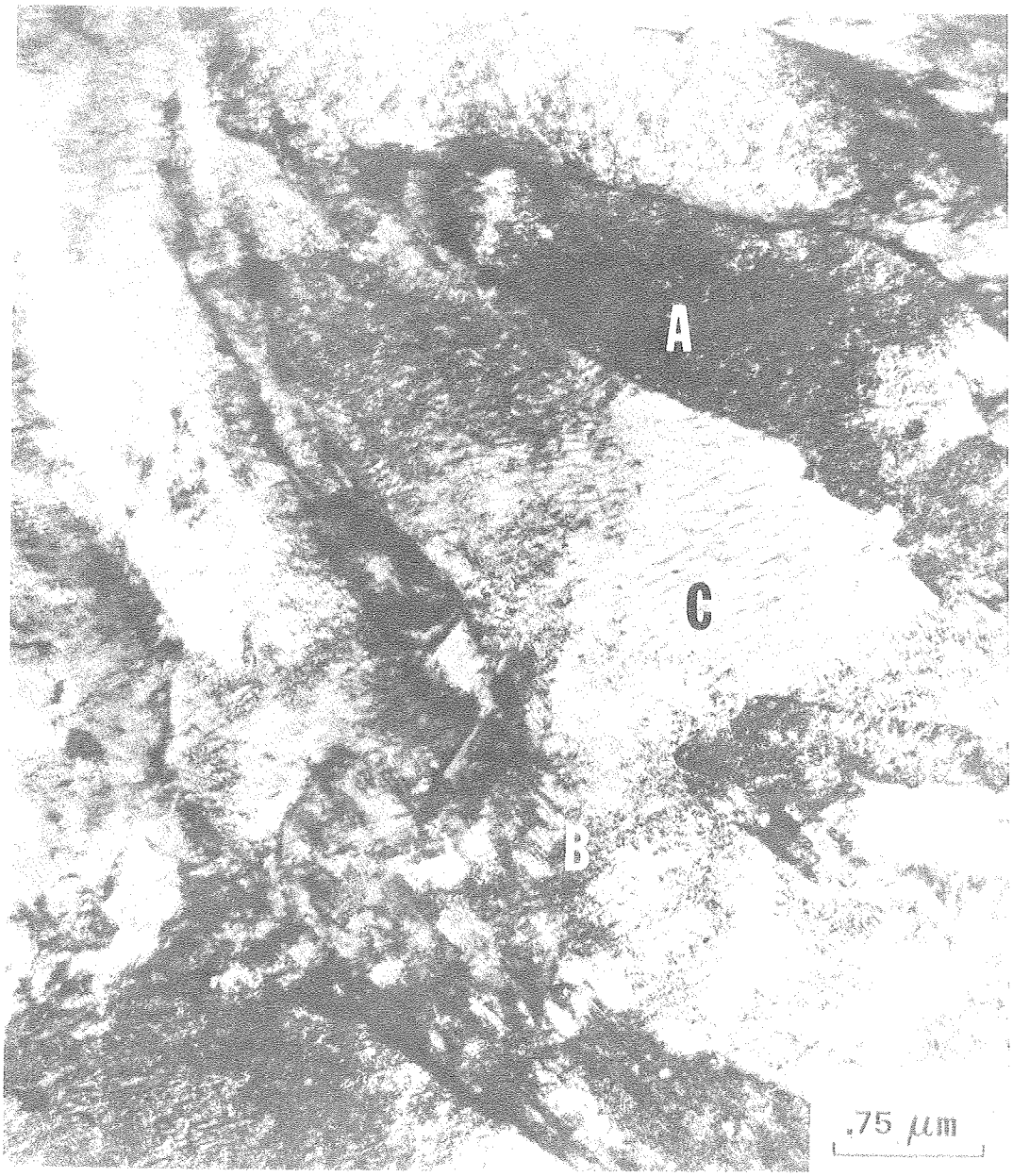

Fig. 56.

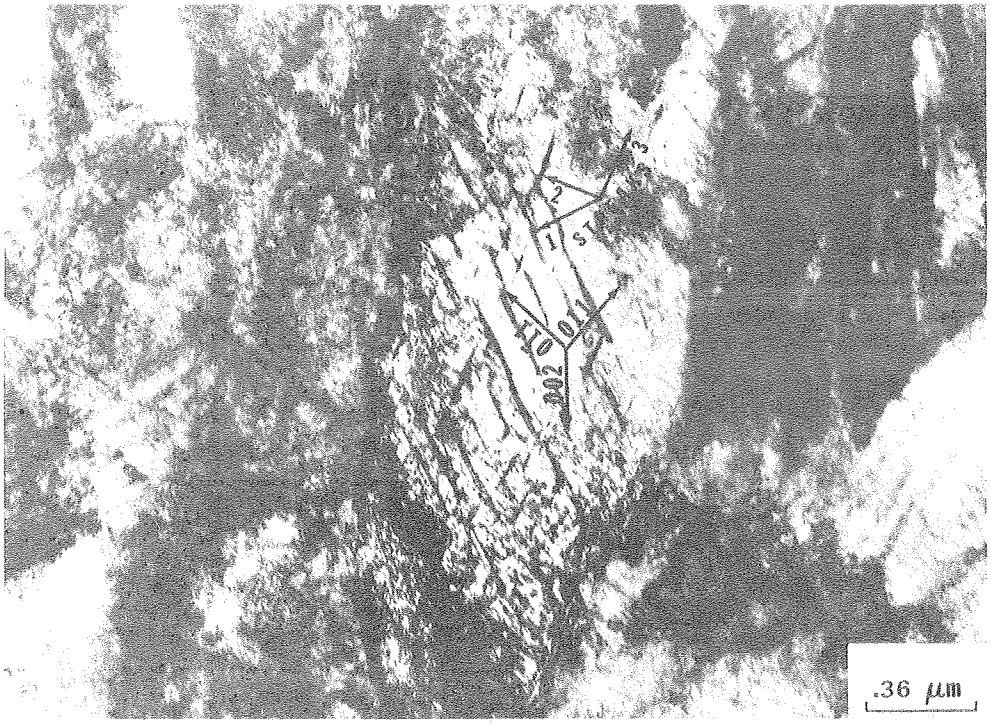
.36 μm

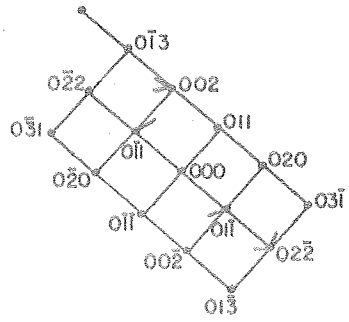
0$\bar{1}$3
0$\bar{2}$2
002
0$\bar{3}$1
011
0$\bar{1}$1
020
0$\bar{2}$0
000
03$\bar{1}$
01$\bar{1}$
01$\bar{1}$
00$\bar{2}$
02$\bar{2}$
01$\bar{3}$

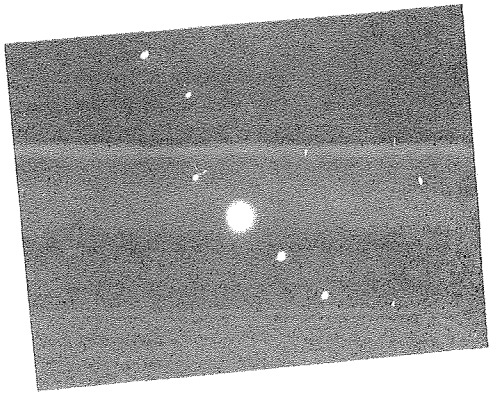

Fig. 57.

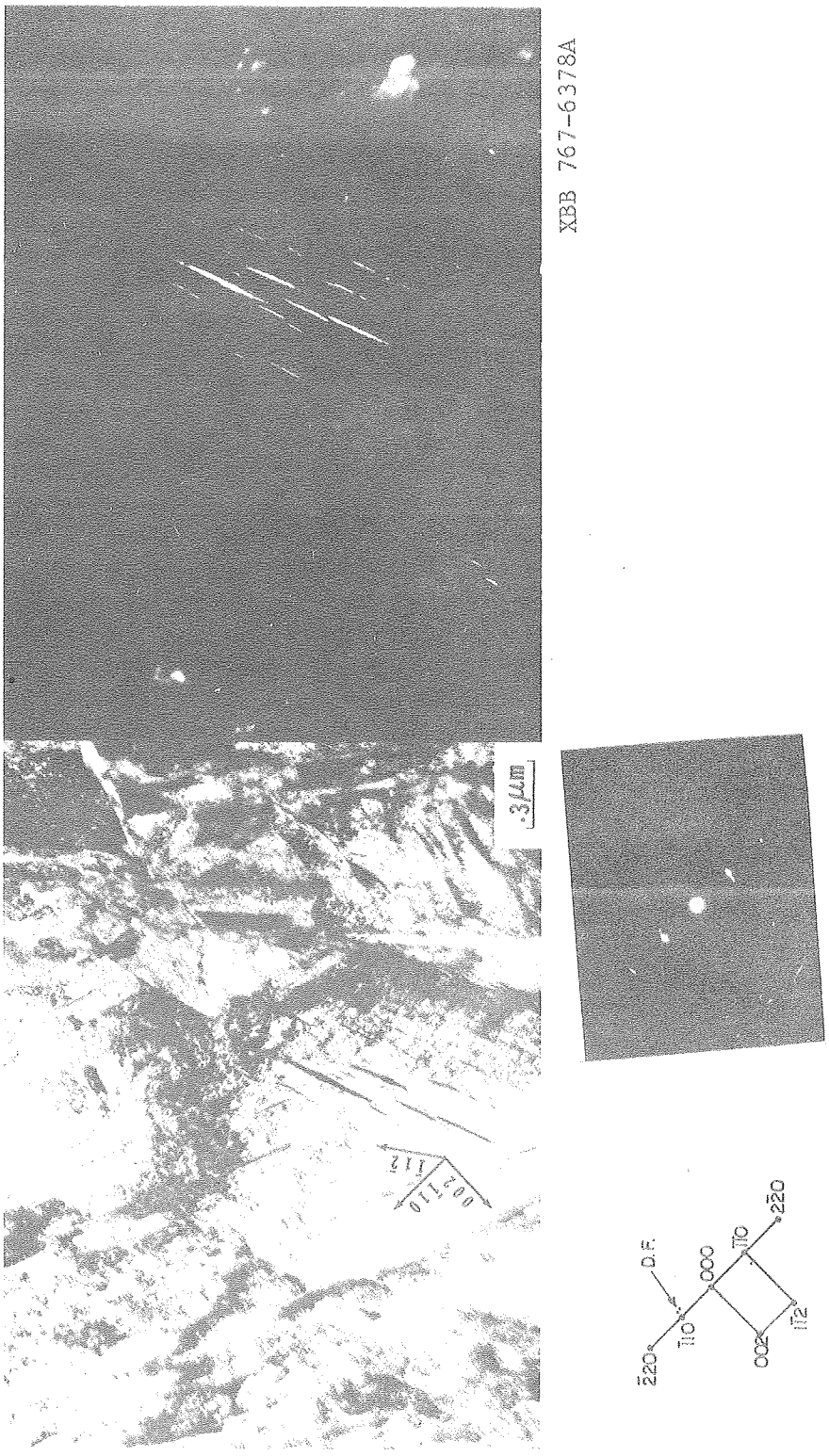

XBB 767-6378A

Fig. 58.

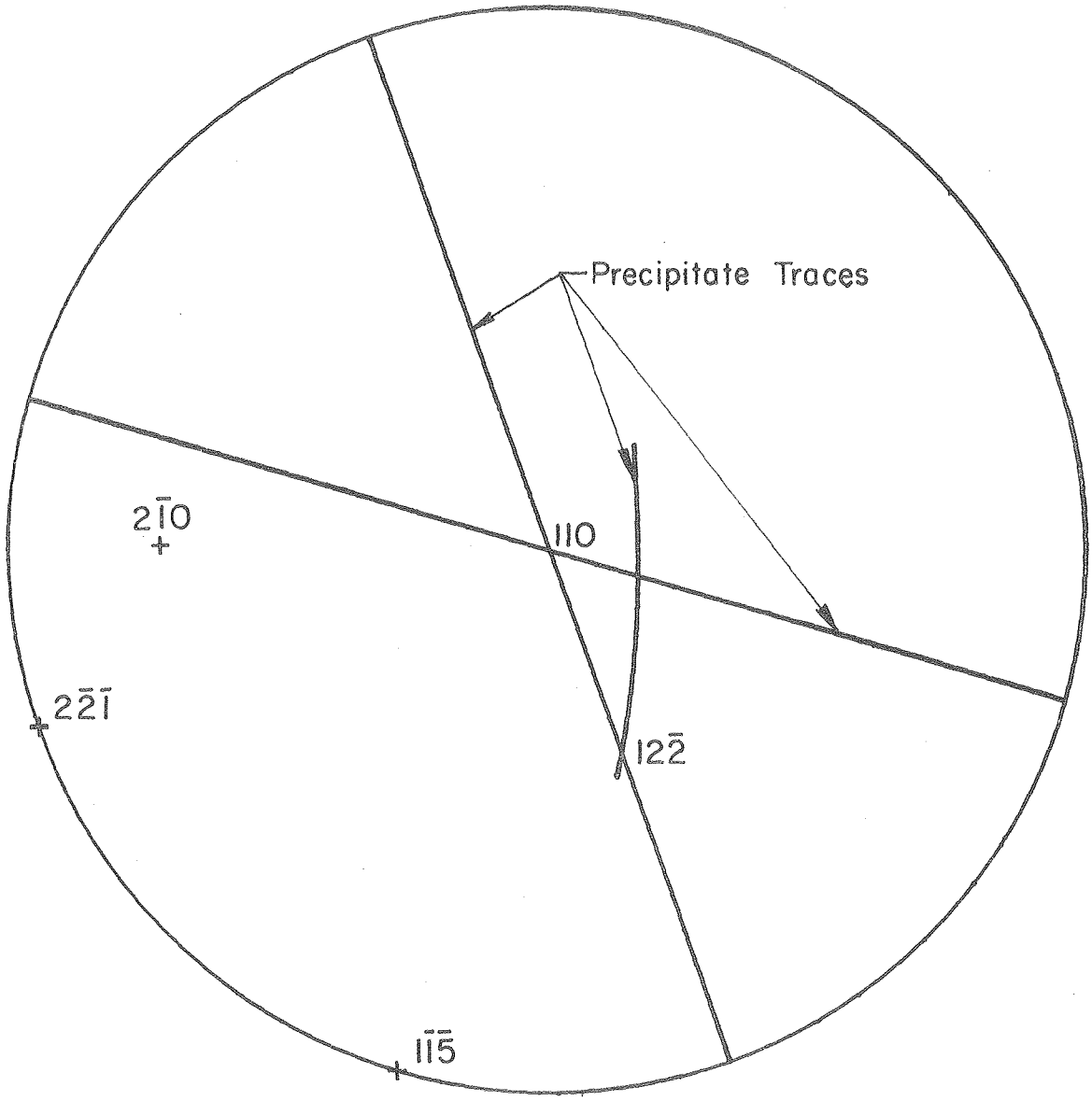

XBL 771-5018

Fig. 59.

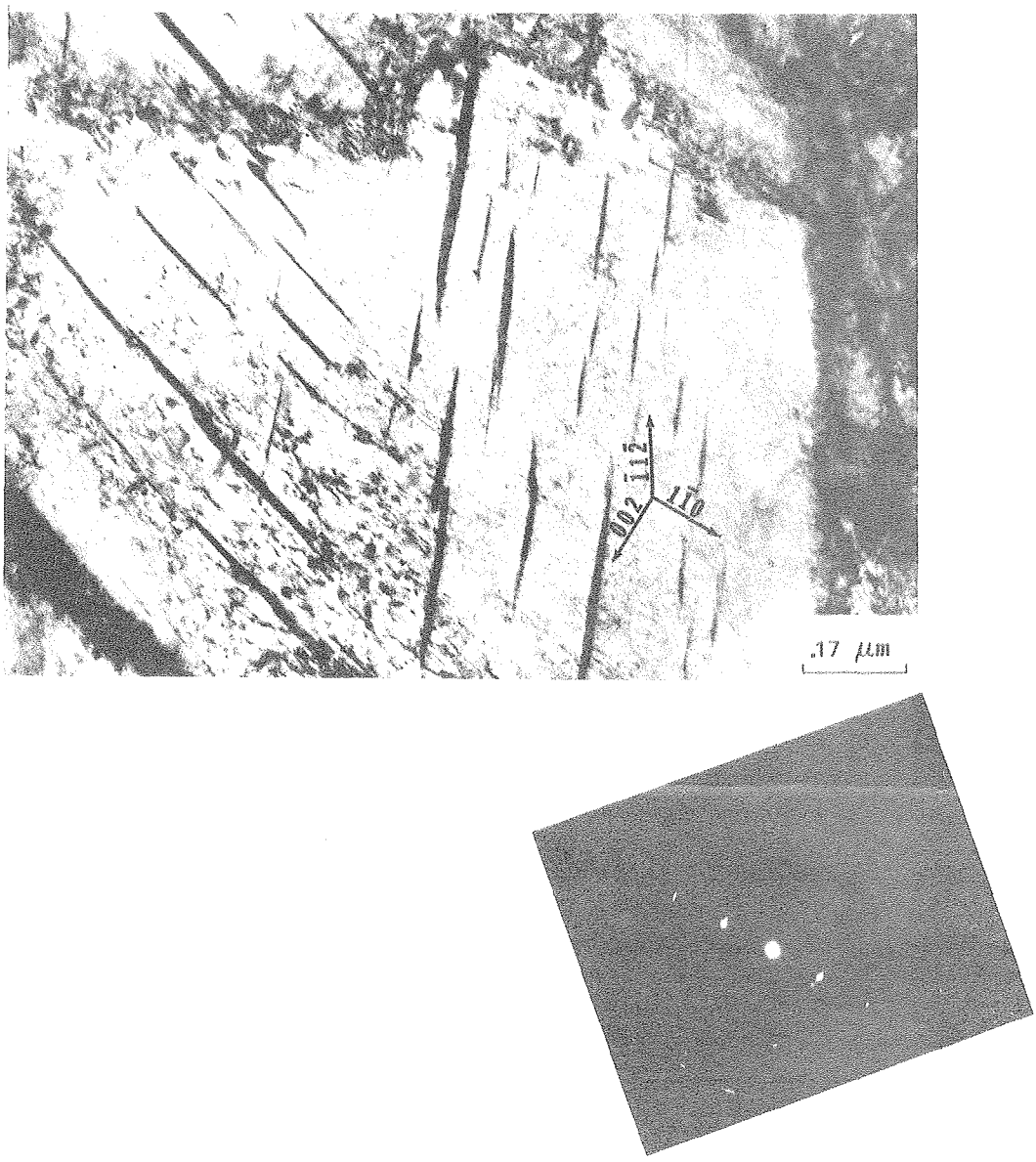

Fig. 60.

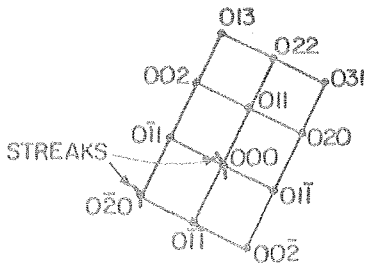

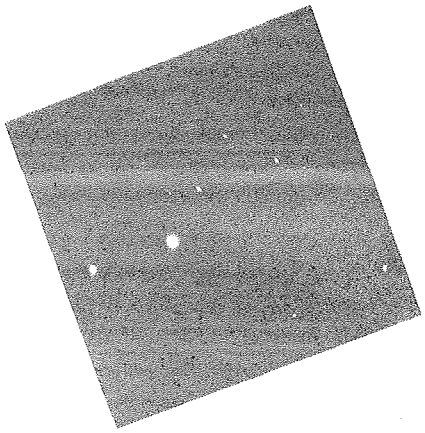

Fig. 61.

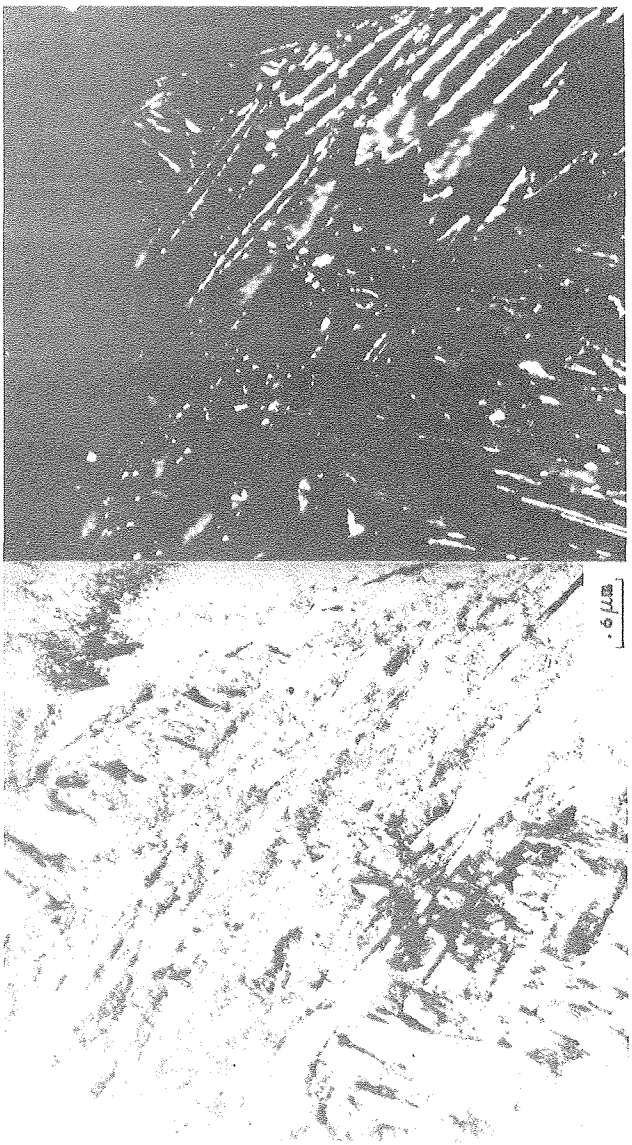

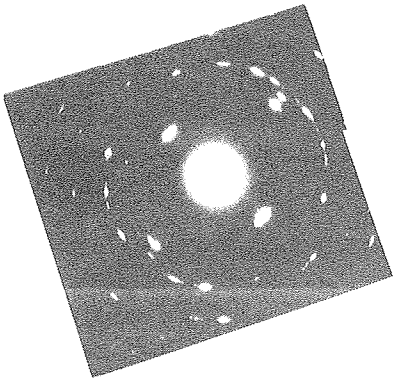

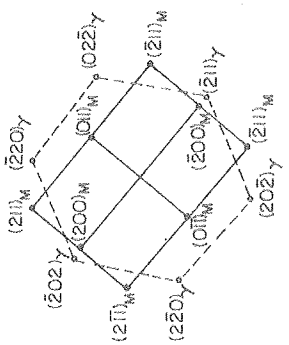

XBB 767-6379A

Fig. 62.

XBB 767-6382

Fig. 63.

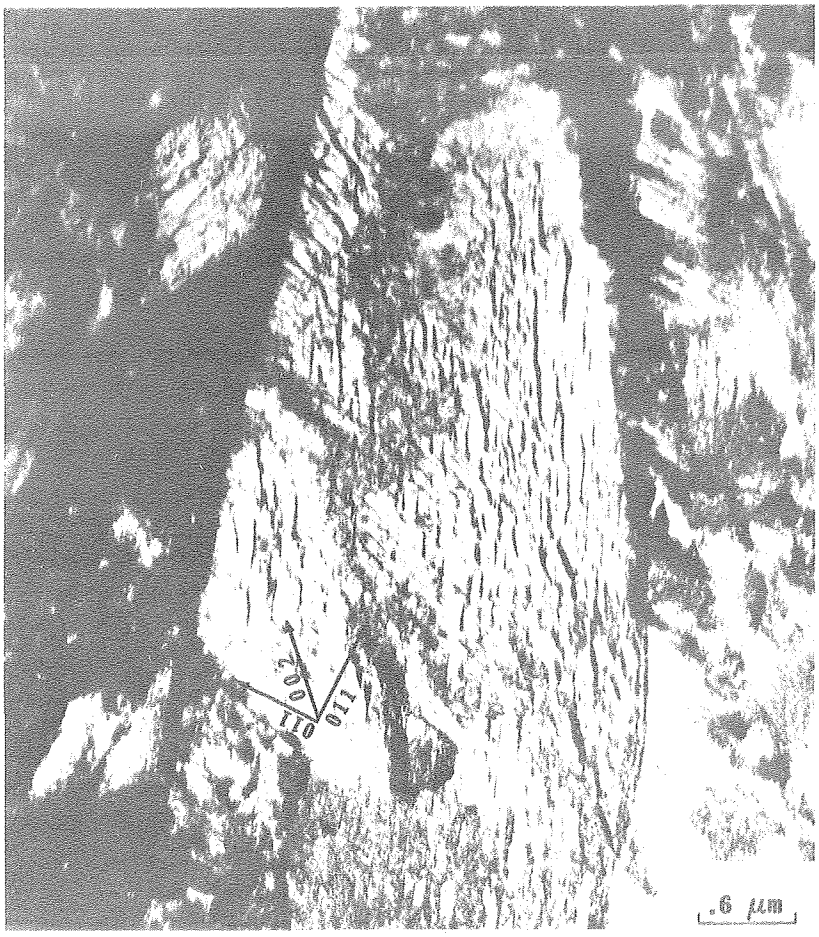

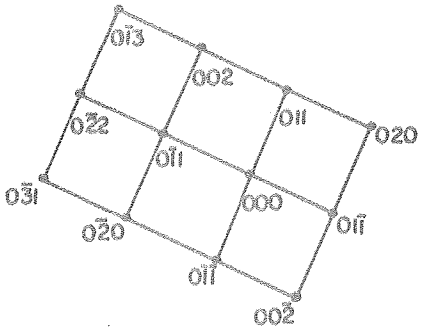

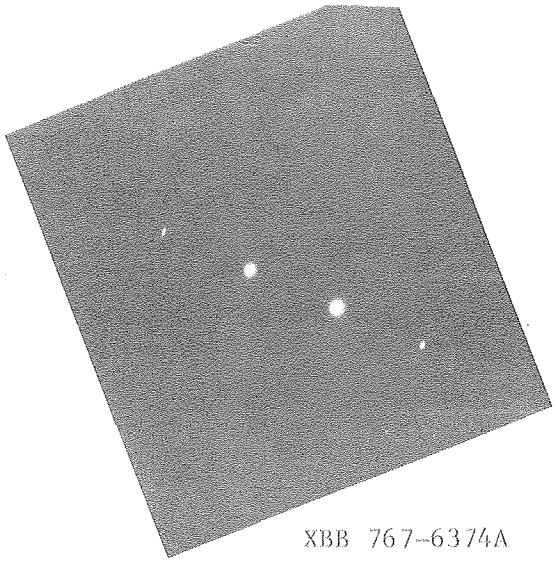

XBB 767-6374A

Fig. 64.

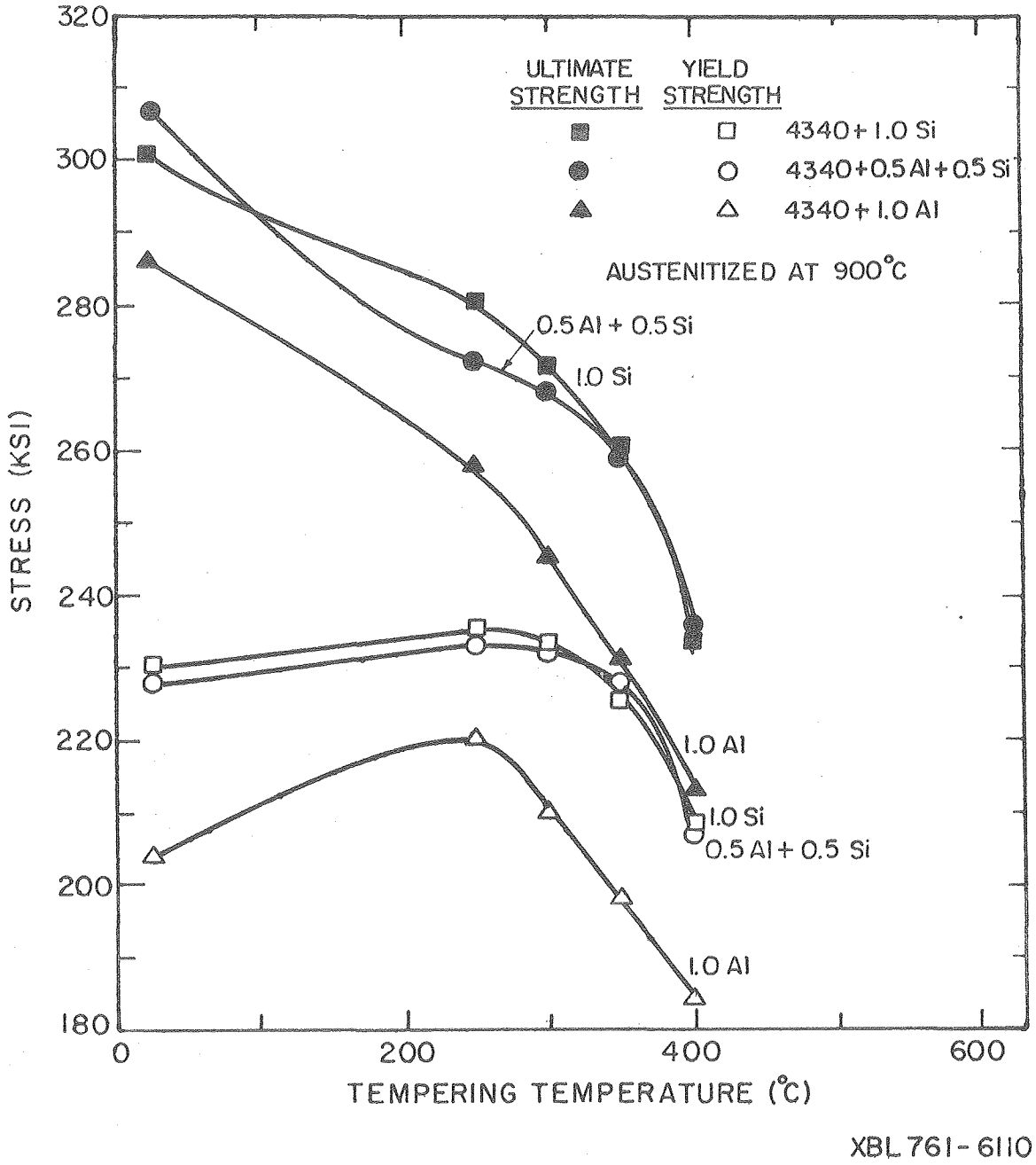

Fig. 65.

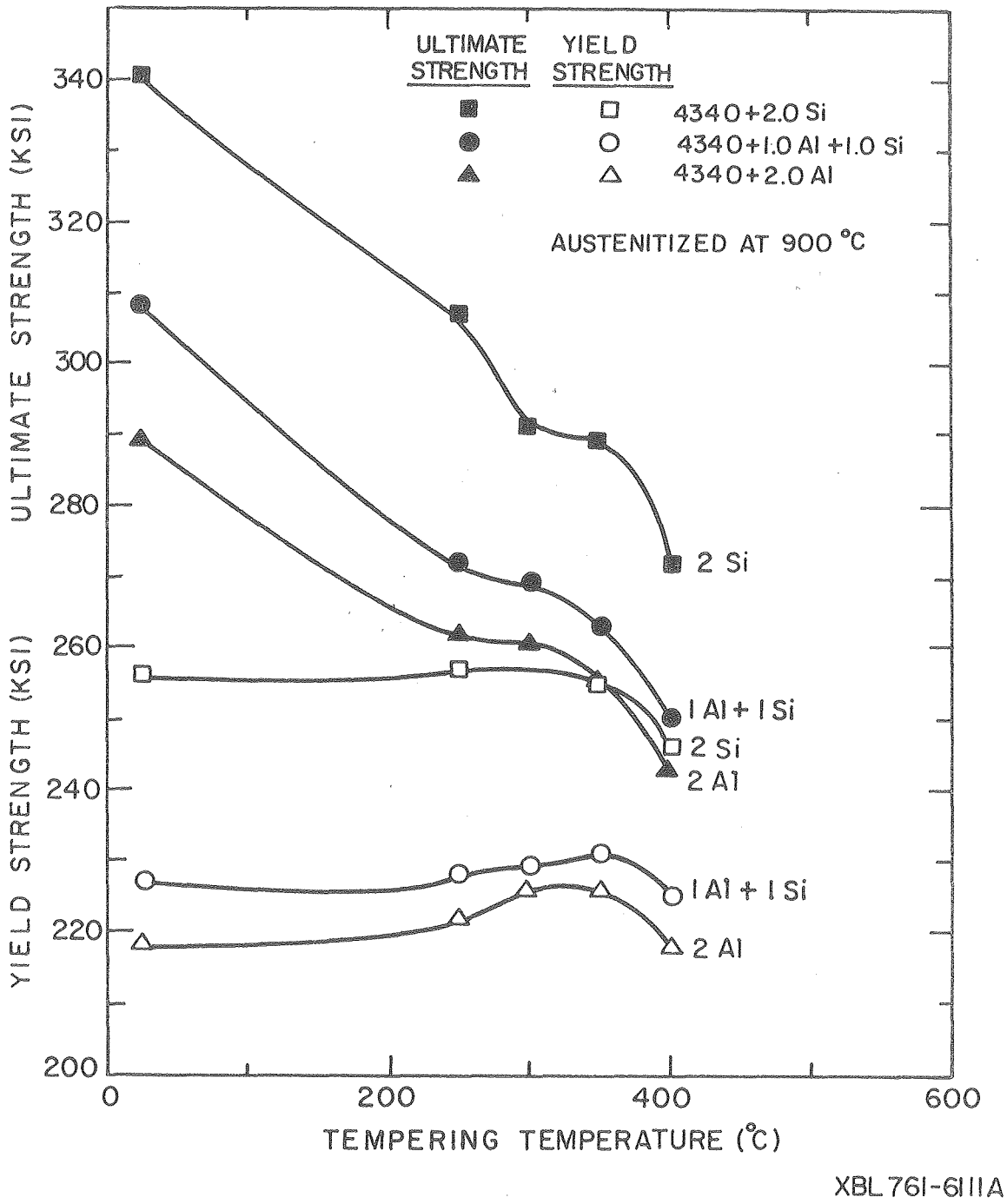
ULTIMATE STRENGTH
YIELD STRENGTH
4340+2.0 Si
4340+1.0 Al +1.0 Si
4340+2.0 Al
AUSTENITIZED AT 900 °C
2 Si
1 Al + 1 Si
2 Si
2 Al
1 Al + 1 Si
2 Al
ULTIMATE STRENGTH (KSI)
YIELD STRENGTH (KSI)
340
320
300
280
260
240
220
200
0
200
400
600
TEMPERING TEMPERATURE (°C)
XBL 761-6111A

Fig. 66.

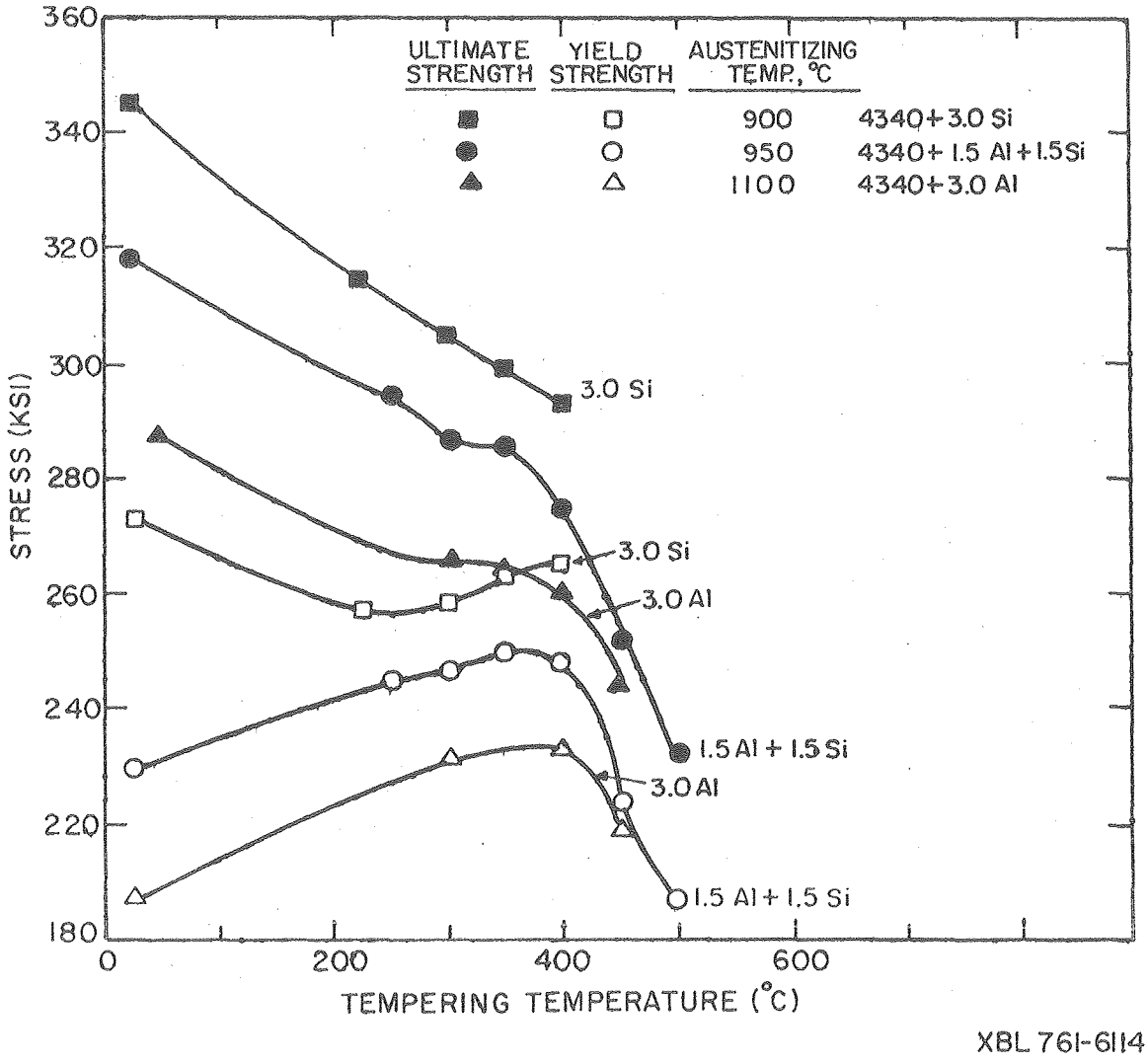

Fig. 67.

XBB 760-11129

Fig. 68.

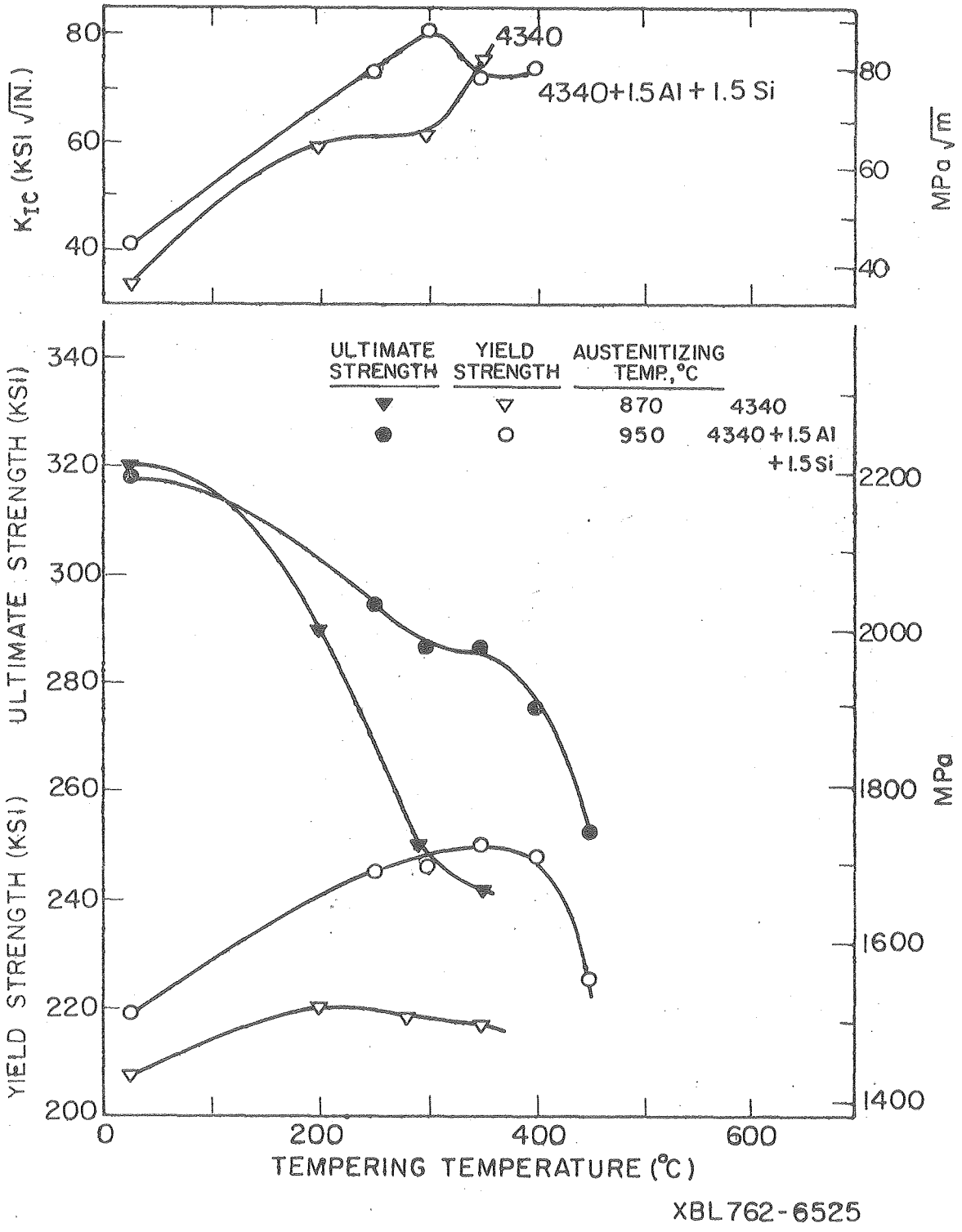

Fig. 69.

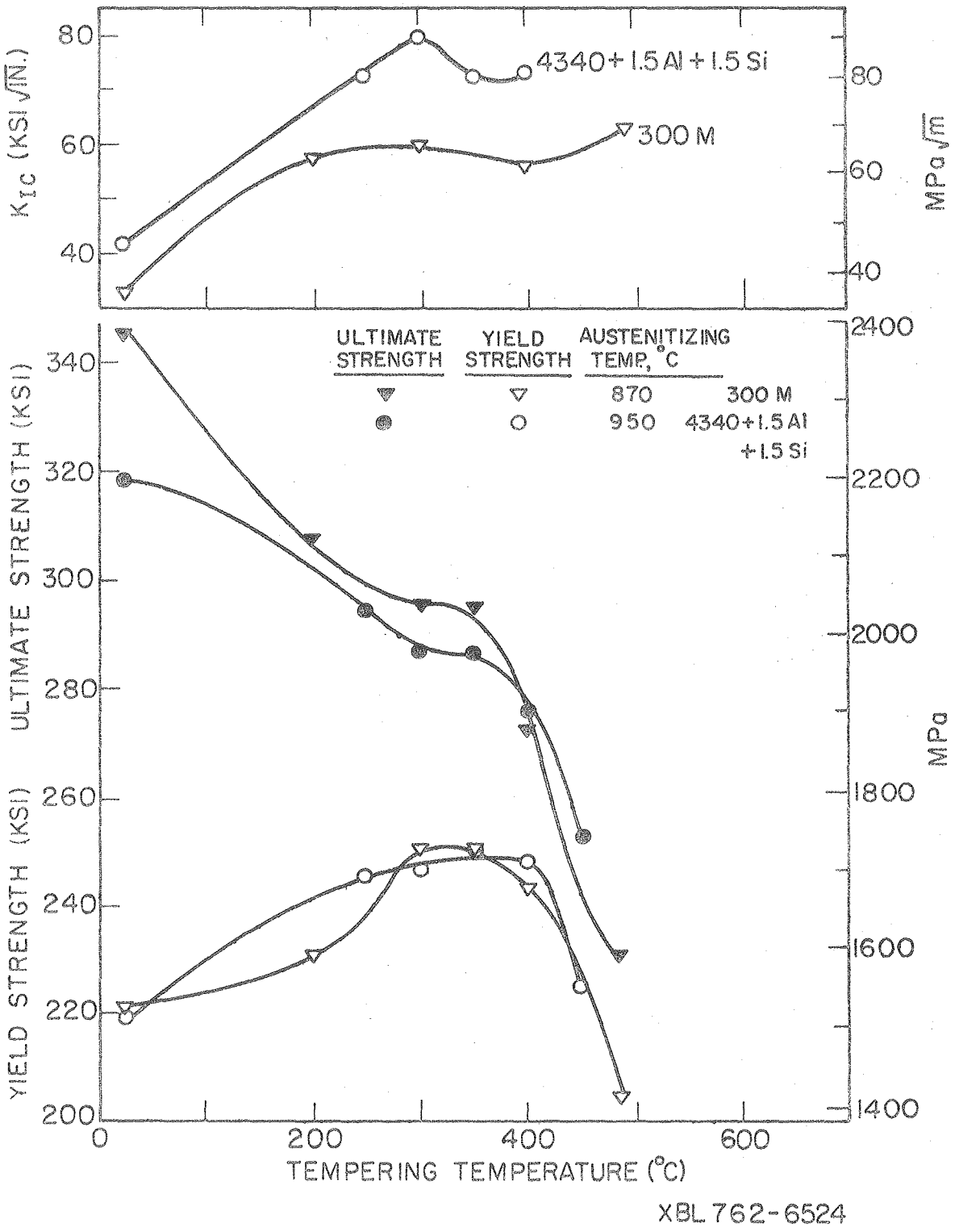
80
60
40
K_{IC} (KSI $\sqrt{IN.}$)
4340+1.5Al+1.5Si
300 M
80
60
40
MPa $\sqrt{m}$
ULTIMATE STRENGTH
YIELD STRENGTH
AUSTENITIZING TEMP., °C
870 300 M
950 4340+1.5Al +1.5Si
340
320
300
280
260
240
220
200
ULTIMATE STRENGTH (KSI)
YIELD STRENGTH (KSI)
2400
2200
2000
1800
1600
1400
MPa
0
200
400
600
TEMPERING TEMPERATURE (°C)
XBL 762-6524

Fig. 70.

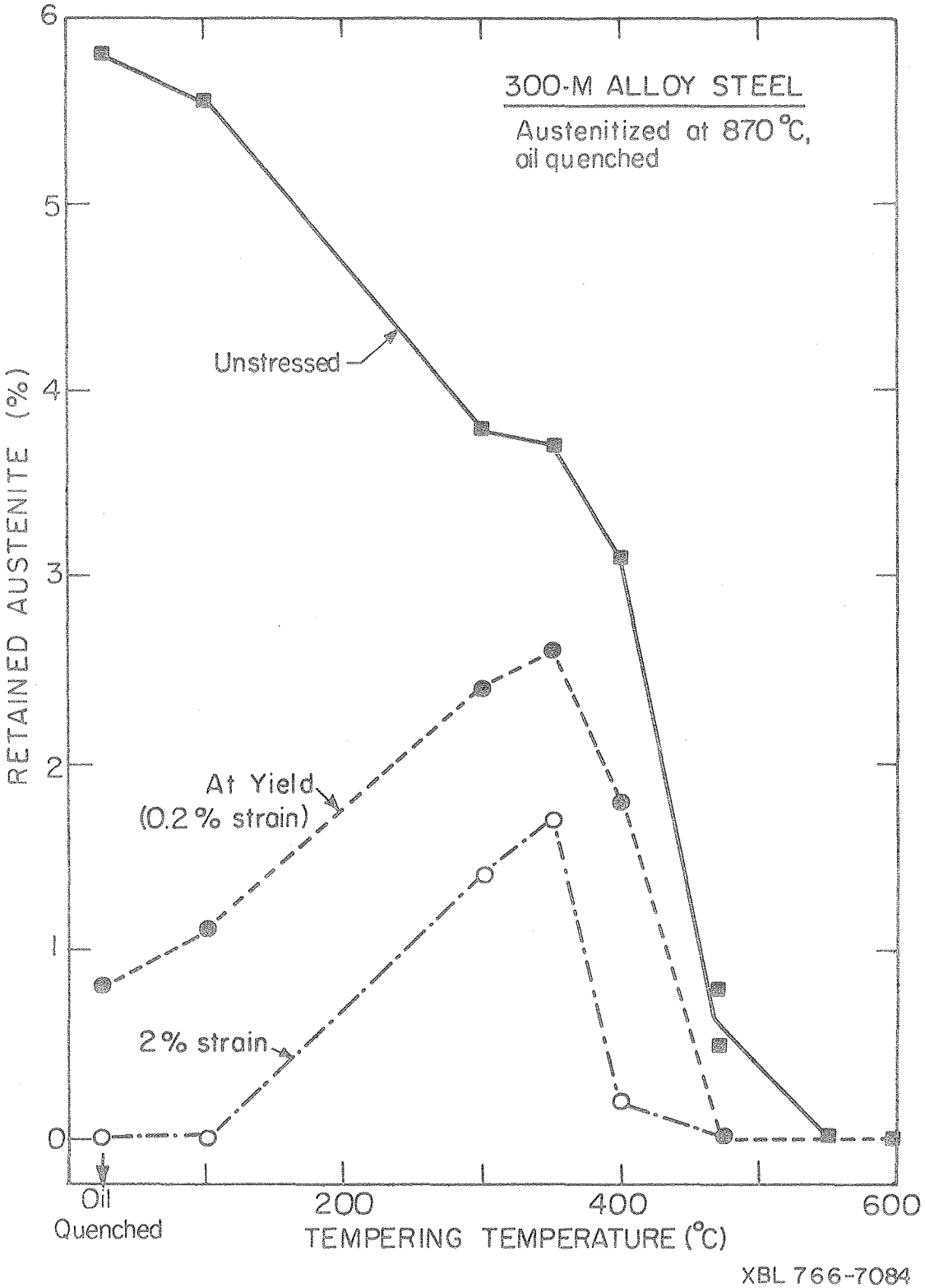

Fig. 71.

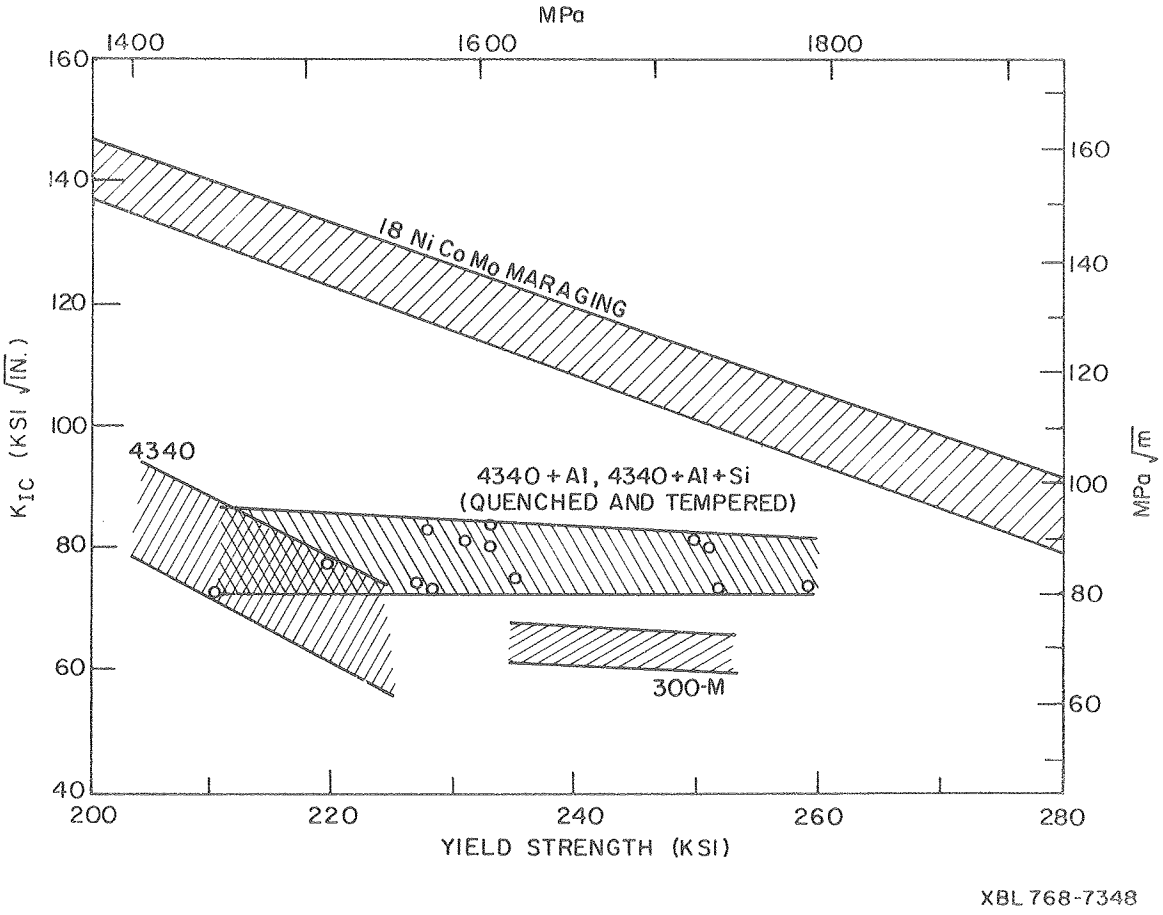
MPa
1400
1600
1800
160
140
120
100
80
60
40
200
220
240
260
280
18 Ni Co Mo MARAGING
4340
4340 + Al, 4340 + Al + Si
(QUENCHED AND TEMPERED)
300-M
K_{IC} (KSI $\sqrt{IN.}$)
MPa $\sqrt{m}$
YIELD STRENGTH (KSI)
XBL 768-7348

Fig. 72.

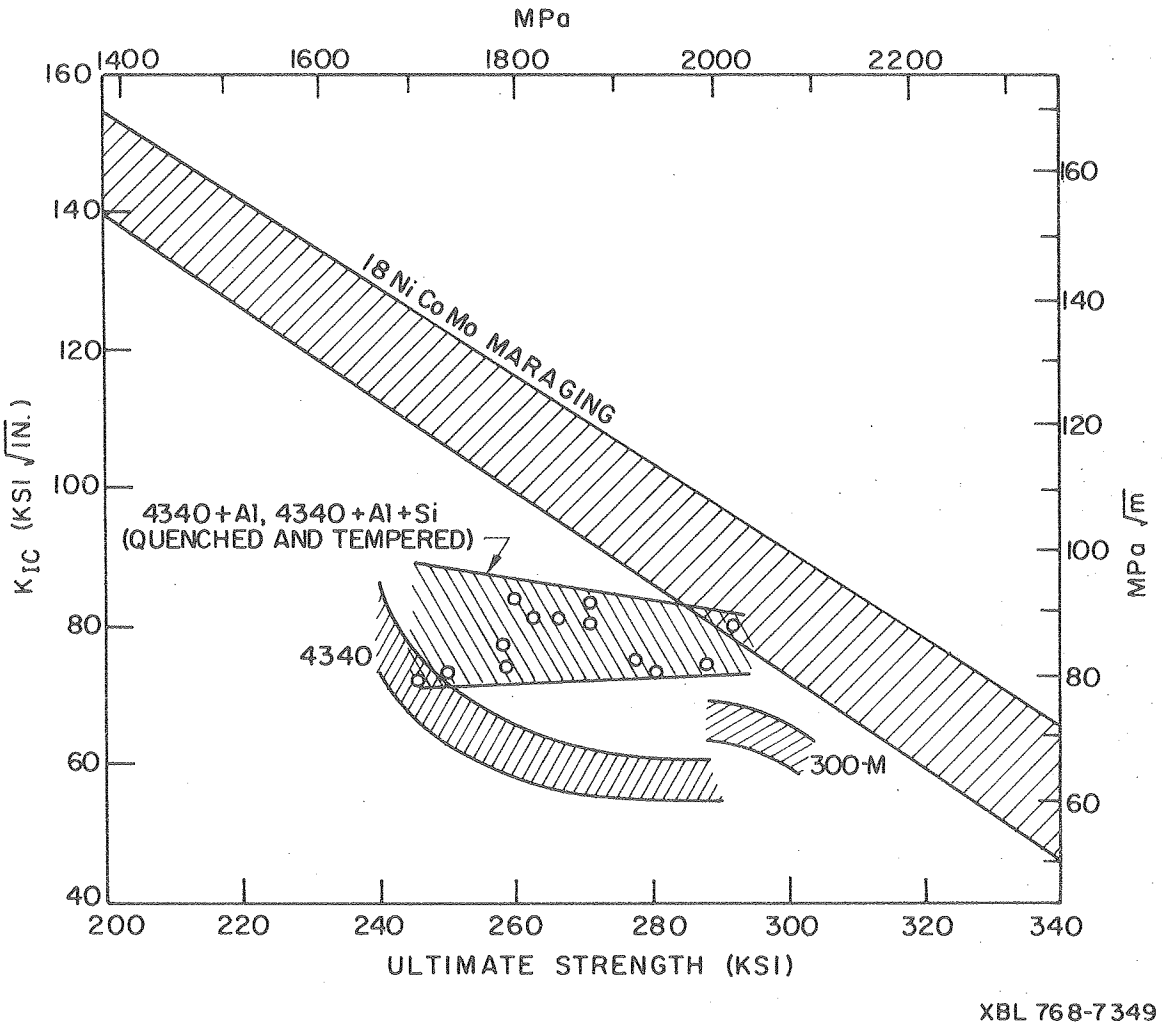
MPa
1400
1600
1800
2000
2200
160
140
120
100
80
60
40
18 Ni Co Mo MARAGING
4340+Al, 4340+Al+Si
(QUENCHED AND TEMPERED)
4340
300-M
K_{IC} (KSI $\sqrt{IN.}$)
MPa $\sqrt{m}$
200
220
240
260
280
300
320
340
ULTIMATE STRENGTH (KSI)
XBL 768-7349

Fig. 73.